Odor Processing and Associative Olfactory Learning in the Moth *Manduca sexta*

ONG, Chik Ying Rose

A Thesis Submitted in Partial Fulfilment

of the Requirements for the Degree of

Doctor of Philosophy

in

Biochemistry

The Chinese University of Hong Kong

April 2010

Thesis committee members:

Prof. Ho Yin Chan (Chair)
Prof. Siu Kai Kong (Thesis Supervisor)
Dr. Mark Stopfer (Thesis Supervisor)
Prof. Wai Yee Chan (Internal Examiner)
Prof. Kin Lam Yung (External Examiner)

Acknowledgements

I would like to thank my advisor Dr. Mark Stopfer for his ideas and for introducing me into this fascinating area of science. I would also like to thank my mentor Professor Siu Kai Kong for his kind guidance, advice, and support. Also, I need to thank my Thesis Committee members for all their time and interest in my research projects.

I am very grateful to Drs. Owen Rennert and Wai-yee Chan for giving me the opportunity to conduct my research in the National Institutes of Health, and for their advice and support throughout my study.

I need to thank all the past and present members of the Stopfer lab, and particularly Drs. Iori Ito, Joby Joseph, and Felice Dunn, for all their suggestions and scientific discussions, and for being great friends that enriched my Ph.D. study.

I would like to thank Dr. Leo Belluscio, and members in his lab for helpful scientific and technical discussions. Especially, I would like to thank Dr. Kai Cheng for all his support and help throughout my study. I would also like to acknowledge help in fluorescent imaging from Drs. James Russell, Vincent Schram, and Louis Dye. Also, I am grateful for Dr. Mark Willis for his help in my moth free flying experiments.

Thanks to Dr. Geraldine Wright for all her help in statistical analyses and advices in my behavioral experiments. Thanks also to Miss Kiriana Cowansage for

developing the moth behavioral training setup in our lab, and for laying the grounds for my olfactory tuning project.

I would like to thank all my classmates, teaching assistants, and principle investigators in the Neural Systems and Behavior summer course in Woods Hole for giving me a busy but memorable summer.

Lastly, I would like to give thanks to my friends in Building 35 for making my Ph.D. experience enriching and enjoyable.

Abstract

Two important focuses in neuroscience are to study how animals process sensory stimuli, and how such stimuli get associated with other sensory modalities through experience. Often, sensory stimuli elicit the oscillatory synchronization of neurons in different parts of the brain, and thus may constitute an important stage in sensory processing. Odor-evoked oscillatory synchronization has been observed in a wide variety of animals, including mammals and insects. Despite differences in details of anatomical structure, animals from widely different phyla appear to use similar strategies to encode odors. Here, using the moth *Manduca sexta*, I examined the factors that cause odor-evoked oscillatory synchronization of olfactory neurons and that determine the frequency of these oscillations. I found that frequency of oscillations decreased from ~40 Hz to ~20 Hz during the course of a lengthy odor pulse. This decrease in oscillatory frequency appeared in parallel with a decrease in net olfactory receptor output, suggesting that the intensity of olfactory receptor neuron input to the antennal lobe, the first olfactory relay center, may determine oscillatory frequency. However, I found that changing odor concentration had little effect on oscillatory frequency. Combining the results of recordings made *in vivo* and computational models, I found that increasing odor concentration recruited additional, but less well-tuned olfactory receptor neurons to respond to the odor. Firing rates of these neurons were tightly constrained by adaptation and saturation. My work established that, in the periphery, odor concentration is mainly encoded by the size of the olfactory receptor neuron population that responded to the odor, whereas oscillatory frequency is determined by the adaptation and saturation of this

response.

Neural representations of odors get associated with other stimuli through experience. Are action potentials the neural representation that directly gets associated with reinforcement during conditioning? In *Manduca*, I found that odor presentations elicited only one or two spikes at odor onset (and sometimes offset) in each of a small portion of Kenyon cells, a population of neurons known to be crucial for olfactory associative learning. By using a series of odor-taste associative conditioning paradigms with various sucrose presentation timings, I carefully controlled the temporal overlap between Kenyon cell spiking and sucrose reinforcement timing. I found that in paradigms that led to learning, spiking in Kenyon cells ended well before the reinforcement was given. Further, increasing the temporal overlap between Kenyon cell spiking and sucrose reinforcement actually reduced learning efficacy. Therefore, spikes in Kenyon cells are not the neural representation that gets directly reinforced, and Hebbian spike timing–dependent plasticity in Kenyon cells alone cannot underlie this learning.

論文題目： 烟草天蛾嗅覺系統運作及氣味學習的原理研究

學生姓名： 王植櫻

導師姓名： 江紹佳教授，Mark Stopfer

修業學位： 哲學博士

學系： 生物化學

肄業日期： 二零一零年一月

摘要

神經科學研究的其中兩項重要項目，是研究動物如何處理感官刺激，與該刺激如何與其他刺激透過經驗聯繫起來。通常，感官刺激會令位於大腦不同部位的神經細胞產生同步式的振動。因此，這同步式的神經細胞振動可能是大腦處理感官刺激的一個重要階段。由氣味激起的神經細胞的同步式振動已在多種動物中發現， 其中包括哺乳類動物和昆蟲。雖然各種動物的嗅覺系統在細節上有解剖結構的差異，但是不同動物門的動物似乎是用大致一樣的策略來作氣味編碼。在此工作中， 我用烟草天蛾研究了產生嗅覺系統神經細胞同步式振動的的因素，及影響此振動頻率的要素。我發現神經細胞的振動頻率在一個較長的氣味刺激中從~40 赫茲下降至~20 赫茲。這振動頻率的下降與嗅覺受體神經元的淨輸出同時下降，因此， 振動頻率可能取決於嗅覺受體神經元的反應烈度。然而，我發現，氣味濃度的變化對振動頻率的影響不大。結合在活體內記錄的細胞活動和電腦模型的結果，我發現加強氣味濃度增加了對該氣味有反應的嗅覺受體神經元數目。這些嗅覺受體神經元的反應嚴格地受制於適應作用和飽和。我的研究確定了在周邊神經系統，氣味濃度主要是以有反應的嗅覺受體神經元的多少來編碼，而振動頻率則取決於適應作用和飽和。

氣味的神經代表透過經驗與其他感官刺激產生聯繫。動作電位是在訓練過程中直接得到加強的神經代表嗎?在煙草天蛾中我們發現，氣味只在一小部分的凱尼恩細胞(已知是聯想學習中至關重要的細胞)中激起了一個或二個動作電位。這些動作電位通常發生在氣味剛開始的時候，但有時也會發生在氣味剛結束的時候。通過使用一系列的氣味與味覺聯想訓練程序，我仔細地控制了凱尼恩細胞動作電位與蔗糖獎賞在時間上的重疊。我發現在那些可導致學習的訓練程序中，凱尼恩細胞的動作電位早在給予蔗糖獎賞之前結束。此外，增加凱尼恩細胞動作電位與蔗糖獎賞的時間重疊減少了聯想學習的效果。因此，凱尼恩

細胞的動作電位不是直接獲得蔗糖獎賞所強化的神經代表，而且，這種學習不能單靠在凱尼恩細胞中海扁式動作電位時間依賴可塑性作為基礎。

Table of contents

List of Publications

The work during my Ph. D. study led to the following publications:

Ong RC, Stopfer M. Olfactory coding: Unusual conductances contribute to sparse neural representation. Focus on "Intrinsic membrane properties and inhibitory synaptic input of Kenyon cells as mechanisms for sparse coding?", *J Neurophysiol* 103:2-3, 2010.

Ito I, Bazhenov M, Ong RC, Raman B, Stopfer M. Frequency transitions in odor-evoked neural oscillations., *Neuron* 64: 692-706, 2009.

Ito I, Ong RC, Raman B, Stopfer M. Olfactory learning and spike timing dependent plasticity., *Commun Integr Biol* 1:170-171, 2008.

Ito I*, Ong RC*, Raman B, Stopfer M. Sparse odor representation and olfactory learning., *Nat Neurosci* 11: 1177-1184, 2008.

*equal contributions

Ong RC, Stopfer M. Peripheral and central olfactory tuning in a moth. *In preparation.*

List of Abbreviations

AL	Antennal lobe
EAG	Electroantennogram
GPCR	G-protein coupled receptor
ING	Interneuron Network Gamma
ISI	Inter-spike interval (in Chapter 2)
	Inter-stimulus interval (in Chapter 3)
KC	Kenyon cell
LFP	Local field potential
LH	Lateral horn
LHI	Lateral horn interneuron
LN	Local neuron
MB	Mushroom body
OB	Olfactory bulb
OBP	Odorant-binding protein
OR	Olfactory receptor
ORN	Olfactory receptor neuron
PBP	Pheromone-binding proteins
PCT	Picrotoxin
PER	Proboscis extension reflex
PING	Pyramidal-Interneuron Network Gamma
PN	Projection neuron
PSTH	Peri-stimulus time histograms
SL	Lifetime sparseness
SP	Population sparseness
STDP	spike timing–dependent plasticity

List of Figures

1 Introduction

My thesis addresses two important questions in olfaction. Olfactory stimuli elicit oscillatory synchronization in groups of neurons in many species. However, what determines the properties of these oscillations is poorly understood. I found that, in the moth *Manduca sexta*, odor stimuli evoke oscillatory synchronization in the antennal lobe (AL) and mushroom body (MB), much like that found in locusts and *Drosophila*. Combining results from *in vivo* electrophysiological recording and computational models, I found that the frequency of this oscillatory activity is determined by the adaptation and saturation of olfactory receptor neurons (ORNs).

The MBs of insects receive neural input about both odors and food; thus, these structures have long been proposed to be the site where odor-food associative memory forms. Here, I investigated odor-activated spiking in MB intrinsic neurons, the Kenyon cells (KCs). By providing food at different specific times during such spiking, I examined the mechanism that can link odor with food information in the MB. This dissertation begins with an overview of olfaction.

1.1 Overview

1.1.1 The nature of olfaction

Animals perceive the chemical world around them through the chemical senses – olfaction and gustation. Chemosensory neurons react with volatile molecules in the environment without necessarily metabolizing them. This allows for the fast detection and recognition of chemicals that are present, or any changes in concentration of chemicals, allowing prompt behavioral responses. Gustation requires the animal to make direct contact with the source of chemicals, but olfaction detects the sources from a distance. This makes olfaction an excellent modality for animals to navigate, explore, orient, and detect changes in air- or water-borne chemical components in the environment. In fact, olfaction plays crucial roles in almost all animals for survival and reproductive success. Animals use olfaction to locate food sources, find mates and offspring, recognize territories, induce oviposition, and to avoid danger. In humans, interestingly, olfaction is also extremely evocative. Many report it evokes emotions and stimulates the imagination most deeply among all the senses (Dethier, 1994).

Whereas the visual or auditory systems detect stimuli that fall along a single, continuous function of wavelength or frequency, the olfactory system has to recognize discrete molecular structures of odorants. Unlike vision or audition, it's not easy to provide a compact description of the odor world. Odorants vary in molecular size, functional groups, branching patterns, three-dimensional structures, and numerous other physio-chemical features. Thus, olfaction requires an enormous capacity for detection, description, and recognition. This fundamental

difference among the different senses is reflected in the number of receptor genes in the system – in humans, there are only three classes of photoreceptors to absorb light from the whole visual spectrum (Nathans *et al.*, 1986), but there are about 400 olfactory receptor (OR) genes expressed in ORNs. In rodents whose primary sense is olfaction, as many as 1,200 functional OR genes are expressed (for review, see Nei *et al.*, 2008).

For terrestrial animals, odorants are carried by air to reach the olfactory organ. Odorants are typically hydrophobic molecules that weigh between 26 and 300 daltons (Mori and Yoshihara, 1995). One obvious reason for the upper size limit of odorants is that volatility falls rapidly with molecular size, so that heavier molecules are less able to remain in the air and reach the olfactory organs. Another reason may be that the ORs cannot accommodate molecules larger than certain sizes (Turin and Yoshii, 2003).

The dispersion of odorant molecules after being released from the source depends on two simultaneous processes: (1) molecular diffusion – the random, heat-related Brownian motion of molecules, and (2) turbulent diffusion – the transport and scattering of odor molecules caused by uneven movements in the medium carrying the molecules (Murlis *et al.*, 1992). While molecular diffusion is a slow and small-scale phenomenon, turbulent diffusion is vigorous and displays a wide range of spatial and temporal scales depending on the ambient environment. Therefore, turbulent diffusion generally dominates odor plume development in nature (Murlis *et al.*, 1992). With the use of an ionized air tracer, Murlis and Jones (1981) showed that odor molecules released from a point source become organized into a series of discrete packets separated by clean air. As they encounter olfactory organs,

typically, odor packets are 100 ms long and 500 ms apart, but are widely variable in concentrations and durations depending upon environmental factors (Murlis and Jones, 1981). Thus, as animals encounter them, odor traces in the natural environment are usually not continuous but are rather highly intermittent.

1.1.2 The pheromone system

In most animals, the olfactory system really consists of two subsystems that are generally both anatomical and functionally distinct: the pheromone system and the general olfactory system. The pheromone system detects and processes highly species-specific molecules. To describe these molecules, Karlson and Luscher (1959) coined the term 'pheromone' (derived from the Greek *pherein*, which means to transfer; and *hormōn*, which means to excite) to define substances which are secreted to the outside by an individual and received by a second member of the same species, in which they release a specific reaction (Karlson and Luscher, 1959).

Responses to pheromones are instinctual – no learning is required after birth (Hudson, 1985; Moncho-Bogani *et al.*, 2002). Most pheromones cause an immediate behavioral response upon reception, like aggregation, aggression, or courtship behaviors. These pheromones are referred to as releaser pheromones. Another type of pheromone has a physiological effect on the recipient, such as changes in hormone levels, and the effect is often delayed. Exposure to the odor of an unfamiliar male mouse within the first few days after coitus, for example, causes the blockage of ovoimplantation in female mice by inhibiting release of prolactin (Bruce, 1970; Parkes and Bruce, 1962). This type of pheromone is referred to as primer pheromone. Some pheromones, on the other hand, can cause both behavioral and endocrine changes in the recipient (Johnston, 2003).

Reactions to pheromones can be mediated by single pheromone compounds or blends of pheromone compounds. In the case of pheromone blends, a mixture of several chemicals in precise proportions is released. Responses to the blend strictly depend on the proper proportions of the components – if the proportion of the same component chemicals is altered, no response, or much reduced effects can be observed (Linn *et al.*, 1987). Most insect sex pheromones are blends rather than single chemical compounds (Linn and Roelofs, 1989); often, different insect species use the same chemicals in different proportions (Sorensen, 1996). For odors used for individual (Gorman, 1976; Smith *et al.*, 2001) or kin recognition (Gamboa *et al.*, 1996), a 'mosaic signal' containing a large number of compounds is commonly used. In this case, the proportions might vary considerably across individuals (Johnston, 2005).

Extensive studies in mammals and insects have established the importance of pheromones. Pheromones are well-known to influence sexual activities in rodents. Five compounds found in adult male urine are shown to accelerate female puberty (Jemiolo *et al.*, 1989; Novotny *et al.*, 1999). Male urinary proteins are also found to influence estrous cycles in females (Marchlewska-Koj *et al.*, 2000; Morè, 2006). Pheromones in urine from female rodents, on the other hand, signal its ovulation stage and can serve as attractants to males and inducers of sexual activity (Rekwot *et al.*, 2001).

Pheromones also guide innate feeding behavior in mammals. Pheromones from the maternal breast, for example, guide pups searching for nipples for feeding. The nipple-search pheromone plays an especially crucial role in rabbit pup survival, because female rabbits leave their young immediately after giving birth, and only

return to nurse their pups for a few minutes a day (Hudson, 1985). Similar roles of pheromones appear to present in humans also – maternal breast odors are found to elicit preferential head orientation by infants and help guide them to the nipples (Porter and Winberg, 1999). But the possible effects of pheromones on adult humans, who rely relatively little on olfactory cues, are poorly understood and probably minimal (Tirindelli *et al.*, 2009).

Although pheromones are found throughout the animal kingdom, our current knowledge about these chemicals mostly came from research in insects. Honeybees are known to use a wide variety of pheromones to establish efficient communications within the colony. The order of the hive in a colony is strongly determined by pheromones produced by the queen, worker bees, brood and possibly drones. The queen mandibular pheromone secreted by queen honeybee, for example, stimulates the colony to forage, build comb, and to rear larvae (Wright, 2009b). Worker bees responsible for guarding and defense, on the other hand, can present several alarm pheromones that attract other worker and guard bees and make them more aggressive when confronting noxious stimuli or enemies (Breed *et al.*, 2004).

Sex pheromones emitted by female moths can attract males from several kilometers away. Upon detecting a sex pheromone plume, male moths approach the source not directly, but through counterturning: a zigzagging track with successive alternate turns, crossing back and forth through the plume's boundaries (Kanzaki *et al.*, 1992; Willis and Arbas, 1991). Counterturning appears to be a result of a self-generated behavioral program triggered by pheromones. In male moth *Bombyx mori*, a single pulse of pheromone elicits a series of counterturns (Kanzaki *et al.*, 1992). A group of interneurons with descending axons to the thoracic ganglia appears to play

important roles in counterturning by switching their firing rates between high and low firing frequencies. Spiking in these interneurons is correlated with the activity of motor neurons that contribute to the zigzag turning behavior (Kanzaki and Mishima, 1996; Olberg, 1983).

Studies have indicated that the temporal profile of a pheromone plume affects the way moths orient toward the plume source. Male moths do not fly upwind in an airstream uniformly permeated with pheromone, but will fly towards the source of pulses of pheromone (Baker *et al.*, 1985; Kennedy *et al.*, 1980; Kennedy *et al.*, 1981). This behavior is not due to adaptation in pheromone receptor neurons because moths readily responded to a pheromone plume added on top of a background of continuous pheromone stream (Baker *et al.*, 1985; Kennedy *et al.*, 1981). Studies in various species of moths showed that males flew or walked straighter upwind to fast-pulsed plumes than to slow-pulsed plumes (Kanzaki *et al.*, 1992; Mafraneto and Carde, 1994; Vickers and Baker, 1994). Therefore, fluctuations in pheromone concentration in air strongly influence pheromone tracking in male moths.

The pheromone system is generally considered to operate like a labeled-line system, one in which separate, non-interacting pathways connect specific sensory structures with the appropriate response structures. In both insects and mammals, pheromones are detected by highly specific receptors located in the periphery – in the mammalian vomeronasal organ and in the insect antenna. The detected pheromone information is then sent to specialized clusters of neurons in the first olfactory relay where it is processed separately from general odors (Christensen *et al.*, 1995; Sorensen, 1996; for review, see Bigiani *et al.*, 2005; Hildebrand, 1995; Vosshall, 2008). This processing scheme provides fast and precise knowledge about the odor. However,

since a dedicated channel is required for each compound, this system can only serve to detect a few odorants that are crucial for the animal.

My study focuses on the insect general olfactory system. In contrast to the pheromone system, the general olfactory system employs ORs that probe different molecular features of odorants. Thus, each receptor neuron can be activated by a variety of odorants, and each odorant can activate a number of different ORN types. In contrast to the labeled-line system for pheromones, it is the combined activity of all activated ORNs that forms the neural representation of the non-pheromonal odorant. A description of the processing and coding of general, non-pheromonal odors appears later in this chapter.

1.1.3 The general olfactory system

Unlike the highly specific pheromone system, the general olfactory system (referred to as the olfactory system hereafter) detects and processes almost any volatile chemical in the environment. This generality is important to ensure that animals can collect as much information as possible from the surroundings because such information could determine the life or death of the animal. The general nature of this task makes the non-pheromonal olfactory system a good model for exploring how the brain processes information.

The olfactory system is remarkable in that it can detect, recognize, analyze, distinguish, and memorize an enormous number of different odor molecules. It has been estimated that more than 400,000 compounds are odorous to the human olfactory system (Mori and Yoshihara, 1995). Even subtle differences in molecular structure can result in profound changes in the perceived odor. Further, odors in

nature are generally blends of odorants. Most floral scents, for example, consist of tens of chemical compounds released at particular proportions. It is the combined effects of these chemicals that give rise to the unique scent of the flower (Dudareva and Pichersky, 2000). Given the huge number of chemicals that can activate the olfactory system, and the astronomical number of possible combinations of these chemicals, the number of smells we can perceive is almost without limit.

Olfactory neuropils of animals in different phyla have surprisingly similar neuroanatomical structures and physiological responses to odors (Ache and Young, 2005; Benton, 2006; Hildebrand, 1995; Kay and Stopfer, 2006). The olfactory glomeruli, spherical clusters of complex synapses clearly distinguishable from surrounding tissues, are found in animals from invertebrates like insects and crustaceans to vertebrates like fish and mammals (Hildebrand and Shepherd, 1997). In both mammals and insects, there is a tremendous convergence of ORNs onto the glomeruli, and then modest output divergence from the glomeruli to higher brain areas (Hildebrand and Shepherd, 1997). Within the glomeruli, excitatory projection neurons (PNs) and inhibitory local interneurons (LNs) interact with each other and with ORNs. The outcome of these interactions is to create temporally dynamic patterns of activity in the output neurons that consist of bursts of spikes and periods of inhibitions (fish: Friedrich and Laurent, 2001; insects: Ito *et al.*, 2008 - this work, see Chapter 3; Laurent *et al.*, 1996; Stopfer *et al.*, 1997; mammals: Bathellier *et al.*, 2008; Fuentes *et al.*, 2008). Because of the reciprocal interactions with local inhibitory neurons, the spikes of these excitatory output neurons are highly synchronous – these activities can be observed as odor-evoked neural oscillations in a variety of animals (fish: Friedrich and Laurent, 2001; mammals: Eeckman and Freeman, 1990; Kashiwadani *et al.*, 1999; insects: Ito *et al.*, 2009 - this work, see

Chapter 2; Laurent and Davidowitz, 1994; Stopfer *et al.*, 1997).

However, despite these striking similarities, phylogenetic analyses show that these common features are not homologous across phyla (Eisthen2002). It is therefore often proposed that evolution of the olfactory system is convergent, that animals having distinct origins evolved to acquire the same features because there is a unique efficient way to process odors, given common selective pressures such as physiological and chemical constraints (Ache and Young, 2005; Eisthen2002; Strausfeld and Hildebrand, 1999; Vosshall *et al.*, 2000).

1.1.4 Advantages of insects as animal models for the study of olfactory processing

The insect olfactory systems are similar to, but contain fewer total numbers and types of neurons than the vertebrate olfactory system (Benton, 2006; Hildebrand and Shepherd, 1997; Strausfeld and Hildebrand, 1999). Yet, like mammals, insects can perform well in odor-guided and learning behavioral tasks. Thus, the insect olfactory systems present a good model for the study of fundamental principles of olfactory processing and odor-guided behaviors that are common among animals in different phyla. Also, findings in the insect olfactory systems can provide important insights for research on other olfactory systems, and for understanding more general principles of information processing by neurons.

Besides, insect olfactory systems are easily accessible to electrophysiology. Insect ORNs on the antennae are remote from the brain, and external to the animal. Therefore, extracellular recordings from receptor neurons can be done without dissection. The early olfactory processing centers, the ALs and MBs, are on the

dorsal surface of the brain – only minimal surgical exposure of these areas is required to make recordings *in vivo*. These advantages allow the study of olfactory processing in a multi-layer system in almost-intact animals. Anatomical details of the insect olfactory system appear in the next section.

Further, insects are capable of a variety of odor-driven behaviors. Attraction to food odors is common among insects. Without learning, naïve moths *Manduca sexta* approach paper flowers with floral odors added (Raguso, 2002). Odors from bananas and mangos are consistently attractive to different wild-type strains of *Drosophila malenogaster* (Ruebenbauer *et al.*, 2008). Interestingly, whereas carbon dioxide is an attractant to mosquitoes, it is a potent stress odor that evokes robust avoidance behavior in *Drosophila* (Gillies, 1980; Suh *et al.*, 2004). Higher-level behaviors like odor discrimination, and olfactory learning and memory behaviors have also been observed in many insect species (Daly *et al.*, 2001; Davis, 2005; Heisenberg, 2003; Skiri *et al.*, 2005; Stopfer *et al.*, 1997; Wright *et al.*, 2009). Among all insects, honeybees display perhaps the most impressive learning ability. Honeybees can learn to associate an odor with food in just one pairing trial (Bitterman *et al.*, 1983), and can differentiate odors differing in length by a single carbon (Stopfer *et al.*, 1997). These capabilities allow the study of neural basis of complex behaviors in insects.

Finally, genetic tools are now available in some insect species. The whole genome sequences of several insects are now available (e.g. the fruit fly *Drosophila melanogaster* (Adams *et al.*, 2000), the silkmoth *Bombyx mori* (Xia *et al.*, 2008) and the honeybee *Apis mellifera* (Weinstock *et al.*, 2006). Among these, a variety of tools has been developed for measuring and manipulating neural activity in

Drosophila (for review, see Luo *et al.*, 2008; Olsen and Wilson, 2008). Expression of GFP, a fluorescent protein, in a known, genetically tagged population of neurons guides experimenters to the desired cell type for intracellular recordings. Neural activity can be monitored in neurons expressing a genetically-encoded fluorescent activity reporter in restricted population of neurons (Jayaraman and Laurent, 2007). Further, expression of channelrhodopsin in neurons allows temporally well-controlled activation of selected neurons by light (Zhang *et al.*, 2007a). By raising the ambient temperature by a few degrees, neurons can be reversibly silenced by blocking neurotransmitter release (Kitamoto *et al.*, 2002). With the use of these tools and others, there have been tremendous advances in understanding insect learning and memory mechanisms in recent years (for review, see Davis, 2005; Heisenberg, 2003). Taken together, such fundamental information necessary for genetic manipulations allows sophisticated functional studies in insects.

1.2 Anatomy and physiological responses of the insect olfactory system

In insects, processing of odorants begins mainly in the antenna, a structure composed of three parts – the basal scapus, the pedicellus, and the flagellum. The basal scapus and the pedicellus are the first two segments from the proximal end, and contain surface mechanoreceptors that project to dorsal neuropils of the deutocerebrum (Lee and Strausfeld, 1990). The flagellum, on the other hand, carries mostly chemoreceptors, although receptors sensing other modalities like humidity and temperature are also found there (Altner *et al.*, 1981; Lee and Strausfeld, 1990; Nishikawa *et al.*, 1995; Tichy and Loftus, 1990; Zimmermann, 1991). Receptor neurons are housed in spine-like structures called sensilla. Sensilla are small, porous, cuticular encasements that typically contain a few ORNs and accessory cells that are bathed in sensillum lymph (Lee and Strausfeld, 1990; Shields and Hildebrand, 2001; Steinbrecht, 1998).

In moths and many other insects, the flagellum is sexually dimorphic. In the moth *Manduca setxa*, for example, the male flagellar segments are keyhole-shaped in cross-section, whereas female flagellar segments are oval or circular. The additional surface area in the male antennae is occupied by sensilla containing pheromone receptor neurons (Vosshall, 2008). In insects, ORNs can also be found in the mouth part, the maxillary pulp, as well.

1.2.1 Odorant-binding proteins

Most of the protein components of nasal mucus in mammals and the sensillum lymph

in insects are odorant-binding proteins (OBPs) (Pelosi, 1994; Vogt and Riddiford, 1981). OBPs were first discovered in the moth (Vogt and Riddiford, 1981) and then in the cow (Pelosi *et al.*, 1982) with the use of ligand-binding assays. Insect OBPs are small globular proteins of about 135 to 220 amino acids, and are characterized by a specific domain made of six α-helices linked by three disulphide bonds (Leal *et al.*, 1999; Scaloni *et al.*, 1999). OBPs are synthesized by accessory cells in the sensilla and are then secreted to the sensilla lymph.

The existence of OBPs in both vertebrates and invertebrates suggests an evolutionary convergent adaptation. In both, OBPs appear to play crucial roles in olfactory processing. However, despite more than two decades of research, the precise functions of OBPs remain poorly understood. By far, most of our understanding of insect OBPs came from studies of pheromone-binding proteins (PBPs). Odorant molecules need to dissolve in and move through the aqueous sensilla lymph in order to reach the receptor dendrites. For large and highly hydrophobic molecules like pheromones, this process would be very inefficient. It has therefore been proposed that OBPs bind to and transport these hydrophobic molecules to the receptor neurons (Sánchez-Gracia *et al.*, 2009; Steinbrecht, 1998). In support of this, Van den Berg and Ziegelberger (1991) showed, with electrophysiological recordings from the perfused sensilla of a moth, that PBPs can solubilize pheromones, reduce the concentration threshold required to activate receptor neurons, and that the PBP-pheromone complex is capable of activating receptor neurons (Berg and Ziegelberger, 1991).

Another potential function of OBPs is to perform an initial screening for molecules, regulating those that can activate ORNs located in the same sensillum. Multiple

OBPs have been found in a single species (in insect: Maida *et al.*, 1997; Maida *et al.*, 2005; McKenna *et al.*, 1994; Pikielny *et al.*, 1994; in mammals: Felicioli *et al.*, 1993; Garibotti *et al.*, 1997; Pes and Pelosi, 1995), and the expression of OBPs appears to correlate with different types of sensilla (Shanbhag *et al.*, 2001; Vogt *et al.*, 1991). Binding assays showed that different OBPs bind selectively to different odorants (Prestwich *et al.*, 1995). Two PBPs from the same species of moth, for example, showed opposite preferences to two pheromone blend constituents (Du and Prestwich, 1995). Moreover, anti-sera against the PBPs of one moth species showed cross-reactivity towards the lymph from sensilla that are tuned to the same pheromone in other moth species (Steinbrecht, 1996). These results are consistent with a role for OBPs as initial filters that influence the types of odorants that can reach ORs.

OBPs may also act as deactivators of odorants. These two possible roles of OBPs – as transporters and deactivators of stimulant molecules – may at first seem to be in conflict. However, Ziegelberger observed that PBPs in a moth can exist in two forms, one reduced and one oxidized, differing only in the number of disulphide bridges (Ziegelberger, 1995). Kinetic experiments showed that pheromone molecules first bind to the reduced form of PBP. After activating the receptor, the receptor catalyzes the redox shift in PBPs and the resulting oxidized PBP-odorant complex is no longer able to activate the receptor (Kaissling, 1998; Ziegelberger, 1995). This limits the duration of activation of receptor neurons and contributes to sensory adaptation.

Other proteins, including the odorant degrading enzyme, esterases, and the transmembrane protein SNMP, are also found in the peri-receptor space. The

functional roles of these proteins, however, remain unclear.

1.2.2 Olfactory receptors

The very first step of the olfactory system toward odor recognition is to detect and discriminate the tens of thousands of odorants in the environment. The OR repertoire of an animal determines the range of odorants it can process. However, the molecular basis of odorant recognition remained speculative until Buck and Axel cloned the OR multigene family in mouse in 1991 (Buck and Axel, 1991).

Buck and Axel screened the RNAs expressed in the mouse olfactory epithelium based on the assumptions that ORs are likely to belong to the seven-transmembrane domain superfamily characteristic of many types of biological receptors, and that, from the large variety of odorants that ORs can recognize, ORs themselves should exhibit significant diversity and thus be encoded by a large multigene family (Buck and Axel, 1991). This work opened new avenues of research for understanding the molecular recognition of odorants. Because of this ground-breaking work, Buck and Axel were awarded the Nobel Prize in Physiology or Medicine in 2004.

The OR multigene family constitutes the largest gene family in the genome. In human, it comprises about three percent of the genome. The number of functional OR genes varies extensively among vertebrate and insect species. To date, 1391 OR genes have been discovered in mouse, among which 328 are pseudogenes. In human, about 800 OR genes have been found, but more than half are pseudogenes (Nei *et al.*, 2008). Among mammals, the gene-to-pseudogene ratio is lowest in human, higher in other primates, and highest in mouse and rat. This may reflect that olfaction plays a more crucial role for survival in rodents than in human

(Olender *et al.*, 2008), and the relatively lesser requirement for olfaction in primates (Gilad *et al.*, 2004). The number of OR genes is much smaller in insects. By far, the largest number OR genes was found in the red flour beetle *Tribolium castaneum* (Abdel-Latief, 2007; Engsontia *et al.*, 2008), which expresses as many as 163 OR genes (Robertson and Wanner, 2006). The variation in OR gene number among species appears to reflect evolutionary specialization for different environmental habitats (for review, see Nei *et al.*, 2008).

The first insect OR gene superfamily was discovered in *Drosophila* by two separate groups of American scientists (Gao and Chess, 1999; Vosshall *et al.*, 1999). Because of the availability of powerful genetic manipulations in *Drosophila*, by far, the most comprehensive information about insect ORs came from studies in this species. In *Drosophila*, there are 60 functional OR genes. Two of these genes undergo alternative splicing, thus there are 62 OR types in total (Robertson *et al.*, 2003). On the antenna, different OR genes are expressed in different regions along the proximal-distal and dorsal-ventral axes (Vosshall *et al.*, 1999).

While each mammalian ORN expresses a single OR, each *Drosophila* ORN expresses two ORs: a divergent, conventional OR, and a highly conserved OR encoded by the gene *Or83b* (Jones *et al.*, 2005; Krieger *et al.*, 2003; Larsson *et al.*, 2004). The co-expression of a highly conserved receptor subunit appears to be ubiquitous in insects – *Or83b* orthologs have been found in other insects like other flies, mosquitoes, moths, honeybees and beetles (Krieger *et al.*, 2003; Melo *et al.*, 2004; Pitts *et al.*, 2004).

Although neurons expressing OR83b alone do not respond to any of a large panel of odors (Elmore *et al.*, 2003), genetically deleting *Or83b* disrupted

electrophysiological and behavioral responses to odors (Larsson *et al.*, 2004). In the absence of odor stimuli, ORNs in mutant flies lacking OR83b showed very little spontaneous activity. *Or83b* mutants produced no odor-evoked responses to stimuli with general odors in electroantennogram recordings (a recording technique that measures summed ORN activities), or in recordings from an indentified sensillum known to be responsive to these odorants. Further, *Or83b* mutation also caused severe impairments in odor-mediated behaviors in larval and adult flies (Larsson *et al.*, 2004).

In the same study, Larsson and colleagues (2004) also found that OR83b helps localize conventional ORs to the dendritic end of receptor neurons. With biochemical assays, OR83b was found to dimerize with conventional ORs (Neuhaus *et al.*, 2005). Heterologous expression of the conventional OR, OR43a, showed a thousand-fold increase in ligand sensitivity when it was co-expressed with OR83b (Neuhaus *et al.*, 2005). Later, Benton and colleagues (2006) showed that OR83b heterodimerizes with conventional ORs early in the endomembrane system in ORNs. This complex then couples to the conserved ciliary tracfficking pathway, and is transported to the dendritic ends of ORNs. The same study also showed that genetically turning off OR83b expression after flies reached adulthood caused a progressive decline in the amount of conventional OR in the cilia. Therefore, the OR-OR83b heterodimer is critical for both localization and maintenance of ORs in the sensory cilia (Benton *et al.*, 2006).

Proteins in the insect OR superfamily have seven-transmembrane domains and consist of about four hundred amino acids (Abdel-Latief, 2007; Hill *et al.*, 2002; Krieger *et al.*, 2002; Vosshall *et al.*, 1999). Although it has been widely assumed

that insect ORs, like vertebrate ORs, belong to the G-protein coupled receptor (GPCR) superfamily (Clyne *et al.*, 1999; Gao and Chess, 1999; Vosshall *et al.*, 1999), insect ORs are actually evolutionarily unrelated to either mammalian ORs or any other known GPCRs (Benton, 2006). In fact, experimental investigations revealed that *Drosophila* ORs adopt a membrane topology quite different from GPCRs – the N-terminus of the *Drosophila* OR is located in the cytoplasmic side of the plasma membrane, and OR83b associates with conventional ORs through conserved loops on the cytoplasmic side (Benton *et al.*, 2006; Lundin *et al.*, 2007). Thus, relative to the vertebrate version, they are partly inside-out.

The signal transduction mechanism in insect ORs has been controversial for years. Various second messengers like inositol triphosphate, diacylglycerol, cGMP, and calcium have been found to participate in OR signal transduction (Kaissling, 1996; Martin *et al.*, 2001; Zufall *et al.*, 1991; Zufall and Hatt, 1991). However, there has been no strong evidence to show that any of the tested second messengers are necessary for OR signal transduction (for review, see Touhara and Vosshall, 2009). Several recent studies showed that, unlike the classic vertebrate classic GPCRs, the heterodimeric insect ORs, in fact, comprise a new class of ligand-activated non-selective cation channels (Nakagawa *et al.*, 2005; Sato *et al.*, 2008; Wicher *et al.*, 2008). When expressed in heterologous systems, binding of odorant ligand to insect OR complexes induced non-selective cation currents that lead to increase in intracellular calcium (Nakagawa *et al.*, 2005; Sato *et al.*, 2008; Wicher *et al.*, 2008). Further, outside-out patch-clamp recordings showed direct evidence that the OR heterodimer forms odorant-gated ion channels (Sato *et al.*, 2008).

On the other hand, Wicher and colleagues (2008) also observed that, besides a fast

transient current, odor application also leads to a slowly activating and slowly decaying current that is ATP- and GTP-dependent. Expression of OR83b alone results in functional ion channels that are not only directly responsive to odorants, but can also be activated by intracellular cAMP or cGMP. Thus, these authors concluded that insect odorant receptors form both ligand-gated ion channels and cyclic-nucleotide-activated non-selective cation channels (Wicher *et al.*, 2008). However, Sato and colleagues did not detect increases in intracellular cAMP upon ligand stimulation (Sato *et al.*, 2008). Therefore, there is still controversy regarding the role of cyclic nucleotide cascades in OR signal transduction. In spite of this, the consensus appears to be that insect ORs represent a distinct type of ligand-gated ion channel among proteins in the seven-transmembrane domain superfamily. This distinct type of signaling mechanism in insects may have evolved because of the need for fast olfactory responses in flying insects, because insect ORs consistently respond faster (within 18-28 ms) then vertebrate ORs (50-200 ms) to olfactory stimuli (Sato *et al.*, 2008).

The molecular features of odorants that ORs recognize remained elusive. Araneda and colleagues conducted a rigorous investigation of the tuning profile of the rat I7 odor receptor (Araneda *et al.*, 2000). By presenting octyl aldehyde, a potent ligand of the I7 receptor, and many other chemically related ligands to animals overexpressing this receptor in the olfactory epithelium, the authors found that the I7 odor receptor was highly specific for an aldehyde group, and has strict steric requirements around the carbonyl group. The I7 receptor, however, was rather tolerant to the aliphatic tail of the odor molecule (Araneda *et al.*, 2000). This work suggested ORNs respond best when activated by odorant molecules that physically fit well within their binding pockets. In *Drosophila*, using a mutant antennal

neuron that lacks endogeneous ORs (Dobritsa *et al.*, 2003), Hallem and Carlson conducted a comprehensive study of the molecular tuning of all OR types expressed in the antennae (Hallem and Carlson, 2006). In separate experiments, the researchers expressed each one of the different OR types in that "empty neuron," and recorded the responses of these neurons to over a hundred odors. They found that the firing rate of the ORN depends on the chemical class of the odor, and that the receptive range of the ORN population forms a continuum from narrowly tuned to broadly tuned. The experimenters projected the receptors' responses into multidimensional analysis space for visualization. They showed that odors of particular chemical classes often cluster together. However, a cluster never included all odorants of the same chemical class. Therefore, the chemical class is one feature, but not the only feature that determines an ORN's responses (Hallem and Carlson, 2006).

Recent computational studies that use numerous molecular descriptors to quantify physiochemical features of odorants showed some degree of success in predicting neural responses to odors *in vivo*. However, the predictive power of an individual set of molecular descriptors varies among OR types and across studies (Haddad *et al.*, 2008; Schmuker *et al.*, 2007). Taken together, ORs do not appear to rely on one or a few simple chemical features to recognize odorants. Considering the large variety of odorants present, each OR type likely detects a different aspect of the odorant chemical space.

Electrophysiological studies of responses of ORNs to odorants revealed several features of olfactory coding in ORNs. Spiking responses of ORNs showed dynamic changes in firing rates over the course of a stimulus. Also, an individual ORN

could respond in an excitatory or inhibitory fashion, depending on the stimulus odorant (de Bruyne *et al.*, 1999; de Bruyne *et al.*, 2001; Duchamp-Viret *et al.*, 2000; Hallem *et al.*, 2004; Shields and Hildebrand, 2000). Such patterning of action potential timing depended both on the chemical identity of the stimulus odorant, and on the odorant's concentration (de Bruyne *et al.*, 1999; Duchamp-Viret *et al.*, 2000; Heinbockel and Kaissling, 1996; Ito *et al.*, 2009 - this work, see Chapter 2). Further, ORNs showed a wide range of tuning breadth and spectra, and odorants varied widely in the number of receptors they could activate (de Bruyne *et al.*, 2001; Hallem *et al.*, 2004; Hallen2006; Ito *et al.*, 2009 - this work, see Chapter 2; Malnic *et al.*, 1999; Shields and Hildebrand, 2000). Therefore, each odorant activates many different types of ORNs, and different odorants activate overlapping sets of ORNs. So, odors appear to be encoded by the combination of ORNs that they activate, and the firing patterns that they elicit in these ORNs.

1.2.3 Antennal lobe

When presented with odorants, ORNs that detect those molecules send patterns of action potentials along their axons to the AL, the first olfactory relay center in insects, or the olfactory bulb (OB), the mammalian structural and functional analogue of the AL. In most insects, ORN axons terminate in glomeruli in the ipsilateral AL (Tolbert and Hildebrand, 1981; Figure 1.1). A well-known exception to this organization feature is that some fly ORNs send their axons bilaterally to glomeruli in both ALs (Stocker, 1994).

Glomeruli are distinct synapse-dense structures in the AL and OB in which multiple types of neurons interact with each other, in both excitatory and inhibitory fashions. In insects, glomeruli are formed by ORN axons, neurites of PNs, LNs, and some

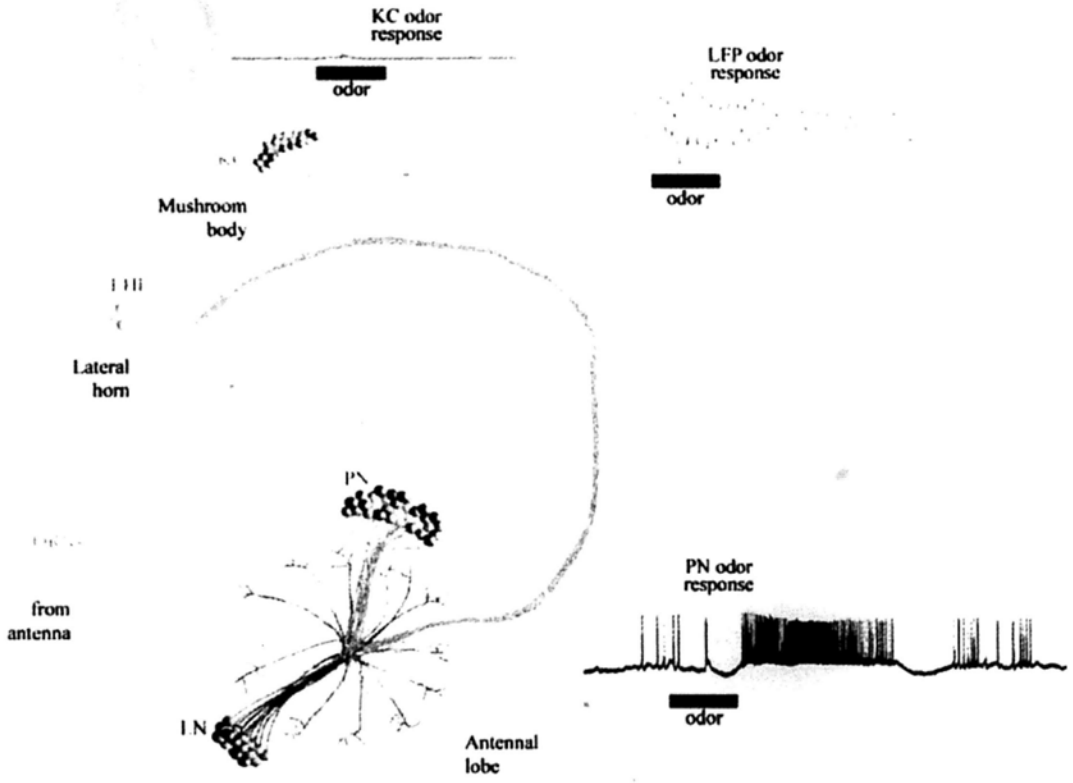

Figure 1.1. Schematic diagram of the insect olfactory system.

centrifugal neurons, together with the synapses among these neurons (Boeckh *et al.*, 1987; Boeckh and Tolvert, 1993; Homberg *et al.*, 1988; Homberg *et al.*, 1989; Tolbert and Hildebrand, 1981). In the moth *Manduca sexta*, the AL houses about 820 PNs and 360 LNs (Homberg *et al.*, 1988). The AL of the honeybee *Apis mellifera* contains 1000 PNs and 750 LNs. Centrifugal neurons that send axons to the AL are not well characterized in any insect species. In *Manduca*, many of these centrifugal neurons have dendritic arborizations in higher olfactory processing centers; therefore, these neurons may send feedback signals to influence olfactory processing in the AL.

Axons of ORNs expressing the same OR converge onto the same glomeruli in the AL

(Bhalerao *et al.*, 2003; Couto *et al.*, 2005; Fishilevich and Vosshall, 2005; Gao *et al.*, 2000; Vosshall *et al.*, 2000), or the OB (Ressler *et al.*, 1994; Vassar *et al.*, 1994). Thus, odor information in each ORN type is channeled to individual glomeruli, generating a spatial representation of ORN activity in the AL and OB.

Odor-evoked patterns of glomerular activation have been observed in diverse animals. With the use of the 2-deoxyglucose uptake method, Gordon Shepherd's group first demonstrated, in rats, that stimulation with different odorants caused activation of different, but overlapping subsets of glomeruli (Sharp *et al.*, 1975; Stewart *et al.*, 1979), and that the extent and density of glomerular activation was greatest with the highest odor concentrations (Stewart *et al.*, 1979). Later, intrinsic signal optical imaging in rats (Rubin and Katz, 1999) and in mice (Belluscio and Katz, 2001) confirmed these findings, and further showed that the odor-evoked activation patterns are bilaterally symmetrical, and are similar across individuals in the same species. In fact, Soucy and colleagues showed, in both rats and mice, that glomeruli having the same odor response profile to hundreds of odors (and thus likely be innervated by the same OR types) are precisely positioned in each OB of a given animal, and across individual animals in the same species (Soucy *et al.*, 2009).

Similar results have been obtained from insects. Calcium imaging in honeybees showed that odors evoked specific, spatio-temporal excitation patterns in the AL (Joerges *et al.*, 1997). Patterns of glomerular activation were similar over repeated presentations of the same odor, but were distinct when stimulated with different odors (Joerges *et al.*, 1997). These activity patterns were bilaterally symmetrical (Galizia *et al.*, 1998), and were highly conserved across individuals (Galizia *et al.*, 1999). Further, in honeybees (Sachse and Galizia, 2003), moths (Skiri *et al.*, 2004)

and flies (Wang *et al.*, 2003), increases in odor concentration resulted in stronger activation of individual glomeruli, and recruited more glomeruli to respond.

Patterns of glomerular activation appear to change over the course of a stimulus. With the use of a calcium-sensitive dye, Spors and colleagues revealed that responses in individual glomeruli in the mouse OB vary over time, with different response latencies and rise times (Spors *et al.*, 2006). However, imaging techniques using intrinsic signals or activity reporter dyes typically have low temporal resolutions (tens of milliseconds or longer) compared to electrophysiological recording techniques (Reiff *et al.*, 2005; Shariff *et al.*, 2006). Therefore, the fine temporal profile of odor-evoked glomerular activation remained unclear.

The subsets of glomeruli that were activated appeared to correlate with chemical features of odorants that were delivered. Two separate studies in flies and moths revealed that compounds in the same chemical class typically activated the same clusters of glomeruli. The glomerular maps activated by odors from one chemical class were different, but partly overlapped with those activated by odorants belonging to other chemical classes (Hansson *et al.*, 2003; Rodrigues, 1988). However, interestingly, Sachse and colleagues reported that, in honeybees, glomerular receptive field mainly depended on carbon chain lengths rather than functional groups (Sachse *et al.*, 1999).

Uchida and colleagues tested the relationship between structural features of odorants and spatial distribution of the activated glomeruli in rats. They found that the dorsal OB responds preferentially to fatty acids and aliphatic aldehydes, and that variations within each group of chemicals, such as differences in carbon chain length or branching pattern, are represented by local differences in activation patterns (Uchida

et al., 2000). They concluded that odorant representation depends on two aspects of molecular features of the odorant – primary features like functional groups characterize each domain, and secondary features like carbon chain lengths and branching are represented by local positions in each domain (Uchida *et al.*, 2000). Consistent with this finding, Belluscio and colleagues showed that, in mice, representations of aliphatic aldehydes with different carbon chain lengths vary systematically along a rostral-caudal axis of the dorsal OB, supporting the presence of a rough chemotopic map primarily based on the functional groups of chemicals (Belluscio and Katz, 2001). However, the specific locations of domains activated by an odorant are likely to be unique to the species (Johnson *et al.*, 2009). It is important to note, though, that a method has never been shown to predict the locations of activated glomeruli when given the chemical structure of an odorant. The relationship between an odorant's structure and the location of glomeruli that respond to it is incompletely understood and may not be simple.

Within the OB or AL, the ORN-specific channels interact extensively. In the insect, ORNs terminating in glomeruli of the AL form excitatory, cholinergic synapses onto PNs and LNs (Distler and Boeckh, 1997; Distler and Boeckh, 1997a; Homberg *et al.*, 1995; Yasuyama *et al.*, 2003). Upon activation by ORNs, cholinergic PNs further excite LNs within the same glomeruli; in turn, inhibitory, GABAergic LNs form reciprocal synapses onto PNs, as well as other LNs (Distler and Boeckh, 1997; Distler and Boeckh, 1997a; Leitch and Laurent, 1996; Olsen and Wilson, 2008a). The multiglomerular LN-LN interactions create a channel of crosstalk among glomeruli which shape the odor responses of PNs (Olsen and Wilson, 2008a). Although the LN population has long been regarded as purely inhibitory, a population of excitatory LN was discovered recently in flies (Shang *et al.*, 2007);

excitatory LNs may exist in other insect species, too.

In the AL, PNs are the only known output neurons, carrying odor information to downstream processing centers. Morphologies of PNs in the AL vary among insect species. Whereas PNs in fruit flies are mostly uniglomerular, innervating a single glomerulus (Stocker *et al.*, 1990), PNs in locusts are all multiglomerular, innervating 10-20 glomeruli each (Ernst *et al.*, 1977; Farivar, 2005; Ignell *et al.*, 2001). In bees (Fonta *et al.*, 1993), moths (Homberg *et al.*, 1988; Ito *et al.*, 2008 - this work, see Chapter 3; Kanzaki *et al.*, 1989) and cockroaches (Strausfeld and Li, 1999), both uniglomerular and multiglomerular PNs are found.

Electrophysiological recordings of PNs allow examination of their responses to odors with a fine temporal resolution and provide clues about how PNs convey information about odorants. PN odor responses display temporal structures at two timescales – a slower, temporally varying pattern of PN spiking activity, and a faster, periodic synchronization of PN spikes, causing local field potential (LFP) oscillations in the AL and MB (Figure 1.1). When stimulated with odor, PNs typically show temporally complex activities that contain both excitatory and inhibitory components, together with periods of quiescence (Figure 1.2A and B). Durations of excitations and inhibitions in PNs are highly variable – odors can elicit bursts of spikes or periods of inhibitions in PNs that last from tens of milliseconds to seconds. Such slow temporal patternings of the odor response of PNs are consistent over repeated exposures to the same odor, different when exposed to another odor or different concentrations of the same odor, and different among individual PNs (Ito *et al.*, 2008 - this work, see Chapter 3; Laurent *et al.*, 1996; Stopfer *et al.*, 2003). Thus, these firing patterns contain information about the odor. Similar temporal dynamics have

also been observed in mitral cells in the OB (Bathellier *et al.*, 2008; Fuentes *et al.*, 2008), although the responses of mitral cells, constrained by the respiratory cycle of vertebrates, are typically less elaborate than those of insect PNs.

The slow temporal patterning in PNs appears to arise mainly from two sources – the activation of slow, $GABA_B$-like receptors on PNs by LNs (Bazhenov, *et al.*, 2001; Macleod and Laurent, 1996; Wilson and Laurent, 2005), and the temporally structured odor response in ORNs (de Bruyne *et al.*, 2001; Hallem and Carlson, 2006; Raman *et al.*, submitted). The population of responsive PNs thus forms a series of spatial activity maps that temporally evolves over the course of the stimulus, producing a spatiotemporal neural representation that is conveyed to higher order olfactory centers.

To analyze odor representations in the PN population, their responses can be projected as trajectories in high dimensional analysis space (Stopfer *et al.*, 2003; Figure 1.2C). These trajectories reveal PN population dynamics that typically consists of three phases – a dynamic transient at the odor pulse's onset, a relatively static fixed point, and a dynamic offset transient at the odor pulse's offset (Mazor and Laurent, 2005). This indicates that individual PNs typically respond to odor with dynamic changes in firing rates at odor onset, settle in a relatively static phase after a few hundreds of milliseconds, and then go through another period of rapid increase or decrease in firing rates after odor is removed. Analysis with simple classification algorithms confirmed that spatiotemporal patterns of PN activity can be used to successfully identify different odors, odor concentrations, and odor timings with optimal stimulus separation during the onset and offset transients (Brown *et al.*, 2005; Ito *et al.*, 2008 - this work, see Chapter 3; Mazor and Laurent, 2005; Stopfer *et al.*,

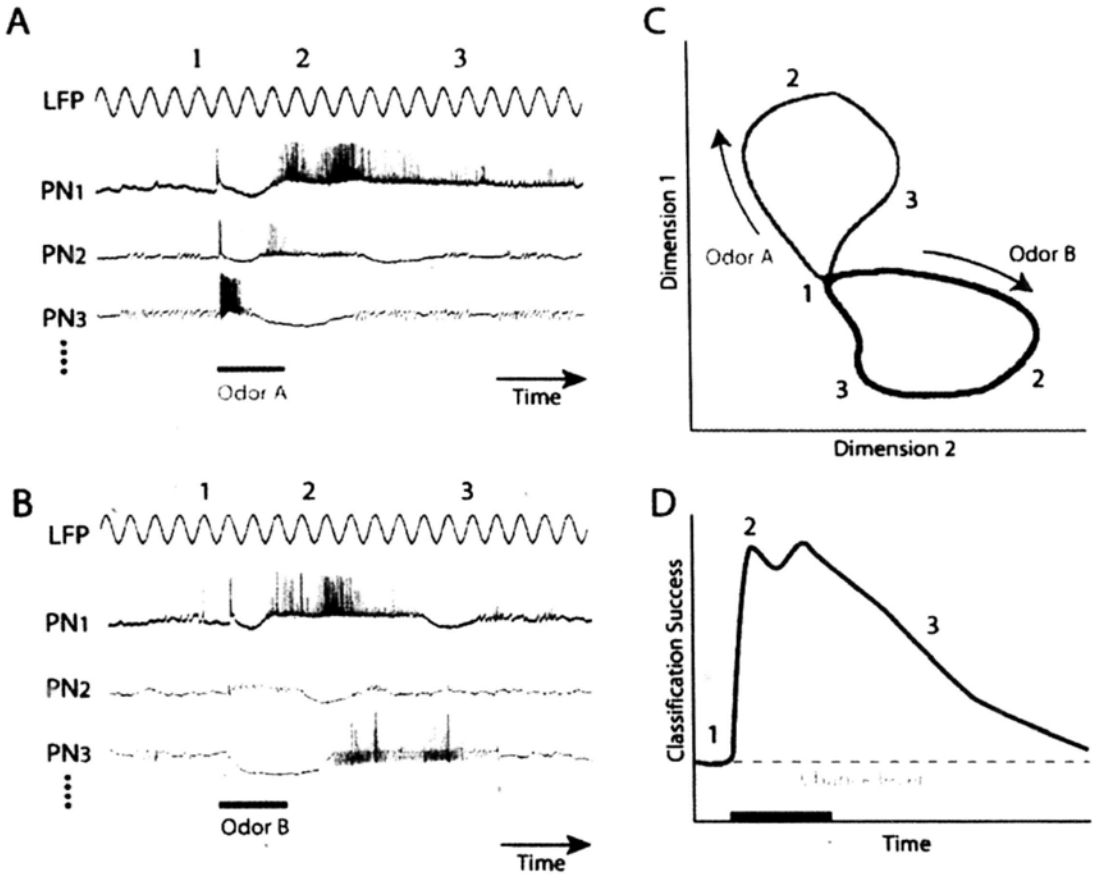

Figure 1.2. Evolution of odor-evoked PN activities.
(A) Odor presentation evokes complex spatial-temporal patterns in PNs, containing excitatory and inhibitory components. Different PNs responded differently to the same odor. Odor presentation timing is indicated by the green bar. (B) The same PNs in (A) responded differently to another odor (blue bar). (C) PN activities can be visualized by dividing the activity of a PN ensemble into a series of points, each point representing PN ensemble firing within a time bin. A trajectory can be formed for each odor-PN ensemble combination by joining each these points (green trace). Over time, the trajectory moves away from the start position (position 1), reaches to a point that is clearly distinguishable from the start position (position 2), and then back to the start position, along a different route, when odor is removed (position 3). For the same PN ensemble, a different trajectory is formed when stimulated with a different odor (blue trace). (D) The difference between the PN ensemble firing patterns can be used to classify odors. Classification is most successful immediately after odor onset and offset, when the PN ensemble responses evoked by different odors are most different. Modified from Kay and Stopfer, 2006.

2003; Figure 1.2D).

On a faster time scale, the reciprocal, excitatory-inhibitory interactions between PNs and LNs cause PNs to fire synchronously. Such synchronous activity can be detected in the AL and MB as 15-20 Hz LFP oscillations in locusts (Laurent and Davidowitz, 1994), and as 20-40 Hz LFP oscillations in moths (Ito *et al.*, 2008 - this work, see Chapter 3). These LFP oscillations are thought to be generated by excitatory and inhibitory pre-synaptic potentials.

In any given oscillation cycle, only a portion of the responding PNs are active. Among the spikes of these active PNs, only a portion fire synchronously at a particular phase relative to the LFP oscillations (Laurent and Davidowitz, 1994). Thus, synchrony between any two PNs is transient, and odor-specific (Wehr and Laurent, 1996). The ensemble of active, synchronous PNs is updated in each oscillatory cycle, and evolves throughout the course of odor stimulation (Laurent *et al.*, 1996). Thus, the evolving maps of PN activity evolve at the rate of the oscillatory cycle. In locusts and moths a new map appears about every 50 ms.

Application of picrotoxin, a specific $GABA_A$ receptor antagonist, within the AL, has been shown to selectively block fast inhibition between LNs and PNs. Picrotoxin injected into the AL abolished synchronization among PNs, and eliminated LFP oscillations in the AL and MB, confirming that oscillatory activities recorded in the MB calyx are primarily caused by synchronized PN activities that arise in the AL (Ito *et al.*, 2009 - this work, see Chapter 2; Macleod and Laurent, 1996). Picrotoxin, however, did not affect the slow temporal patterning of PN odor responses (Macleod and Laurent, 1996; Stopfer *et al.*, 1997), which are mediated in part by $GABA_B$-type receptors.

Oscillatory synchronization in the olfactory network was first observed in the hedgehog by Adrian (1942), and has since been found in mollusks (Gelperin and Tank, 1990), insects (Ito *et al.*, 2009 - this work, see Chapter 2; Laurent and Davidowitz, 1994; Stopfer *et al.*, 1997), fish (Friedrich and Laurent, 2001; Satou, 1990), crustaceans (Sandeman and Sandeman, 1998), rodents (Neville and Haberly, 2003), and primates (Hughes and Mazurowski, 1962), providing further evidence for the use of a similar strategy across species to process odor information. The functional significance of oscillations was tested in honeybees, using an odor discrimination task. Picrotoxin injected, desynchronized honeybees can readily distinguish odorants with very different odorant structures. However, these treated honeybees could not distinguish structurally similar odorants, a task that is well-performed in the control group of bees injected with saline (Stopfer *et al.*, 1997). In locusts, desynchronization of PNs by picrotoxin injection caused degradation of odor specificity in β-lobe neurons, a type of MB extrinsic neurons that read KC outputs (MacLeod *et al.*, 1998). Thus, oscillatory synchronization of olfactory neurons is functionally relevant, and essential for fine odor discrimination.

1.2.4 Mushroom body

The MB receives direct olfactory inputs from PNs. KCs, the intrinsic neurons of the MB, extend dendritic arbors into the MB calyx, the input region of the MB, where they receive synaptic inputs from PN axon terminals. The number of KCs can range from thousands to hundreds of thousands, depending on the insect species (Farris and Sinakevitch, 2003). In locusts, for example, there are about 50,000 KCs in each of the bilateral MBs. In locusts, surprisingly, although KCs greatly outnumber PNs, each KC is connected to about half of the PNs, so each KC receives

inputs from about 400 PNs (Jortner *et al.*, 2007). In addition to olfactory inputs, the calyx appears to receive inputs from visual, auditory, and mechanosensory systems as well (Groneberg, 2001; Strausfeld and Li, 1999). Consistent with receiving such diverse input, the MB has long been found to participate in olfactory learning and memory (Erber, 1980; Heisenberg *et al.*, 1985), and in other higher brain functions like sensory integration (Li 1997; Li and Strausfeld, 1999; Mizunami *et al.*, 1998), place memory (Mizunami *et al.*, 1998) and decision making (Zhang *et al.*, 2007).

Axons of KCs run along the pedunculus and terminate in the lobes of the MB, where they synapse onto the MB's extrinsic neurons. Although KC neurites in the pedunculus and lobes are generally referred to as axons, evidence exists that they actually receive inputs from other protocerebral neurons, MB extrinsic neurons, and other KCs (Li and Strausfeld, 1997; Strausfeld, 2002; Farris, 2005). There are two main classes of KCs, classified according to their branching patterns in the lobes. Class I KCs comprise the largest population of KCs. Class I KCs form dendritic trees in small regions in the calyx, and bifurcate to supply the ventral (or "α") and medial (or "β") lobes of the MB. Class II KCs are also called the "clawed" or "γ" KCs, as they form distinct claw-shaped dendritic terminals that sample all regions of the calyx, and their axons form the "γ" lobe of the MB (Farris, 2005). Each KC receives input from various combinations of PNs that represent different glomeruli (Tanaka *et al.*, 2004).

In the lobes of the MB, KCs synapse onto MB extrinsic neurons. Various types of MB extrinsic neurons showing distinct patterns of branching and physiological responses have been found. Many of these neurons respond to stimuli of more than one sensory modality, and therefore likely integrate multi-modal inputs (Li and

Strausfeld, 1997). A distinct class of MB extrinsic neuron with innervations in the MB calyx and the pedunculus has been found. Some of these neurons are GABAergic and thus may mediate feedback to the calyx (Li and Strausfeld, 1999).

Besides receiving excitatory inputs from PNs, KC dendrites in the MB calyx also receive dense GABAergic innervations from other protocerebral neurons. One main source of these inhibitory inputs to KCs is the lateral horn interneurons (LHIs). Several lines of evidence suggest that the lateral horn (LH) is involved in innate olfactory behaviors (Datta *et al.*, 2008; Heimbeck *et al.*, 2001; Jefferis *et al.*, 2007). Jefferis and colleagues conducted a detailed anatomical study of the projection patterns of PNs into the LH in *Drosophila*. These authors found that the posterior-dorsal LH receives inputs from PNs associated with glomeruli responsive to fruit odors, whereas the anterior-ventral LH receives inputs from PNs associated with glomeruli responsive to pheromones (Jefferis *et al.*, 2007).

After receiving the output of PNs, some inhibitory LHIs send axons to the MB calyx where they impose feed-forward inhibition on KCs. This periodic inhibition reduces the amount of spiking in the odor responses of KCs (Perez-Orive *et al.*, 2002). In the MB, KCs transform the highly active, spike-filled spatiotemporally dynamic odor code in PNs into a much sparser representation. Sparse sensory representation is widely observed in other sensory systems (for review, see Barlow, 1972; visual: Vinje and Gallant, 2000; Weliky *et al.*, 2003; Young and Yamane, 1992; auditory: DeWeese *et al.*, 2003), and in the MB of many insects (locusts: Perez-Orive *et al.*, 2002; moths: Ito *et al.*, 2008 - this work, see Chapter 3; fruit flies: Turner *et al.*, 2008; Wang *et al.*, 2004; honeybees: Szyszka *et al.*, 2005). Sparseness can be measured in two forms – the lifetime sparseness, a measure of the amount of action

potentials in a single neuron over time, and the population sparseness, a measure of the probability that any given member in a neural population will spike in a certain period of time. Lifetime sparseness and population sparseness are not necessarily correlated (Willmore and Tolhurst 2001), and various degrees of sparseness are possible. In the MB, typically, very few KCs in the population will respond to any given odor stimulus, and each responding KC typically fires only one or two spikes at the odor onset, and sometimes at the offset (Ito *et al.*, 2008 - this work, see Chapter 3; Perez-Orive *et al.*, 2002; Stopfer *et al.*, 2003; Figure 1.1). Therefore, KCs show a high degree of both population and lifetime sparseness when activated by odors (Ito *et al.*, 2008 - this work, see Chapter 3; Perez-Orive *et al.*, 2002).

Sparse coding appears to offer some advantages to the processing of sensory information (for review, see Olshausen and Field 2004; Ong and Stopfer, 2009). Since sparse codes use fewer spikes for signaling, neurons require less metabolic energy to restore resting membrane potentials and to recycle neurotransmitters. Also, less coding space is required for stimulus representations and for memory formation. Furthermore, fewer synapses have to be modified to stabilize the learned associations between sparsely encoded stimuli (Laurent, 2002).

Sparse odor representation in KCs is caused by both intrinsic and circuit properties. Intrinsically, active conductances in KCs with strong spike frequency adaptation make these neurons especially sensitive to coincident inputs provided by synchronized PN spikes (Demmer and Kloppenburg, 2009; Perez-Orive *et al.*, 2002; Perez-Orive *et al.*, 2004). From the network point of view, in each oscillatory cycle, synaptic input from PNs to the calyx causes some KCs to fire. LHIs, like the KCs, receive direct olfactory inputs from PNs. Some LHIs then project axons to the

calyx, where they can inhibit KCs with a slight time delay. Thus, each oscillatory cycle originating in the AL reaches the KCs as a wave of excitation followed by a wave of inhibition, with inhibition closing off the cycle. The net effect of this circuitry is that LHIs reduce the time window during which KCs can integrate synaptic inputs from PNs (Perez-Orive *et al.*, 2002). A computational study revealed that changes in odor concentrations modulate the response latency of LHIs, and thus adjust the temporal window over which KCs can integrate PN synaptic input with odor concentration (Assisi *et al.*, 2007). This adaptive mechanism helps maintaining sparse KC responses over a wide range of odor concentrations. Consistent with this, blocking inhibitory inputs from LHIs by injecting picrotoxin to the calyx broadened KC EPSPs, and reduced the odor selectivity and sparseness of KC odor responses (Perez-Orive *et al.*, 2002; Perez-Orive *et al.*, 2004). Thus, this circuit function (likely with help from other inhibitory neurons that are mostly unknown) effectively sparsens the odor responses of KCs.

1.2.5 Overview of olfactory coding in insects

Odorants in the air are detected by ORNs on the antenna. Each ORN type recognizes a different set of physiochemical features of odorants; therefore, some ORNs are more broadly tuned than others, and a given odorant activates multiple types of ORNs (de Bruyne *et al.*, 2001; Haddad *et al.*, 2008; Hallem *et al.*, 2004; Hallem and Carlson, 2006; Malnic *et al.*, 1999; Schmuker *et al.*, 2007; Shields and Hildebrand, 2000). ORNs expressing the same OR type converge onto the same glomeruli in the AL, channeling odor information to PNs and LNs innervating those glomeruli (Bhalerao *et al.*, 2003; Couto *et al.*, 2005; Fishilevich and Vosshall, 2005; Gao *et al.*, 2000; Vosshall *et al.*, 2000). In addition, the multiglomerular LNs

provide channels of crosstalk among glomeruli (Olsen and Wilson, 2008a).

In the AL, each PN responding to the odor develops slow, temporally evolving patterns of spikes that last from tens of milliseconds to seconds. These firing patterns in PNs are odor- and concentration-specific (Ito *et al.*, 2008 - this work, see Chapter 3; Laurent *et al.*, 1996; Stopfer *et al.*, 2003). These patterns are jointly caused by the temporally varying ORN activities (de Bruyne *et al.*, 2001; Hallem and Carlson, 2006; Raman *et al.*, submitted), and the slow, $GABA_B$-like inhibition by LNs (Bazhenov, *et al.*, 2001; Macleod and Laurent, 1996; Wilson and Laurent, 2005). On top of this, the fast excitatory-inhibitory interactions between PNs and LNs transiently synchronize individual PNs with each other, generating LFP oscillations that can be observed in the AL and MB. In each oscillation cycle, a small portion of the responsive PNs will fire reliably at a particular phase relative to the LFP oscillations (Laurent and Davidowitz, 1994; Laurent *et al.*, 1996; Wehr and Laurent, 1996; Figure 1.3). Thus, an odor-specific fraction of the PN population will fire synchronously during each oscillatory cycle. The synchronous firing of PNs appears to be important to activate KCs in the MB – intrinsic properties of KCs allow KCs to summate simultaneous synaptic inputs supralinearly, and therefore KCs may serve as coincidence detectors of PN activities (Perez-Orive *et al.*, 2004). Further, besides synapsing on KCs, PNs also innervate the LH and activate LHIs. Having received PN inputs, LHIs send waves of inhibitions to KCs with a brief delay. Therefore, in each oscillation cycle, KCs receive a wave of odor-specific excitatory inputs from PNs, followed by a wave of inhibitions from LHIs, with LHI inhibitions closing off the cycle (Perez-Orive *et al.*, 2002). These intrinsic and circuitry properties together, and possibly with help from other inhibitory neurons, make KCs almost silent at rest, and fire very few spikes in a small subset of KCs when

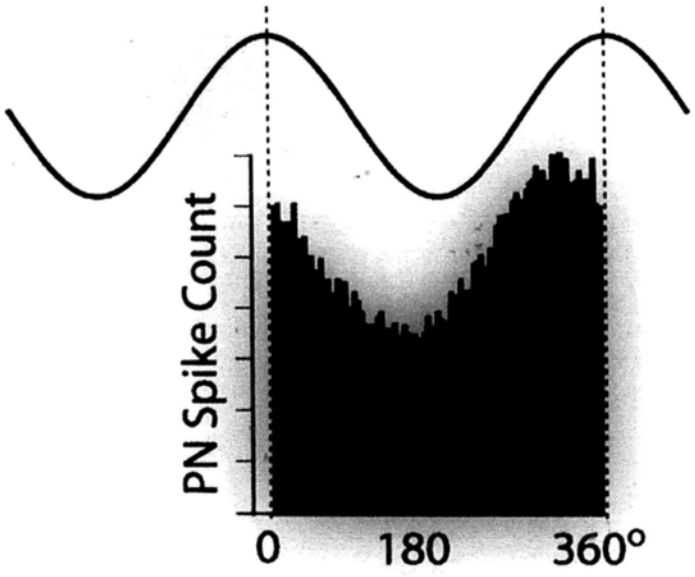

Figure 1.3. PN spiking in each oscillation cycle.
The excitatory-inhibitory interactions between PNs and LNs causes PNs tend to firing synchronously with each other. Nevertheless, not all PN spikes are synchronized. In each oscillation cycle, only a small subset of the responsive PNs fire synchronously with each other, producing the LFP oscillations. A large portion of the PN spikes are not phase-locked to the LFP oscillation cycles. Modified from Kay and Stopfer, 2006.

stimulated with odor.

Information about odor identity appears to be present in the firing patterns of the PN population. Analyses with simple classification algorithms showed that population PN activities can be used to identify odors, odor concentrations, and odor timings, with highest accuracy immediately after odor onset and offset (Brown *et al.*, 2005; Ito *et al.*, 2008 - this work, see Chapter 3; Mazor and Laurent, 2005; Stopfer *et al.*, 2003).

Increasing odor concentration activates more ORNs in the antenna. At low odor concentrations, only ORNs that are specifically tuned to the odor are activated. As odor concentration increases, additional, less specifically tuned ORNs are also activated (Hallem and Carlson, 2006; Ito *et al.*, 2009 - this work, see Chapter 2).

This leads to changes in firing patterns in PNs in a similar way as those caused by changes in odor identity (Stopfer *et al.*, 2003). However, when the responses of many PNs are analyzed together in a high dimensional analysis space, responses elicited by different concentrations of the same odor clustered together. PN responses to different odorants, on the other hand, formed distinct clusters in the analysis space (Stopfer *et al.*, 2003). KC odor responses remained sparse despite increase in odor concentration (Stopfer *et al.*, 2003). This is possibly caused by an adaptive circuitry mechanism that LHIs tend to fire at earlier phases relative to the oscillation cycle when odor concentration increases, therefore limiting the time window over which KCs can integrate PN inputs (Assisi *et al.*, 2007). The result of this circuitry is to transform the responses of broadly-tuned, very sensitive peripheral receptor neurons into extremely sparse and specific responses in the KCs.

Over the course of a lengthy odor stimulus, LFP oscillations frequency suddenly slowed as total ORN output decreased because of sensory adaptation in ORNs. However, LFP oscillation frequency in the MB remained invariant over a wide range of odor concentrations, an apparent contradiction. In this work, I examined the relationship between stimulus intensity and oscillation frequency by using experimental and computational approaches. The results of this study are presented in the next chapter.

2 Frequency transitions in odor-evoked neural oscillations

In many species sensory stimuli elicit the oscillatory synchronization of groups of neurons. What determines the properties of these oscillations? In the olfactory system of the moth we found that odors elicited oscillatory synchronization through a neural mechanism like that described in locust and *Drosophila*. During responses to long odor pulses, oscillations suddenly slowed as net ORN output decreased; thus, stimulus intensity appeared to determine oscillation frequency. However, changing the concentration of the odor had little effect upon oscillatory frequency. Our recordings *in vivo* and computational models based on these results suggested the main effect of increasing odor concentration was to recruit additional, less well-tuned ORNs whose firing rates were tightly constrained by adaptation and saturation. Thus, in the periphery, concentration is encoded mainly by the size of the responsive ORN population, and oscillation frequency is set by the adaptation and saturation of this response.

2.1 Introduction

Sensory stimulus-evoked neural oscillations have been described in many animals (Adrian, 1942; Bresseler and Freeman, 1980; Galambos *et al.*, 1981; Gray *et al.*, 1989; Laurent and Naraghi, 1994; Schadow *et al.*, 2007; Stopfer *et al.*, 1997; Tanaka *et al.*, 2009). For a particular modality in a given species, oscillation frequency often seems unrelated to stimulus intensity. In the locust olfactory system, for example, odors elicit ~20 Hz oscillations that vary little in frequency even when odor concentration varies over 5 orders of magnitude (Assisi *et al.*, 2007; Stopfer *et al.*, 2003). In some cases, though, stimulus intensity does appear to modulate oscillation frequency; the changing velocity of a visual stimulus, for example, can systematically change the frequency of gamma oscillations in the cat visual cortex (Gray and Prisco, 1997). What determines the frequencies of these oscillations?

Here, we used the insect olfactory system to clarify the encoding of odor intensity, and the relationship between stimulus intensity and oscillation frequency. In insects, odor molecules are first detected by ORNs. Axons from ORNs converge upon glomeruli in the AL, where excitatory PNs and LNs interact. PNs send excitatory inputs to LNs, and LNs send rapid inhibitory feedback to PNs via $GABA_A$-like receptors. In locusts, honeybees and *Drosophila*, this feedback circuit has been shown to synchronize groups of PNs, resulting in regular oscillating waves of output that depolarize KCs, the intrinsic neurons of the MB. These waves can be detected as a LFP (Laurent and Naraghi, 1994; Stopfer *et al.*, 1997; Tanaka *et al.*, 2009).

We found that odors evoked oscillatory responses in the moth *Manduca sexta* much like those described in the locust, honeybee and fly. Further, in the moth, we found

that lengthy odor pulses evoked oscillations that began at ~40 Hz but then suddenly decreased to ~15-20 Hz. Simultaneous LFPs and recordings from the moth's antenna (electroantennogram, EAG) showed the net response intensity of ORNs decreased in parallel to the shift in oscillation frequency. This suggested oscillation frequency might be determined by the intensity of the response of the ORN population. In apparent contradiction, though, we also found that odor-evoked oscillation frequency remained remarkably constant across a broad range of odor concentrations. What then is the relationship between stimulus intensity and oscillation frequency?

Our approach, combining experimental and computational methods, led to several conclusions. First, we found the frequency of odor-evoked oscillations in the moth olfactory system is determined by the intensity of input to the oscillatory AL network, but this intensity is determined by sensory adaptation and saturation of ORNs rather than by the intensity of olfactory stimuli. Second, extending prior work, we demonstrated that the vast majority of olfactory dynamic range is encoded in the periphery by the number of responsive ORNs rather than by the firing rates of those ORNs. And third, we characterized a new stable oscillatory regime in which principle neurons participating in an oscillatory network can fire much faster than the oscillation frequency.

2.2 Results

2.2.1 Odors evoke fast and then slow LFP oscillations in the MB

To characterize the moth olfactory system's neural responses, we delivered a variety of odors (non-pheromones, see Methods) over a wide range of concentrations, and a range of durations from 100 ms (as moths might experience while flying in an odor plume), to 4 s (as moths might experience when sampling food from flowers).

All odor stimuli in our panel induced robust oscillations in the LFP recorded in the MB calyx (a target of PNs, Figure 2.1A). Figure 2.1B shows an example of oscillations elicited by a presentation of dilute benzyl alcohol vapor to the ipsilateral antenna of a moth that was mostly intact but with its brain exposed for electrophysiological recording (see Methods). The first of a series of odor presentations typically elicited only weak oscillations in the LFP; however, oscillatory power increased rapidly over the first 4 or 5 presentations (Figure 2.2). Odor pulses briefer than ~1 s elicited fast, 30-40 Hz oscillations in the moth MB; notably, odor pulses longer than ~1 s produced oscillations that were initially fast but then dramatically slowed to 10-20 Hz (Figure 2.1C-E). Others (Laurent and Davidowitz, 1994; Perez-Orive *et al.*, 2002; Perez-Orive, 2004) and we (Figure 2.3) had previously observed similar but less pronounced decreases in LFP oscillation frequency in the locust.

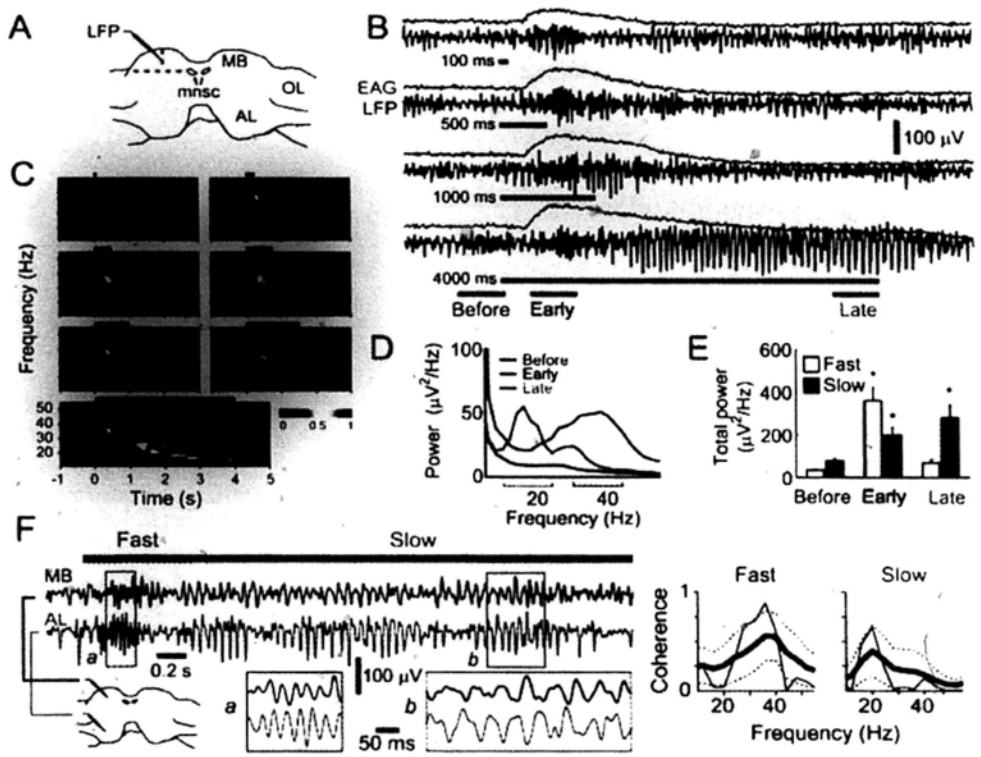

Figure 2.1. Odors evoked LFP oscillations in the moth MB and AL.
(A) Recording site for LFP: center of the calyx in the MB. MB, mushroom body; mnsc, medial neurosecretory cells; OL, optic lobe; AL, antennal lobe. (B) LFP oscillations (black traces) with simultaneously-recorded electroantennogram (EAG, green traces) evoked by different pulse durations of 1% benzyl alcohol, a plant volatile. Black horizontal bars: odor pulses. Color bars: time windows (500 ms) used to calculate the power spectra in [D]. (C) Brief odor pulses evoked fast oscillations; lengthy pulses evoked first fast, then slow oscillations. Normalized, average spectrograms from 18 trials obtained from 6 animals with 3 trials each (see Methods). Black horizontal bars above each spectrogram: odor pulses. (D) Power spectra of oscillatory LFP responses averaged from 22 moths and 8 odors, total of 820 trials. Color brackets: 14 Hz-wide bands used to calculate the total oscillatory powers of fast (red, 30-44 Hz) and slow (blue, 10-24 Hz) oscillations in [E]. (E) Total oscillatory power of fast and slow LFP shifted significantly over lengthy odor pulses. Twenty trials tested for each odor were averaged before pooling, mean±SE. n=41; 2-way ANOVA: $f_{window}(2)=26.62$, $P<0.0001$ (fast oscillations); $f_{window}(2)=9.09$, $P<0.0003$ (slow oscillations). Asterisks: significant differences (Tukey-Kramer multiple comparisons). (F) LFP oscillations in the AL and MB were highly coherent. Left: Example of odor-evoked LFP oscillations recorded simultaneously in the AL and MB; odorant: 1% cyclohexanone (4 s). Areas *a* and *b* are expanded in insets. Horizontal red (0.25-1 s) and blue (1-4 s) bars: times used for coherence analysis at right. Right: Magnitude squared coherence between the AL and MB. Thin black line: coherence of the response shown. Thick black and dotted lines: average coherence and its one standard deviation range (5 AL-MB combinations in 4 preparations, 20 trials each of 2 odorants), respectively.

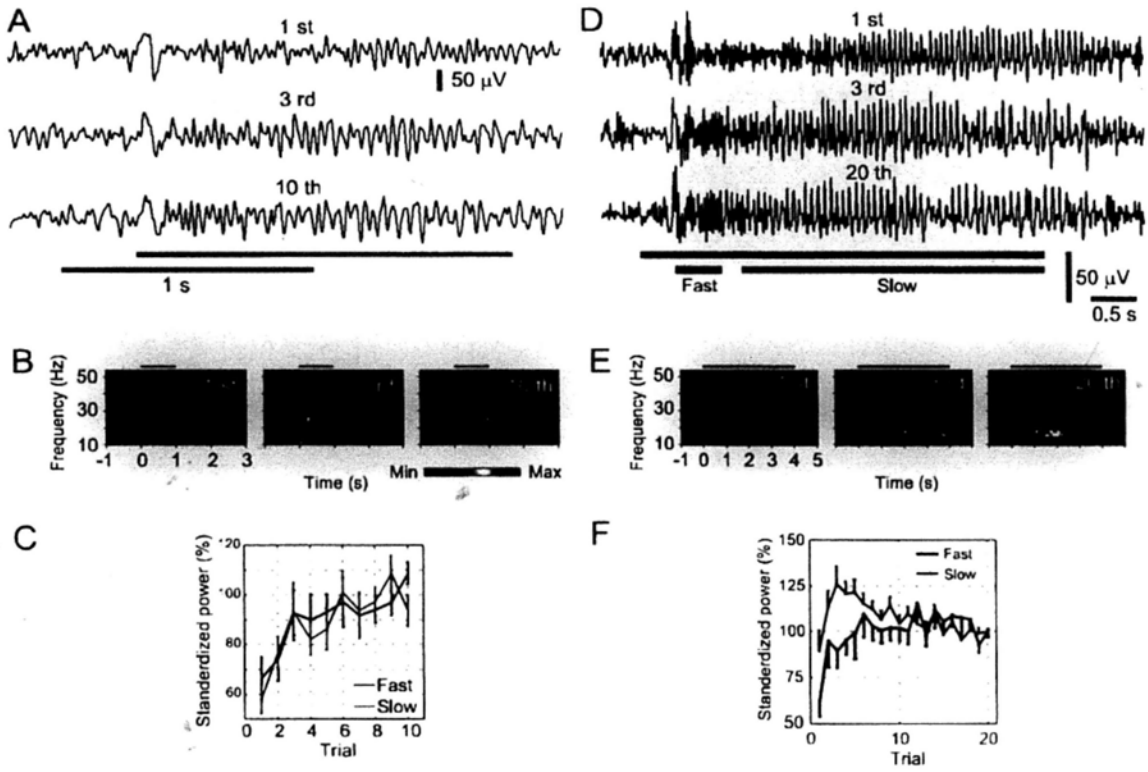

Figure 2.2. LFP oscillatory power increased over repeated stimulus presentations.

(A) LFP recorded in the MB when elicited by repeated brief odor pulses (1 s, 0.05 Hz, 100% Hexanol) increased in oscillatory power. The first (top), 3rd (middle), and 10th trials (bottom) are shown. Black horizontal bar: odor stimulation period; red (0.3-0.8 s) and blue (0.8-1.8 s) horizontal bars: time windows for total power plotted in [C]. (B) Averaged spectrograms (23 MBs from 20 moths included; 1 or 2 odors for each, resulting in 27 experiments) for the first, 3rd, and 10th trials. Odors used include 100% hexanol, 1% and 100% trans-2-Hexen-1-ol, 1% benzyl alcohol, 1% linalool, 1% benzaldehyde. (C) Repeated trials elicited an increase in spectral power of fast (30-44 Hz) and slow (10-24 Hz) oscillations. LFP power (5-55 Hz) was standardized by the average of the last 3 trials of each experiment. Values are expressed as mean±SE. n=27; 2-way ANOVA: $f_{trial}(9)=2.78$, $p<0.005$ (Fast); $f_{trial}(9)=4.14$, $p<0.0001$ (Slow). (D) MB-LFP elicited by repeated deliveries of long odor pulses (4 s, 0.05 Hz, 1% benzaldehyde). The first (top), 3rd (middle), and 20th trials (bottom) are shown. Black horizontal bar: odor stimulation. Red (0.3-0.8 s), light blue (1-3 s), blue (1-2 s), green (2-3 s), and magenta (3-4 s) horizontal bars: time windows for total power shown in [F]. (E) Average spectrograms for the first, 3rd, and 20th trials, replotting same data shown in Figure 2.1E (n=41). The peak of slow oscillation power shifted to earlier in the response gradually over trials. (F)

Standardized total power (5-55 Hz) of fast (30-44 Hz) and slow (10-24 Hz) oscillations elicited by lengthy odor pulses (4s). Even the first odor presentation elicited strong slow oscillations in the latter part of the response.

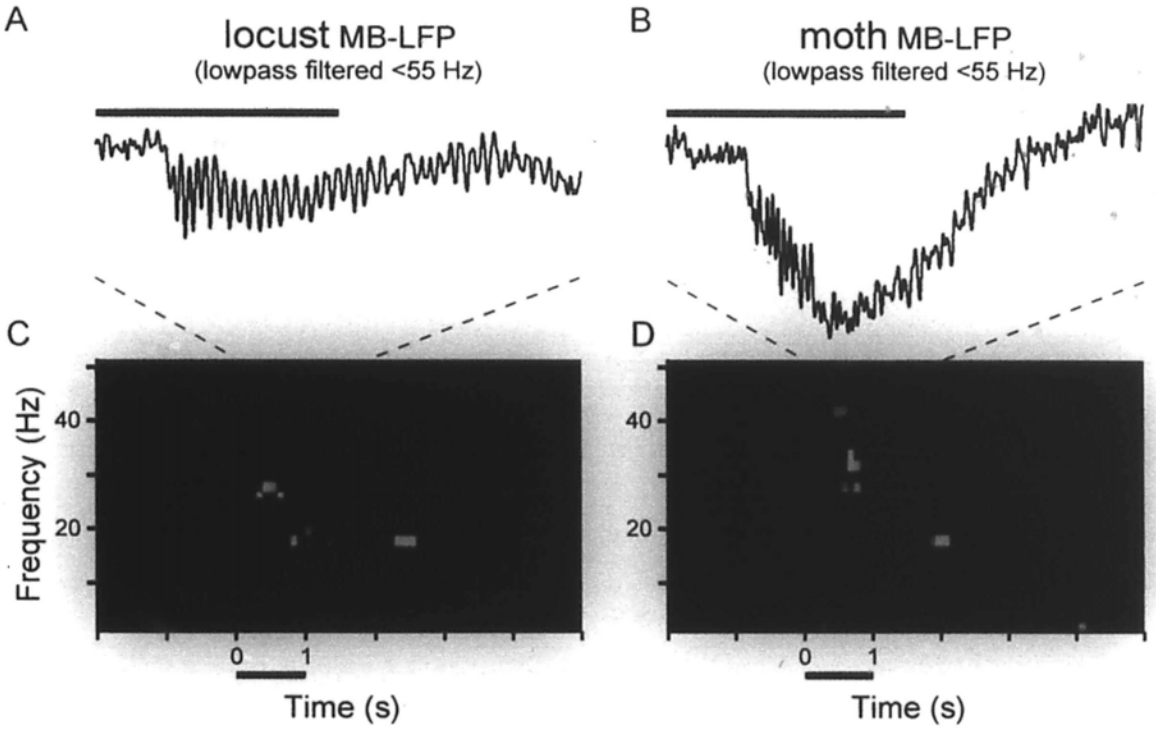

Figure 2.3. Oscillation frequency in locusts also decreases during a response. Representative example odor-elicited LFP oscillations (low-pass filtered below 55 Hz) recorded from the mushroom bodies of the locust (A) and the moth (B). Spectrograms of MB-LFP oscillations in the locust (C) and the moth (D). The frequency shift is less pronounced in the locust than in the moth. However, the deflection amplitude is greater in the locust.

2.2.2 LFP oscillations are generated in the AL

Where, and by what mechanism are the oscillations generated? In the moth, we made simultaneous recordings of LFPs from the AL and the MB. All odors we tested induced both fast and slow oscillations in both the AL and the MB; further, the AL-LFP and MB-LFP signals were highly coherent (n=10, Figure 2.1F).

We next made simultaneous intracellular recordings from pairs of AL neurons together with LFP recordings from the MB (Figure 2.4; all neurons morphologically identified by dye injection and subsequent confocal imaging). Figure 2.4A shows an example of a simultaneous recording of the MB-LFP, a PN, and an LN. For most oscillation cycles, a spike in the PN was closely followed (within ~2 ms) in the LN by either a single spike or an EPSP, suggesting LNs received odor-driven periodic input from PNs. And, reciprocally, the membrane potential of this PN revealed a periodic hyperpolarization and depolarization after each spike, suggesting IPSPs from the inhibitory LNs regulated the timing of spikes in the PN. Sliding-window cross-correlations showed that the membrane potential fluctuations in this LN and PN were tightly coupled to LFP oscillations recorded in the MB (spikes clipped; Figure 2.4B). The oscillations slowed during each trial.

Are the fast and slow oscillations generated in the AL? We made intracellular recordings from 14 PNs and 30 LNs, each simultaneously with LFPs recorded in the MB; Figure 2.4C displays the spike-LFP phase relationships for spikes pooled from all recorded cells. Spikes in PNs reliably phase-locked to the LFP at a point just past the peak of each cycle during fast (mean direction and 95% confidence interval= 2.79° ± 9.1°; 1,950 spikes) and slow (23.4° ± 3.3°; 7,005 spikes) oscillations. Spikes in LNs phase-locked to the LFP just after the PNs during fast (71.4° ± 3.0°;

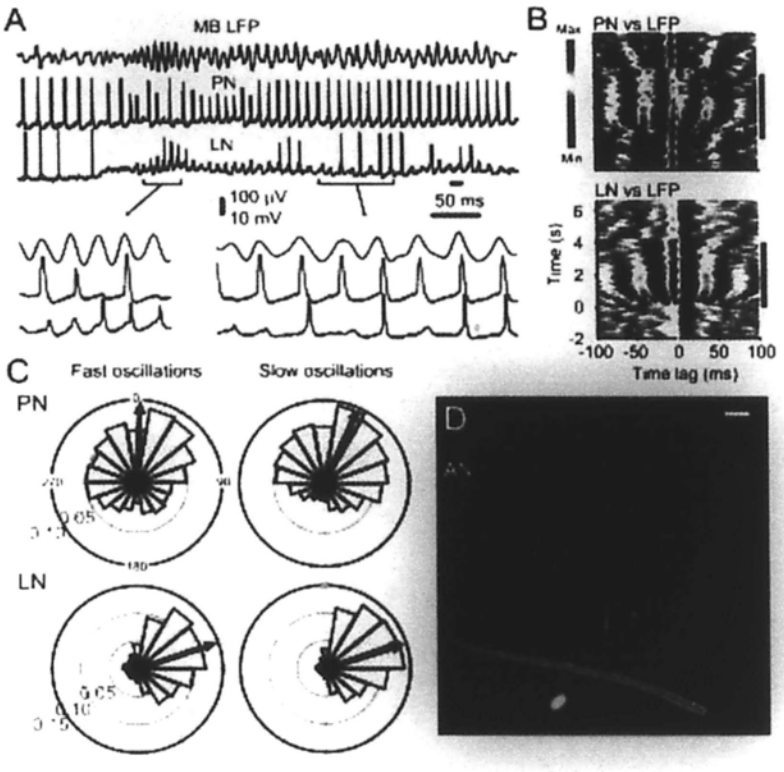

Figure 2.4. PN and LN responses were strongly phase-locked to the LFP.
(A) Example simultaneous intracellular recordings from PN and LN, with LFP recorded in the MB. First 2 s after the odor onset shown; brackets: portions expanded beneath. Odorant: 1% benzyl alcohol. (B) Subthreshold oscillations: 5-trial average sliding-window cross-correlograms show reliable LFP and subthreshold membrane potential oscillations for the PN (top) and LN (bottom) in [A]. Spikes were clipped. Vertical bars: odor pulses. (C) Spike-LFP phase relationships: Polar histograms show phase position, relative to LFP, of spikes recorded in PNs (n=14) and LNs (n=30) for fast and slow oscillations. Concentric circles: firing probability. Black arrows: mean direction. (D) All recorded neurons were filled with dye and later morphologically identified. Example of PN and LN morphology. An Alexa-fluor-633 (red) filled PN and an Alexa-fluor-568 (yellow) filled LN are shown. Scale bar: 50 μm. AN: antennal nerve.

2,623 spikes) and slow (72.6° ± 1.1°; 12,723 spikes) oscillations. The spike phase distributions of PNs and LNs were each significantly different from uniform distributions (Rayleigh test, $p<0.05$) indicating strong phase-locking. The temporal relationships of these populations match those shown in the simultaneously-recorded example (Figure 2.4A).

Together, the reliable, periodic relationships among AL neurons suggested that the timed inhibition of PNs by LNs was important for producing synchronous oscillations. To test this, we selectively abolished fast inhibition from LNs to PNs by locally injecting picrotoxin (PCT, a blocker of the $GABA_A$-like inhibition in *Manduca*, Waldrop *et al.*, 1987) into the AL while recording LFPs from the MB. Injection of PCT (n=6) reversibly and significantly reduced odor-evoked fast and slow oscillations; control injections of saline (n=5) had no effect (Figure 2.5). Thus, inhibition from LNs within the AL is required for the generation of odor-elicited oscillations. Both fast and slow oscillations are generated within the AL and are transmitted to the MB by PNs.

2.2.3 Responses in KCs are shaped by oscillatory input from PNs

To test whether followers of PNs in the MB are sensitive to the oscillatory synchrony of their input, we made intracellular recordings from a set of KCs (n=20, all morphologically identified by dye injection and subsequent confocal imaging).

During odor presentations, the membrane potentials of KCs revealed pronounced sub-threshold fluctuations that were tightly coupled to simultaneously-recorded LFP oscillations. In our four recordings from KCs that revealed sub-threshold activity,

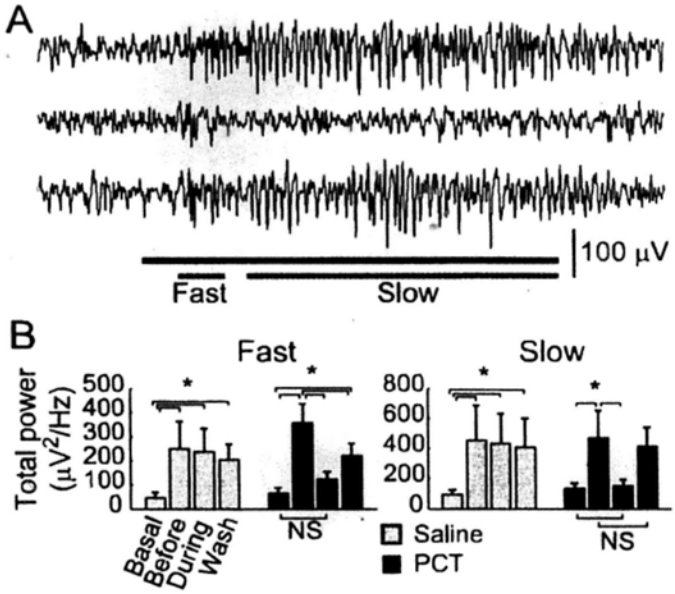

Figure 2.5. Local injections of $GABA_A$ receptor blocker picrotoxin into the moth AL reversibly abolished odor-evoked oscillations.

(A) Example: odor-evoked LFP oscillations recorded in the MB before (top) and after injection (middle), and after washout (bottom). Black horizontal bar: odor presentation, 4s. Odor: 1% trans-2- hexen-1-ol. Short (0.3-0.8 s) and longer (1-4 s) gray horizontal bars: time windows for spectral power (5-55 Hz) shown in [B]. (B) Summary shows PCT significantly reduced the strength of odor-evoked LFP oscillations. Total power calculated as in Figure 2.1E, mean±SE. Saline injection: n=5; 2-way ANOVA: NS (not significant). PCT (picrotoxin) injection: n= 6; 2-way ANOVA: $f_{treatment}(3)=17.09$, $P<0.0006$ (fast 0.3-0.8 s); $f_{treatment}(3)=5.18$, $P<0.0285$ (slow 1-4 s). Asterisks: significant differences ($P<0.05$, Tukey-Kramer multiple comparisons test).

peaks of the membrane potential oscillations reliably occurred during falling phases of the LFP oscillation (Figure 2.6A,B; see Methods). Further, odor-evoked spikes in KCs were phase-locked to the falling phases of LFP oscillations during fast (117.1° ± 12.2°; 329 spikes) and slow (125.7° ± 5.8°; 706 spikes) oscillations (Figure 2.6C). The spike phase distributions for KCs, like those of PNs and LNs, were significantly different from uniform distributions (Rayleigh test, $p<0.05$).

We found that the timing of spikes in PNs, LNs and KCs became more precise (less jitter around the preferred phase) as the oscillation frequency decreased (Figure 2.7). Together, these results indicated that oscillations strongly influence the timing of spikes in the KCs.

2.2.4 Oscillation frequency remains constant over a wide range of odor concentrations

We had observed that long odor pulses elicited oscillations that shifted dramatically in frequency. What causes this shift? We found that, during long odor pulses, EAGs decreased in amplitude with timing roughly matching that of the frequency shift in the LFP (Figure 2.1B). The decrease in EAG amplitude was probably caused by sensory adaptation within the ORNs (Kaissling *et al.*, 1987), a mechanism that reduces the intensity of response to an ongoing stimulus. The nearly parallel changes in ORN output intensity and oscillation frequency suggested to us that the intensity of the stimulus may determine oscillation frequency.

To test this, we delivered a wide range of concentrations of three odors (hexanol, octanol and geraniol), expecting to find that higher concentrations elicited more

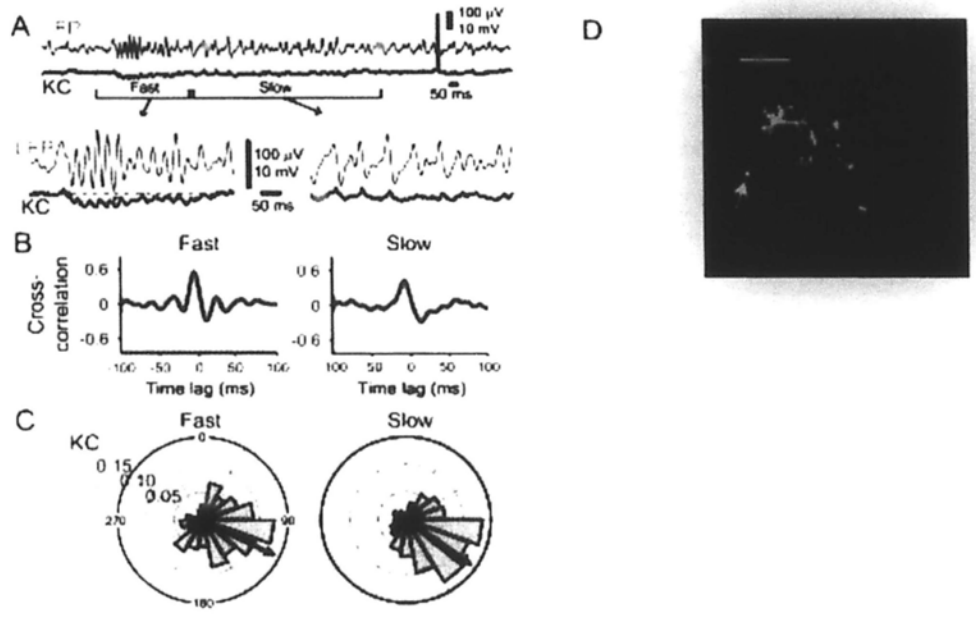

Figure 2.6. Spiking in KCs is sparse, odor specific, and tightly phase-locked to the LFP.

(A) KCs showed odor-elicited subthreshold membrane potential fluctuations that were tightly correlated with LFP oscillations. Example: top, gray: LFP; bottom, black: simultaneous intracellular record of a KC. Bottom: details of fast and slow periods during oscillatory response. Odor: 4 s, 1% benzyl alcohol. Gray broken line: resting potential. (B) Cross-correlations between LFP oscillations and KC subthreshold activity. Cross-correlation was calculated for times bracketed in [A]. Black lines: correlation for the trial shown in [A]; gray lines: 21 other trials from this cell. All 8 KCs showing subthreshold oscillations revealed similarly-shaped correlation functions, 3 with coefficients >0.3. (C) Polar histograms show strong phase-locking between spikes in KCs and the LFP oscillations. Histograms show spikes recorded from 20 KCs during fast and slow oscillations. Arrows: mean phase position. (D) Example of KC morphology; posterior view of MB; KC filled with Alexa Fluor 633. Scale bar: 50 µm. Arrow: soma; CaM: medial calyx; CaL: lateral calyx.

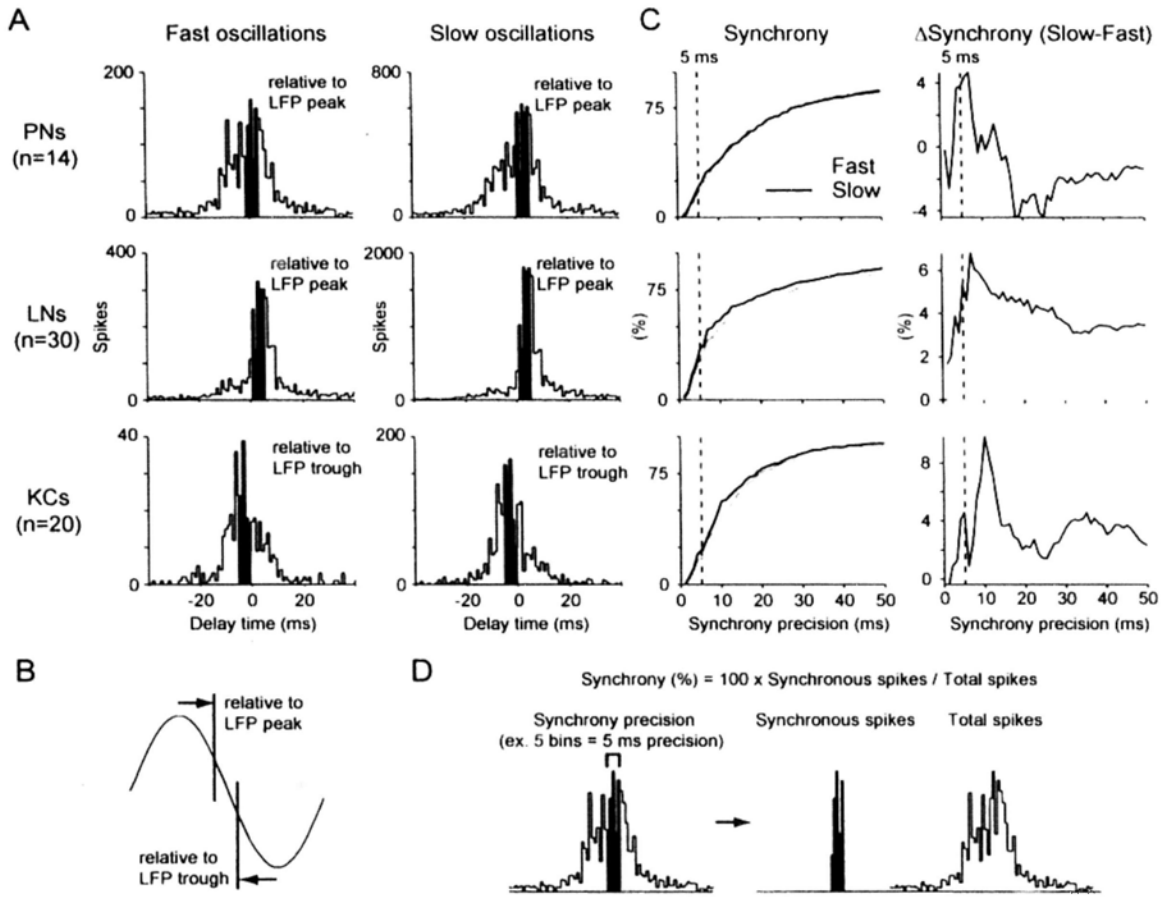

Figure 2.7. Spike timing became more precise within PNs, LNs and KCs as the oscillation frequency decreased.

(A) Distributions of spike timings (relative to LFP peak or trough) in neurons recorded intracellularly. Timing was defined as shown in [B and D]. Note that the distributions of spike timings in PNs revealed two peaks, consistent with our observation that moth PNs tended to fire twice per one cycle (Figure 2.13). (B) Definition of spike timing. To determine spike timing more accurately, we considered our observations that PNs and LNs fired near the peaks of LFP-oscillations and KCs fired near the troughs. (C) Synchrony increased after the frequency transition. Synchrony (%) defined as in [D] was calculated for a range of accuracy (from 1 ms to 50 ms). The increase in synchrony (ΔSynchrony) was obtained by subtracting the synchrony measured during fast oscillations from that measured during slow oscillations. (D) Definition of synchrony. For 1 ms precision, the maximum bin (1 ms) in each histogram was defined as synchronous (the proportion of synchronous spikes divided by the total number of spikes). For broader precision (>1 ms), the spikes in the bins centered at the maximum bin were included as synchronous spikes.

intense responses from ORNs and perhaps faster oscillations in the LFP. Indeed, the range of odor concentrations we used elicited a wide range of responses in the EAG (Figure 2.8A,B) and in the LFP (Figure 2.9) from small, near-basal fluctuations to deep, saturating deflections; thus, the range of odor concentrations we used effectively elicited a wide range of response intensities from the population of ORNs. Lower odor concentrations evoked weaker LFP oscillations; higher concentrations evoked stronger oscillations (Figure 2.8C). However, we found that the initial LFP oscillation frequency remained almost constant across five or more orders of magnitude of odor concentration (Figure 2.8D). Together, these results appeared contradictory: decreasing drive from ORNs appeared to result in dramatically reduced oscillation frequency, yet experimentally changing the intensity of the input to ORNs had little or no such effect.

2.2.5 The ORN population encodes odor concentration spatially and temporally

The EAG aggregates the responses of many ORNs in the antenna. Thus, we next characterized the responses of individual ORNs on the moth antenna while delivering odor pulses of different concentrations (Figure 2.10; n=37 ORNs from 9 preparations; see Methods). We found that individual responsive ORNs revealed a small dynamic range, firing at rates that varied only within narrow spans of concentration. ORNs responding to moderate odor concentrations (e.g. 0.01%-1% of hexanol; see Methods) showed firing rates that quickly saturated (Figure 2.10F green lines) or even decreased (Figure 2.10F red lines) as odor concentration increased. And,

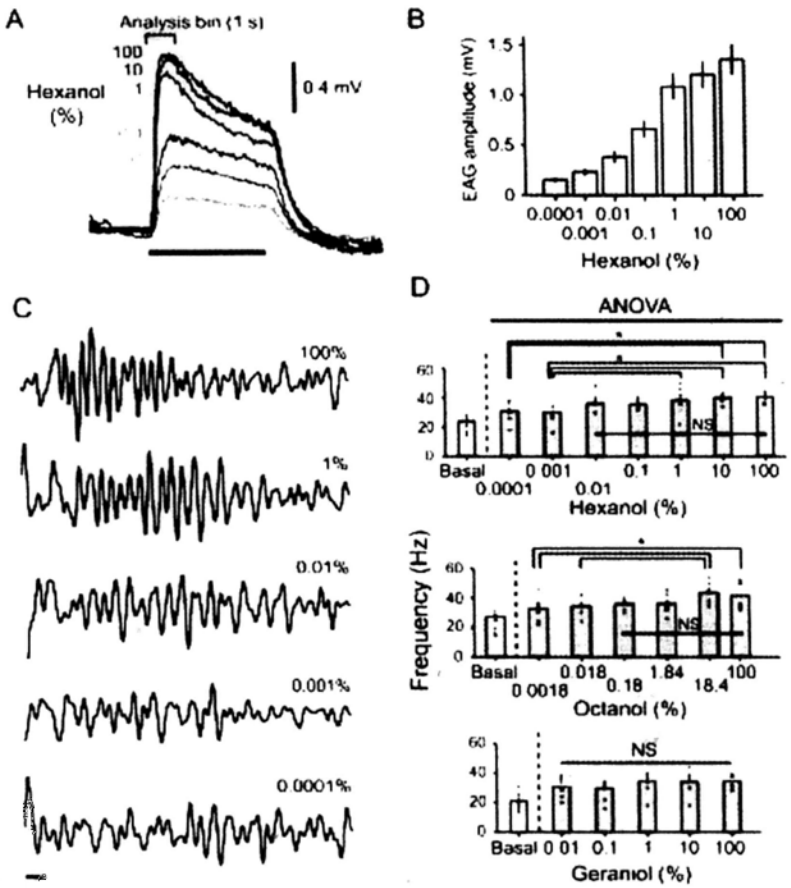

Figure 2.8. Odor concentration determines oscillation coherence, not frequency.

(A) EAG traces revealed total ORN output increased with odor concentration. Example from one antenna; horizontal bar: 4 s. (B) Summary. EAG amplitude (first 1 s, see bracket in [A]) evoked by a range of odor concentrations. Mean±SE; n=8; 2-way ANOVA: $f_{odor\_concentration}$=16.84, p<0.0001. (C) Higher concentrations of odor evoked stronger LFP oscillations. Initial portions of the odor response are shown. Scale bar: 50 ms. (D) The frequency of fast oscillation changed not at all or only slightly across a broad range of odor concentrations. All results are shown (dots); bar graph shows means, n=9. Leftmost bars: basal oscillatory power in absence of odorant. Hexanol: 2-way ANOVA: $f_{hexanol\_concentration}$=6.16, p<0.001; post hoc Tukey-Kramer tests found small but significant differences between three highest and two lowest concentrations (p<0.05). Octanol: $f_{octanol\_concentration}$=4.98, p<0.001; post hoc tests: significant differences between highest two and lowest two concentrations of octanol (p<0.05); Geraniol: 2-way ANOVA: $f_{geraniol\_concentration}$=1.4, p>0.25, ns.

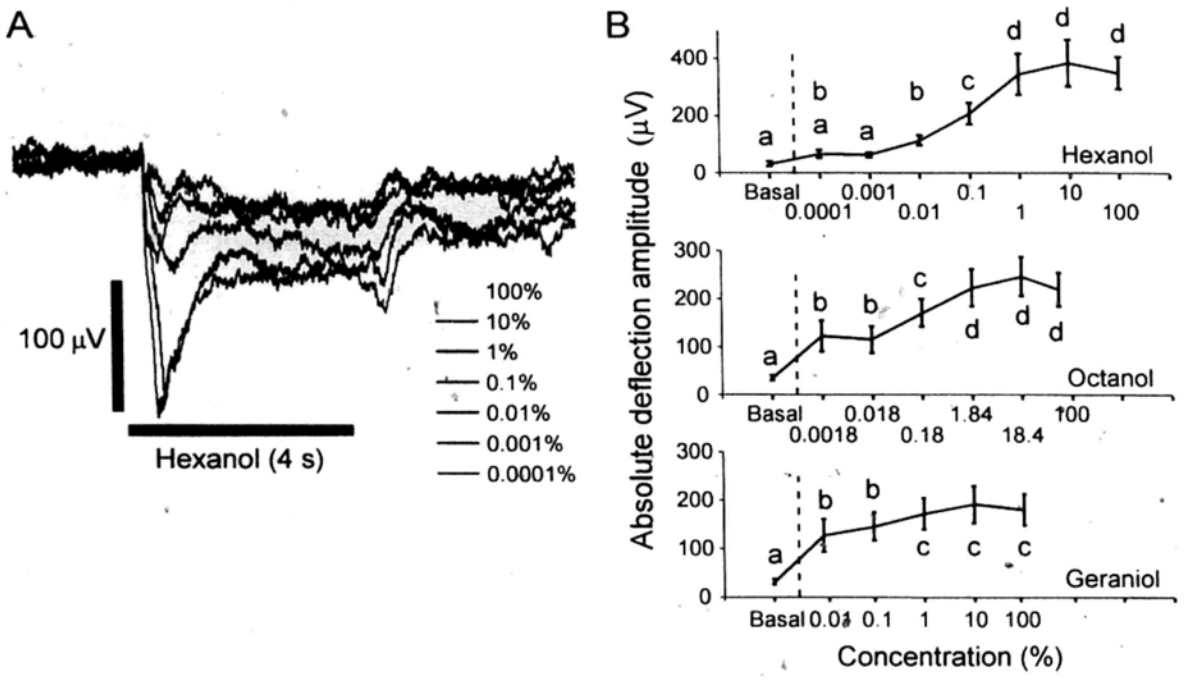

Figure 2.9. LFP deflection amplitude increases with odor concentration.
(A) LFP deflection (low-pass filtered at 55 Hz) evoked by a range of concentrations of hexanol. (B) Summary. LFP deflection amplitude increased with odor concentrations. 2-way ANOVA: f_{hexanol} concentration=113.32, $p<0.0001$. f_{octanol} concentration=183.57, $p<0.0001$. f_{geraniol} concentration=102.27, $p<0.0001$. For all three odors, responses to the three highest concentrations showed saturation (Tukey-Kramer multiple comparisons).

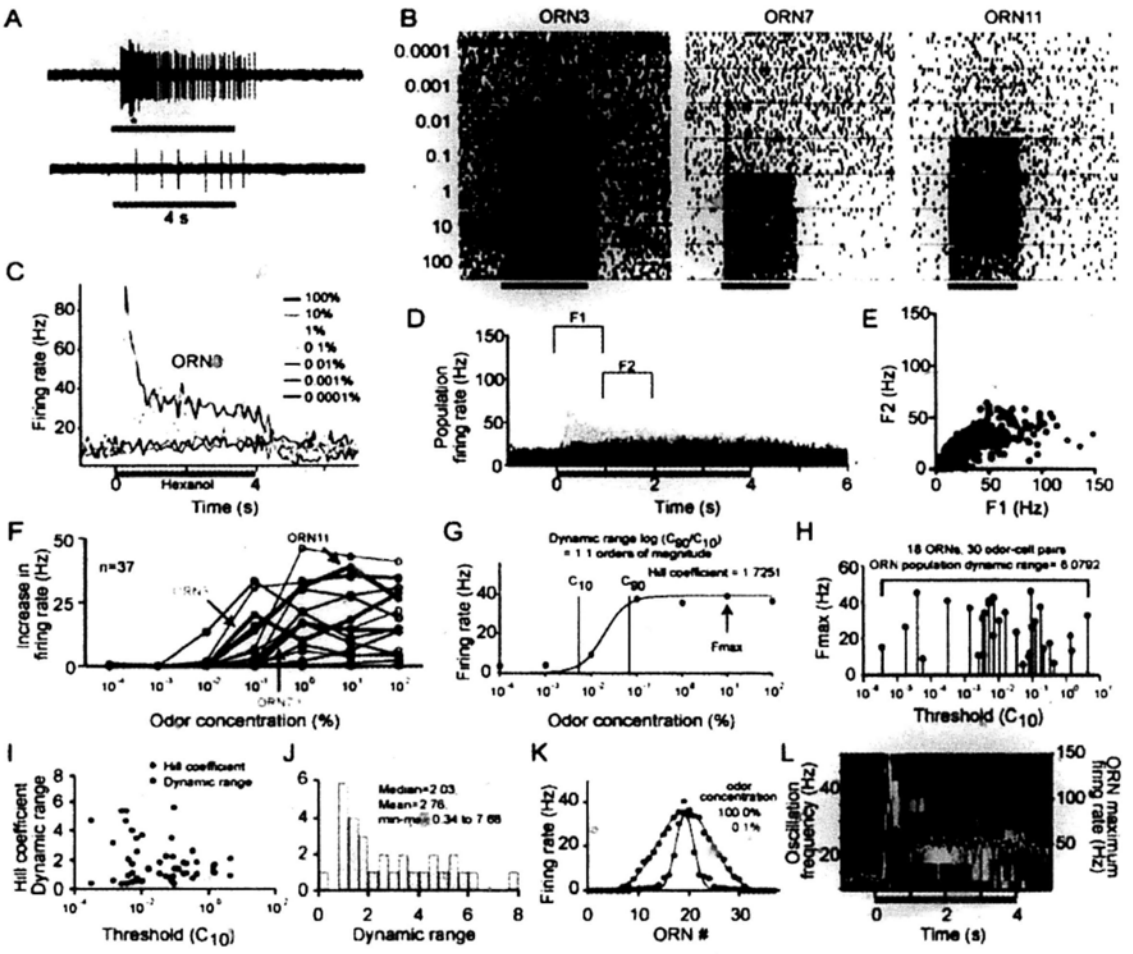

Figure 2.10. Saturation and adaptation constrained the ORN firing rates.
(A) Example extracellular recordings from a sensillum on the antenna show responses to odor pulses (4 s) of 10% hexanol (top) and jasmine oil extract (bottom). Two ORNs were recorded in this sensillum, one with short spikes and sustained firing, and one with large, transiently firing spikes (marked by *). Tan bars: odor pulses. (B) Spike rasters of three ORNs tested with a wide range of concentrations of hexanol. Blocks of 10 trials for each concentration were tested in random order. Tan bars: odor pulses (4 s). (C) Instantaneous firing rates of a representative ORN. Spikes were binned (100 ms); spike count in each bin averaged over 10 trials. (D) The most active ORNs quickly adapted. Instantaneous population firing rate; firing rate averaged over 10 trials for each odor-sensillum combination; 1,011 odor-sensillum combinations (32 sensilla tested with up to 20 odors each). Responses to odor-sensillum combinations were divided into 2 groups based on initial peak firing frequency (>40 Hz: light gray; <40Hz: dark gray). Brackets: 1 s

analysis bins used to calculate initial (F1) and late peak (F2) frequencies. For this analysis multiunit activity was included. (E) Relationship between peak frequencies F1 and F2. Dots under the diagonal line indicate adaptation. Almost all odor-sensillum combinations showing initial spike frequency >40 Hz (F1) underwent adaptation during the stimulus. (F) Concentration tuning curves for 22 ORNs. Mean firing rates of most ORNs saturated after the odor onset. Red traces: ORNs with firing rates that decreased after the peak concentration; Green traces: ORNs with firing rates that saturated after the peak concentration. (G) ORN concentration response curves were fit with the Hill equation. Example: ORN22, tested with different concentrations of hexanol. Parameters (C_{10}, C_{90}, Hill coefficient, F_{max}) in panels H-J were obtained from this fitting. (H) Lack of correlation between maximum firing rates (F_{max}) and the thresholds (C_{10}) of individual ORNs. Response thresholds (C_{10}) spanned about 6 orders of magnitude, indicating our sample of ORNs, as a population, offered a wide dynamic range. Only responsive odor-ORN combinations (n=25, >5 Hz change in mean firing rate during odors) were included in this analysis. (I) Hill coefficient (red) and dynamic range (blue) as function of threshold. ORNs responding to low concentrations typically showed low Hill coefficients and relatively wide dynamic ranges. (J) Histogram of Hill coefficients. Most ORN-odor combinations showed Hill coefficients >1, indicating a dynamic range <2 orders of magnitude.

(K) Firing rates in the ORN population followed Gaussian distributions. The numbers of spikes in the first 1 s of odor responses (indicated by colored dots) were counted in 37 ORNs tested with hexanol. The ORN firing rates were fit with Gaussian distributions (colored lines). As the odor concentration increased, the width of the distribution (sigma) broadened but the height of the distribution remained about the same. All odor concentrations evoked responses with Gaussian distributions. (L) Frequency of MB-LFP oscillations changed in parallel to the odor input (1% hexanol) to the AL network. Odor input: firing rate of the most active ORN (at each 50 ms time slice across 22 ORNs). Power spectrogram: average of 9 preparations.

ORNs that initially responded vigorously to an odor presentation (e.g. with firing rates >40 Hz) quickly slowed their firing (Figure 2.10B,C). This sensory adaptation was evoked by all odors tested and all concentrations whenever the initial firing rate exceeded ~40 Hz (Figure 2.10D,E). Faster-firing ORNs underwent greater adaptation (Figure 2.10E), suggesting ORNs better-tuned for a given odor would adapt more. Thus, we found that each ORN fired at a rate tightly constrained by adaptation and saturation.

To quantify the dynamic range of individual ORNs relative to that of the population, we fit concentration response curves with the Hill equation (Figure 2.10F,G; Firestein *et al.*, 1993; Wachowiak and Cohen, 2001; Koulakov *et al.*, 2007). In our sample of ORNs and odors we found response thresholds were widely distributed across concentrations spanning about 6 orders of magnitude (C_{10}, Figure 2.10H). Consistent with this, increasing numbers of ORNs participated in the response as odor concentrations increased (Figure 2.10F,H). And, most ORNs had Hill coefficients greater than 1 (mean = 1.1269; median = 0.802), corresponding to a dynamic range spanning less than 2 orders of magnitude (Figure 2.10I,J; Koulakov *et al.*, 2007). The 2 orders of magnitude encoded by individual ORNs corresponded to only about 2/6, or 33% of the dynamic range provided by the whole ORN population. Further, we found that the firing rates in the ORN population fit Gaussian distributions (Figure 2.10K). As odor concentration increased, the width of the distribution (number of responsive ORNs) broadened but the height of the distribution (firing rate) remained about the same (Figure 2.10K). These results indicate that, in the moth, the great majority of olfactory dynamic range is encoded as changes in the size of the population of responsive ORNs.

2.2.6 Firing rate adaptation in ORNs determines oscillation frequency

Our analysis of individual ORNs revealed that the frequency transition in LFP oscillations followed a temporal profile closely matching that of the adaptation rate of the most active ORNs (Figure 2.10L; Figure 2.11). Yet, experimentally changing the intensity of input to the ORNs (odor concentration) had little if any such effect. To explain these apparently contradictory findings and to understand how oscillation frequency is determined, we incorporated our physiological measurements into a full-scale, map-based model (reduced type, Rulkov *et al.*, 2002; Rulkov *et al.*, 2004; Rulkov and Bazhenov, 2008) of the moth AL (Figure 2.12A). We simulated input to the AL network as synaptic currents applied to odor- and concentration-specific populations of PNs and LNs (Assisi *et al.*, 2007; see Methods). In our model, as *in vivo*, this input caused the population of PNs to spike and to synchronize through feedback inhibition mediated by LNs (Figure 2.12B). Synchronized spiking in the model AL was manifest as periodic oscillations of the LFP (Figure 2.12B, top; calculated as the average activity of all PNs).

We had found that the adaptation of ORN firing rates followed a temporal profile matching that of the frequency transition in LFP oscillations (Figure 2.10L; Figure 2.11). How does adaptation influence the dynamical properties of the AL network? To simulate activation and adaptation of the odor responses of ORNs, we drove our network model with a rapidly rising and then slowly decaying input (Figure 2.12B, bottom) with the size of the AL population receiving external stimulation (input "width") held constant. During the simulated odor's onset, the rapid increase in input intensity quickly entrained the network to generate ~40 Hz oscillations (Figures

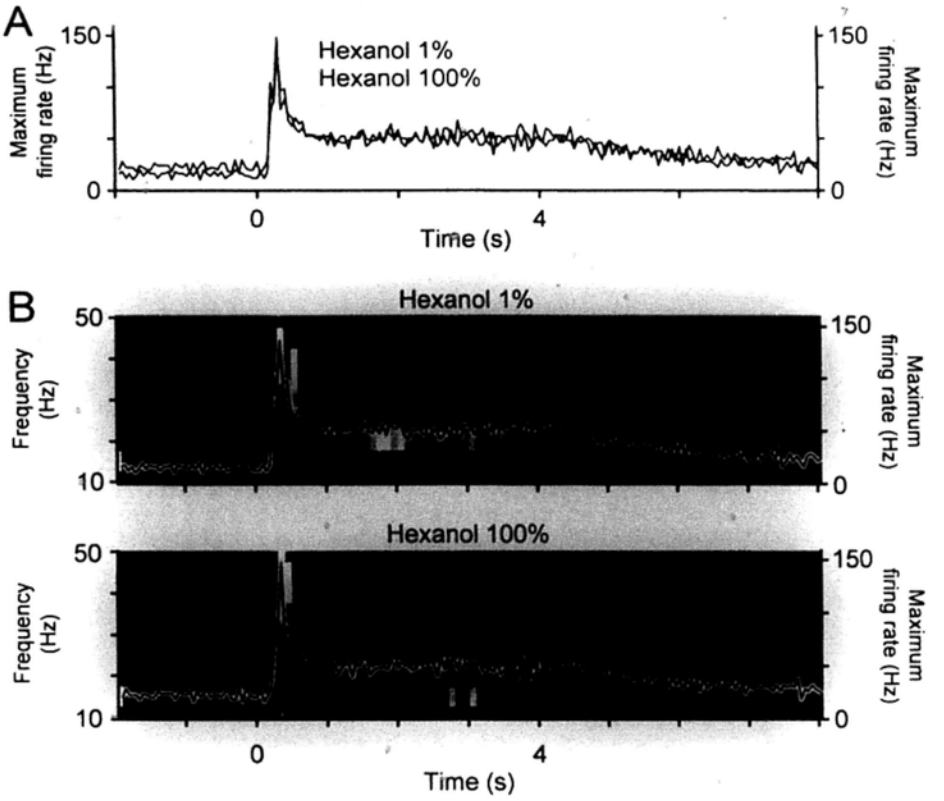

Figure 2.11. Saturation of firing rates in ORNs and in the frequency of MB-LFP oscillations

(A) The instantaneous maximum firing rates of most active ORN in the population (calculated every 50 ms) adapted in a nearly identical manner for two different concentrations (1% and 100%) of hexanol. (B) The oscillation frequency followed the strength of odor inputs very closely at both concentrations.

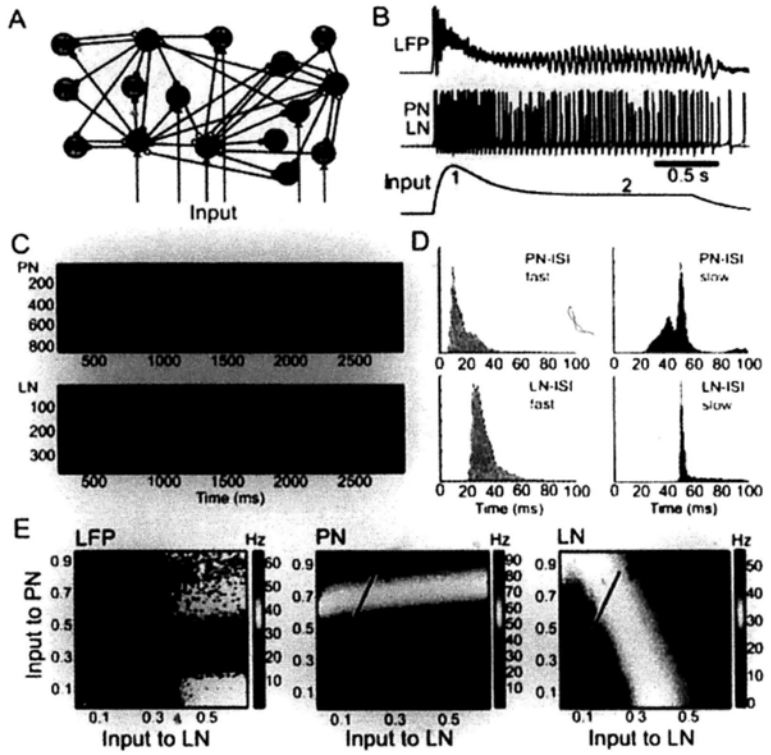

Figure 2.12. Odor evoked oscillations in model of moth AL.

(A) Full-scale, map-based model included randomly connected populations of 820 PNs and 360 LNs. Odor pulse input was simulated by external currents delivered to a subset of neurons. (B) Amplitude of the input was set to resemble the EAG (bottom). LFP (top) and neuronal (middle) responses resembled those recorded *in vivo*. The input to the model was tuned to match results of our physiological recordings and corresponded to points '1' and '2' in the parameter space shown in [E]. (C) Raster plots show spikes in all PNs (top) and all LNs (bottom) evoked by one odor pulse (applied from 500-2500 ms). (D) Interspike interval (ISI) distributions during fast and slow phases of LFP oscillations. Many PNs fired two spikes in a single oscillatory cycle (ISI < 25 ms during fast and ISI < 50 ms during slow phase); LN frequency was typically limited to the LFP frequency. (E) Frequency of LFP, PN and LN oscillations as a function of input from ORNs to PNs and LNs. Sweeping the points between '1' and '2' in parameter space mimicked the ISI distribution (compare [D] and Figure 2.13) and the abrupt change in oscillatory frequency (compare [B] and the Figure 2.1C) we observed *in vivo*.

2.12B,C). The subsequent decrease in stimulus amplitude initially led to a reduction in the LFP amplitude, signaling a decrease in the synchrony of spiking across the population of responsive PNs. But as the input intensity continued to decrease, synchrony suddenly resumed, although now at ~20 Hz. During this transition the inter-spike interval (ISI) distributions of both PNs and LNs (Figure 2.12C,D) lengthened. Our intracellular recordings from PNs and LNs had revealed qualitatively similar changes in ISI distribution (Figure 2.13). In our model, a 40-50% decrease in stimulus intensity caused a frequency shift (Figure 2.12B) matching what we had observed *in vivo* (Figure 2.1D,F). This result suggested that a change in stimulus intensity similar to what occurs *in vivo*, and not the size of the responsive ORN population, could explain much of the change in oscillation frequency. Other factors such as the strengths and the time constants of synaptic currents could influence oscillation frequency as well (Figure 2.14).

We next analyzed the steady-state network dynamics of our model as a function of input intensity. Throughout these stimulations we held constant both the size of the AL population receiving external input and the amplitude of the input; in separate experiments we systematically changed the input amplitude to explore a broad space of parameters. Our model showed that the AL network could generate oscillations with a wide range of frequencies, including 20-40 Hz, depending on the net intensity of its input (Figure 2.12E, left panel). Further, individual PNs and LNs could change average firing rate as a function of excitatory and inhibitory input intensity (Figure 2.12E middle and right panels). In our model, inhibitory LNs almost always spiked at the frequency of the LFP oscillations; notably, excitatory PNs could fire faster with either one or two spikes during each oscillatory cycle (Figure 2.12C,D). These results match those of our intracellular recordings (Figure 2.13).

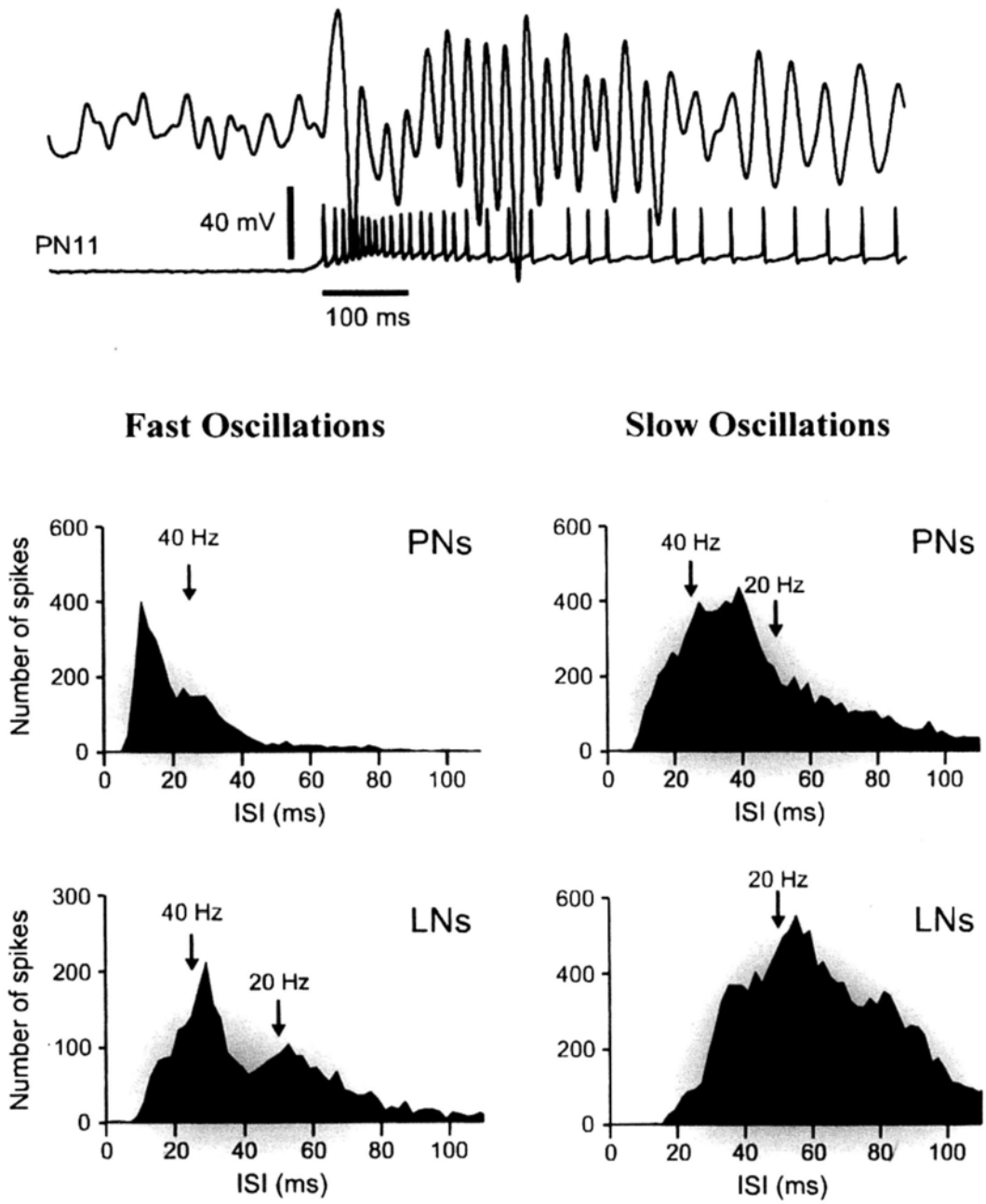

Figure 2.13. Inter-spike interval (ISI) distributions *in vivo* match results from the model.

ISI was computed from spikes occurring during fast (0.5 s analysis bin starting from 0.3 s after the odor onset) and slow (3 s analysis bin starting from 1 s after the odor onset) oscillations in each trial. The same dataset used in Figure 2.4C (spikes pooled from all trials in all animals) was analyzed.

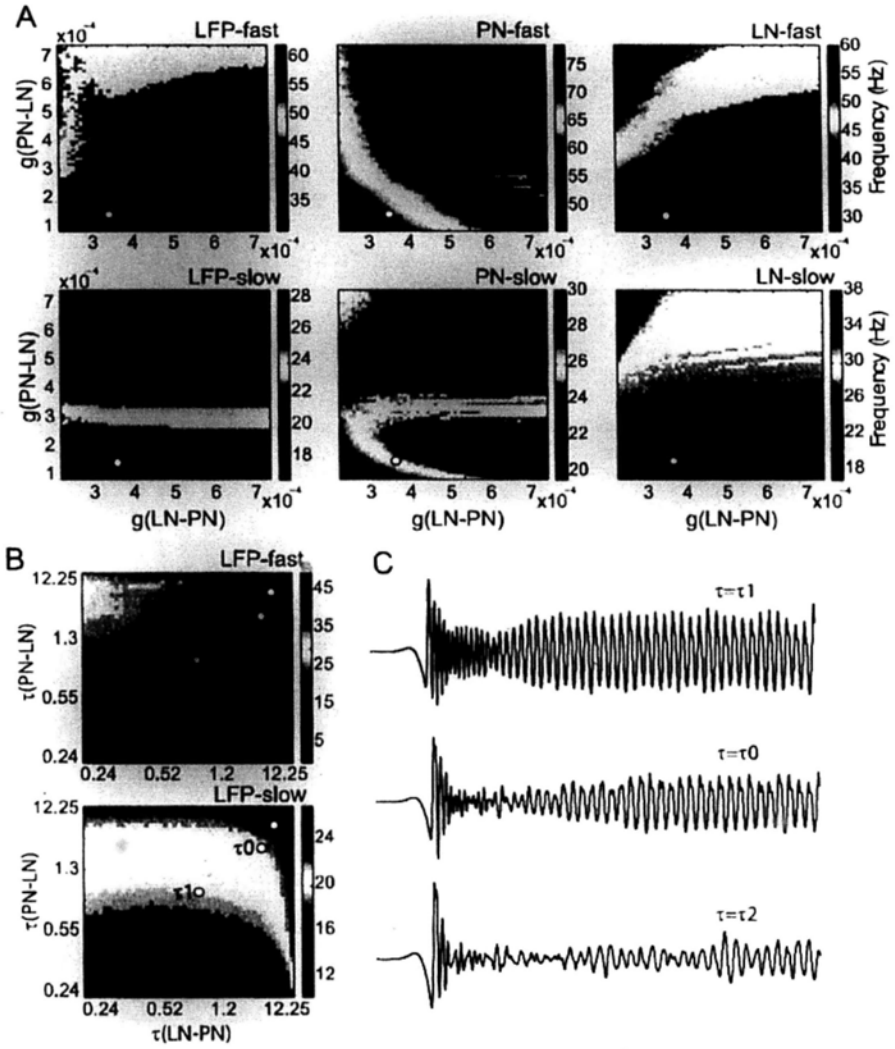

Figure 2.14. Effect of synaptic potential strength and synaptic time constant on oscillation frequency.

(A) Changing the maximal conductances of excitatory (PN-LN) and inhibitory (LN-PN) synapses profoundly affected the frequency of oscillations. Color: frequency; white dots: parameters used for the following simulations. The same frequency of LFP oscillations could be attained in two different network states: (1) PNs fire faster than LFP or LNs (top/left area of the plot) or (2) PNs fire at about the same frequency as LFP or LNs (top/right area of the plot). Increasing the strength of excitatory input from PNs to LNs generally increased the frequency of odor-triggered oscillations (Figure 2.14A, LFP), and the firing rates of LNs usually increased to match the LFP oscillation frequency. However, increasing the strength of PN-LN coupling actually reduced the firing rates of PNs during the initial fast phase of oscillation but increased the firing rates of PNs during the slow phase. In contrast, increasing inhibition from LNs to PNs (beyond the minimal level required to maintain oscillations) had little impact on the frequency of LFP or LN oscillations.

It did, however, decrease the firing rates of PNs, at least, for the lower range of PN-LN conductances (Figure 2.14A, middle column). This fact may explain the difference between the dynamical responses of the moth AL where excitatory PNs fire typically faster than LFP, and in other systems (e.g., cortical gamma oscillations) where spikes in excitatory cells typically skip cycles of LFP oscillations (see Discussion). Notably, the time constants of synaptic input had relatively little influence upon LFP frequency as long as synaptic weights were scaled to keep the integral of postsynaptic current stable over time. (B) Changing the decay time constants of excitatory and inhibitory synapses had less dramatic effects on oscillation frequency. Increasing the time constant of excitation slightly reduced the frequency of oscillations, probably because smaller and longer-lasting EPSPs less efficiently drove spiking in LNs. Varying the time constant of inhibition had minimal impact upon the frequency of oscillations (see Discussion). Oscillations failed when decay time constant of inhibition exceeded ~12 msec. Time constant modifications were accompanied by conductance changes to keep the area under PSP profile constant. (C) Examples of LFP oscillations elicited with different combinations of synaptic time constants shown in [B] (circles). Increasing the decay time constant reduced the amplitude of LFP oscillations, indicating a decrease in synchrony.

How do changes in odor concentration influence the dynamical properties of the AL network? Our model had shown that, for a network with a fixed number of responsive neurons, increasing the amplitude of external stimuli led to a progressive increase in oscillation frequency (Figure 2.12E). But, our recordings from ORNs had shown that, as the concentration of an odorant increased, more types of receptors began to respond (Figure 2.10K; see also Duchamp-Viret *et al.*, 2000; Hallem and Carlson, 2006; Stewart *et al.*, 1979; Wachowiak and Cohen, 2001). To simulate this effect of changing odor concentration we varied the proportion of the PN and LN populations (parameter σ, width of the curve in Figure 2.15A; compare to Figure 2.10K) driven by external excitatory input. We found that varying the size of the stimulated neuronal population only slightly varied the frequency of oscillations (Figure 2.15B-D). When driven by very low odor concentrations ("narrow" input, i.e. σ=0.2), the frequency of LFP oscillations increased slowly upon odor onset (Figure 2.15C left); several oscillatory cycles were required to engage all the neurons in oscillatory dynamics. Our model suggested that the main effect of varying the size of the responsive neuronal population was to vary the coherence of the moth AL network, but not its frequency.

Our results showed that when sensory input underwent adaptation, two factors changed: 1) active PNs decreased their firing rates; and 2) the size of the active PN population decreased (Figure 2.12B,C). To test which factor most directly underlies the oscillator's frequency shift, we provided our model a simplified square input profile rather than a realistic Gaussian input profile; the simplified input drove all stimulated PNs and LNs identically and gave zero input to all non-stimulated PNs and LNs, thus holding the size of the active PN population constant over time even

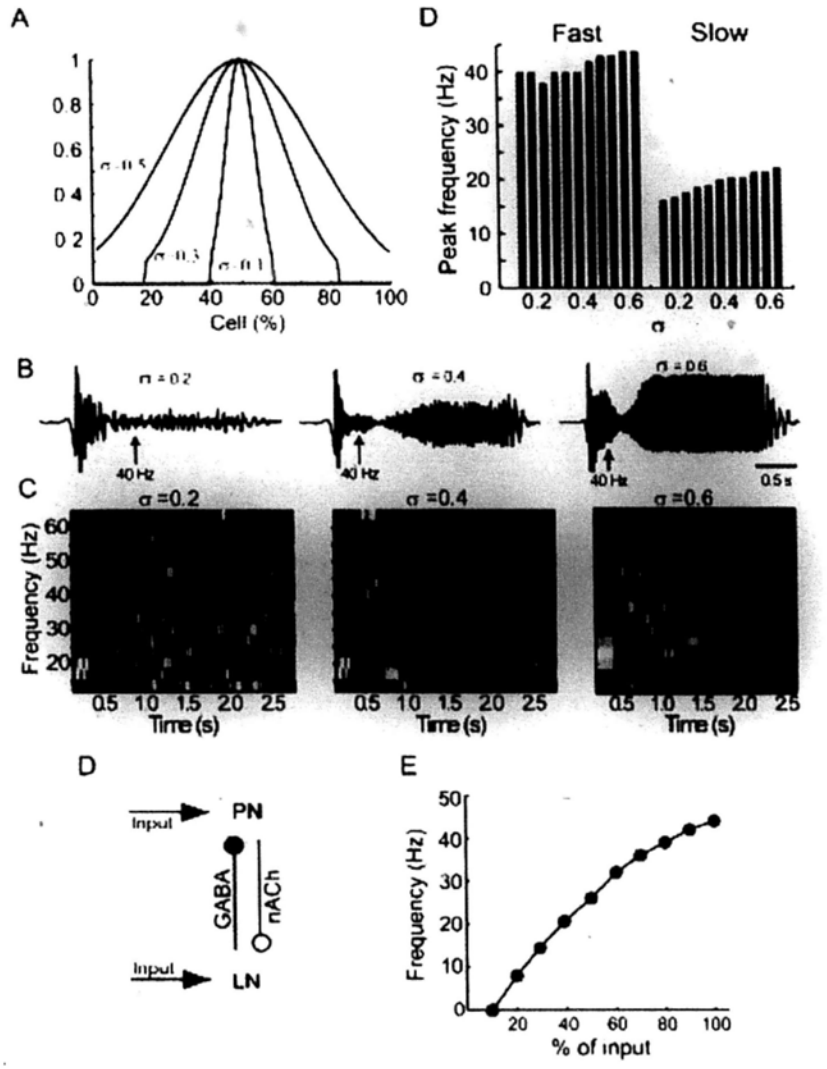

Figure 2.15. Effect of odor concentration upon LFP frequency in moth AL model.

(A) Odor input to the network was simulated by synaptic currents applied to an odor-specific population of PNs and LNs. The size of stimulated population (defined by a Gaussian distribution with width σ; see Figure 2.10K) was varied to simulate different odor concentrations. (B) Examples of LFP oscillations elicited by three odor concentrations. As *in vivo*, during lengthy odor stimuli the network shifted from fast to slow oscillatory states. LFP was band-pass filtered (5-50 Hz). (C) Spectrograms of LFP oscillations (those shown in B) for three odor concentrations. (D) Minimal network consisting of a single PN and LN. (E) Frequency of oscillations in the minimal network increased sub-linearly as a function of input amplitude.

as the input adapted. With this constrained input, adaptation still caused the oscillatory frequency to decrease (Figure 2.16A). In contrast, decreasing the size of the stimulated AL population (to model a decrease in odor concentration) did not affect oscillation frequency (Figure 2.16B). Consistent with this result, an even simpler model consisting of only a single PN and a single LN, reciprocally-coupled (Figure 2.15D), showed that changing the intensity of the input caused a shift in oscillation frequency (Figure 2.15E). Taken together, these models suggest that input intensity regulates the firing frequency of active PNs, which directly determines the network oscillatory frequency.

2.2.7 A subset of strongly activated PNs regulates oscillatory frequency

To test the robustness of our results and to gain a more intuitive understanding of the mechanism that underlies the oscillatory response transition in the AL, we designed an additional, simplified "firing rate" version of our more realistic map-based model of the AL network (see Methods).

To test whether the oscillatory frequency of the AL network is determined by the firing rates of activated PNs, we systematically varied the threshold required to activate PNs, effectively removing weakly-activated ORNs from the network (Figure 2.17A). Even though this manipulation (like decreasing odor concentration) greatly decreased the size of the active population of neurons and caused the overall input to the network to change dramatically (Figure 2.17B), the oscillatory frequency remained constant (Figure 2.17C). Next, we simulated the effect of sensory adaptation by altering the response intensity of the most strongly activated PNs

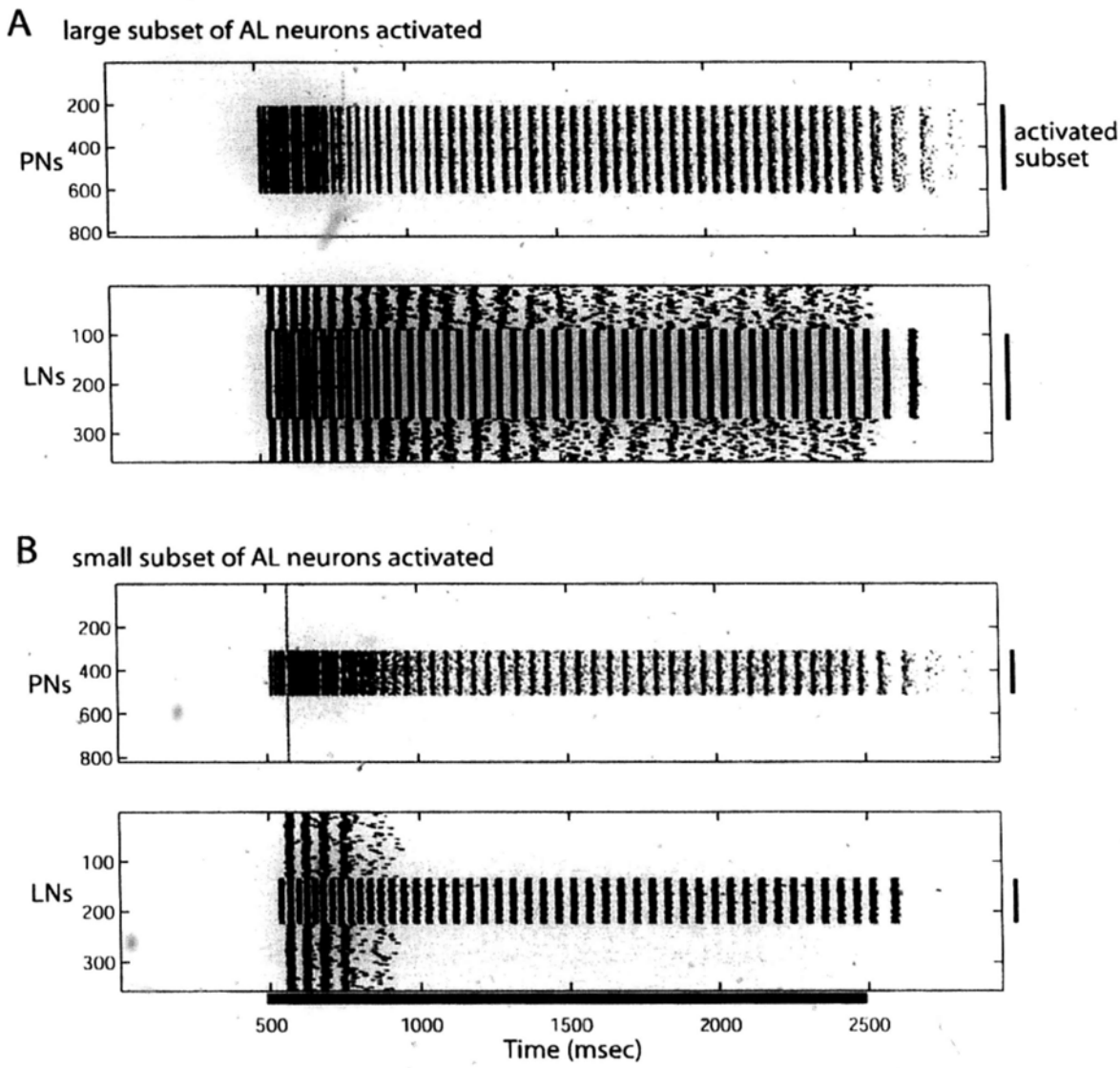

Figure 2.16. Changes in the size of the PN population do not determine oscillation frequency.

(A) The size of the active PN population remained constant over time even when the input underwent adaptation, leading to a frequency shift. (B) To model changes in odor concentration, we reduced the width of the input profile; however, the frequency remained identical to that for wider stimulus.

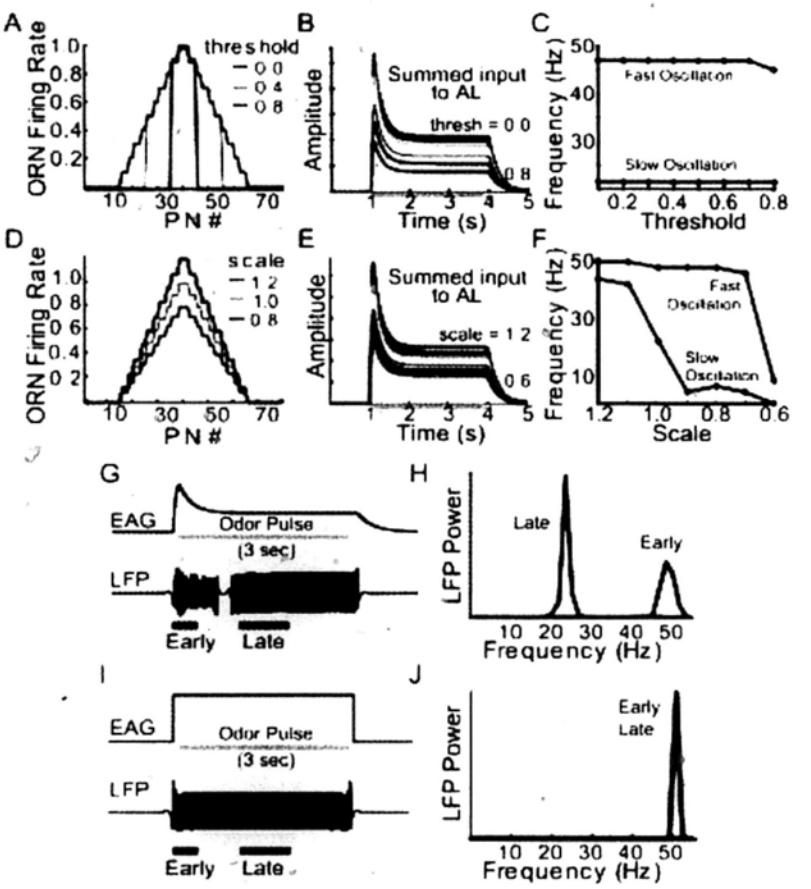

Figure 2.17. Simplified firing-rate model of the moth AL

(A-C) Varying the width of the distribution of responsive PNs (simulating changes in odor concentration, see Figures 2.10K and 2.15A) had no effect on oscillation frequency. (A) Width was varied by adjusting the threshold level for activating PNs. (B) Adjusting the threshold greatly altered overall input to the modeled AL network. (C) The oscillation frequency remained constant despite simulated changes in odor concentration. (D-F) Varying the height of the distribution of responsive PNs (simulating adaptation in ORNs) caused changes in oscillation frequency. (D) Height was altered by scaling the response intensity of activated PNs. (E) Adjusting the intensity greatly altered overall input to the modeled AL network, as in [B]. (F) The frequency of LFP oscillations decreased when adaptation of ORNs was simulated. (G-H) Model EAG (green) and LFP response (black) when ORNs are permitted to adapt. Adaptation alone is sufficient to shift the oscillatory frequency (power spectra for early and late oscillations shown in H). (I-J) Model EAG (green) and LFP response (black) when ORNs are not permitted to adapt. Without adaptation oscillation frequency remains constant (power spectra in J).

(Figure 2.17D). This manipulation, which kept the number of active neurons constant but reduced overall input to the network (compare Figure 2.17B and E), greatly altered oscillatory frequency (Figure 2.17F), consistent with results we obtained with our map-based model and with our physiology experiments.

Further, our simplified rate model showed that adaptation of the ORNs was sufficient to shift the oscillatory frequency of the AL network (Figure 2.17G-H); a version of the model lacking adaptation showed no shift in frequency (Figure 2.17I-J). These results, combined with those of our physiological recordings and map-based model show that, for any given odor or concentration, oscillation frequency is controlled by a small subset of ORNs and PNs, those that are most highly responsive.

In summary, our computational models (Figures 2.12, 2.15, and 2.17) demonstrated that the shifts in LFP frequency we observed *in vivo* during lengthy odor stimulations can be explained by gradual changes in the intensity of output from a stable group of ORNs to the AL. This intensity level is determined mainly by the adaptation and saturation of the ORNs rather than by the intensity of the environmental stimulus (odor concentration). Our results show that, in the periphery, the great majority of the olfactory system's dynamic range is encoded by the size of the responsive receptor population rather than by its firing rate. Our results also resolve an apparent contradiction, that oscillation frequency follows the intensity of the net receptor output (amplitude of the EAG) but not the concentration of the odor. These findings are summarized in Figure 2.18.

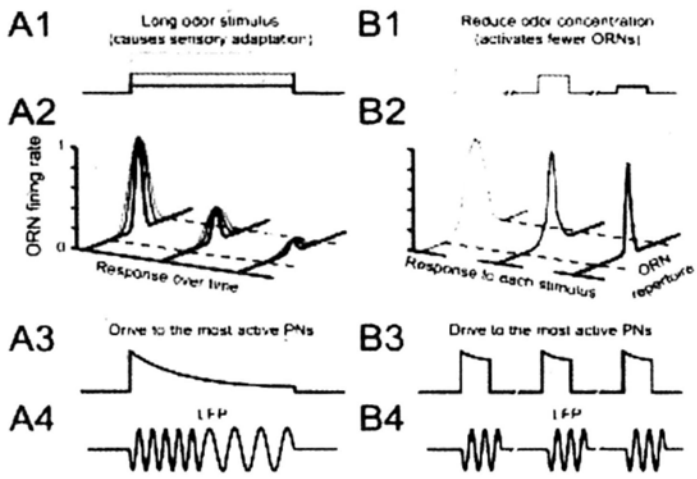

Figure 2.18. Summary of the mechanism to determine oscillation frequency. (A1) Long odor pulses cause ORNs to undergo sensory adaptation. (A2) When odor exposure is lengthy, active ORNs adapt, decreasing their firing rates. (A3) The lower ORN firing rates reduce excitatory drive to PNs. (A4) As each PN receives less intense input, its firing rate decreases and oscillations slow. (B1) When odor concentration is reduced, smaller populations of ORNs respond. (B2) However, the responsive ORNs continue to fire at high rates. (B3) Thus, the most active PNs continue to receive strong input from responsive ORNs. (B4) and oscillation frequency remains stable across broad ranges of odor concentration.

2.3 Discussion

2.3.1 Odor elicited oscillations in the moth

In the moth *Manduca sexta*, our intracellular recordings from PNs, LNs and KCs together with recordings of the LFP from the MB and AL (Figures 2.1, 2.4, and 2.6) revealed that moths employ essentially the same neural mechanism as that characterized in the locust and *Drosophila*: oscillations are generated in the AL via $GABA_A$-type inhibition (Figure 2.5), build up gradually over repeated odor presentations (Figure 2.2; Stopfer and Laurent, 1999) and influence the fine spike timing of downstream KCs (Assisi *et al.*, 2007; Laurent, 2002; Perez-Orive *et al.*, 2002; Tanaka *et al.*, 2009).

This result contradicts several earlier reports. Previously, in the moth, pulses of pheromone were found to induce highly localized LFP oscillations only within the AL, with spikes in pheromone-sensitive PNs phase-locked to the AL-LFP oscillations (Heinbockel *et al.*, 1998). However, such stimuli were described as never producing coherent LFP oscillations between the MB and the AL (Christensen *et al.*, 2003). Further, in a multi-unit recording experiment (Christensen *et al.*, 2000) and a double intracellular recording experiment (Lei *et al.*, 2002), cross-correlation analyses detected no sustained oscillatory synchrony between pairs of PNs but rather only brief, stimulus-locked, non-oscillatory synchrony. These observations led to the proposal that, in *Manduca*, only transient, non-oscillatory synchronous activity among PNs supports odor coding, likely by promoting coincidence detection by downstream elements (Lei *et al.*, 2002). Our experiments employed general, non-pheromonal odors, such as host plant volatiles and common food blends at a

wide range of concentrations. The differences in our results from those reported earlier probably arise both from our focus on the general olfactory system rather than the pheromone system, and from differences in recording techniques (likely the electrode's shape and internal solution; see Methods). The moth pheromone system, which, within the AL, consists of three specialized glomeruli anatomically separate from the ~60 glomeruli of the general odor system (Rospars and Hildebrand, 1992), may not provide an ideal model for all aspects of general olfaction.

Indeed, our results show that, to a remarkable extent, odor coding mechanisms in *Manduca* are similar to those of other species, including *Drosophila* (Tanaka *et al.*, 2009), honeybee (Stopfer *et al.*, 1997), and locust (Laurent and Naraghi, 1994; MacLeod and Laurent, 1996; Perez-Orive *et al.*, 2002). This was perhaps unexpected because these species differ in details of olfactory anatomy and physiology. The ~60 ordinary glomeruli in the AL of *Manduca* compare roughly in number to many other insects (Anton and Homberg, 1999), and the great majority of its PNs are uniglomerular (Homberg *et al.*, 1989). By contrast, in the locust, the AL is organized into ~1000 microglomeruli (Ernst *et al.*, 1977) which are heavily interconnected through multiglomerular PNs (each visiting 12-24 glomeruli), and extensively arborized LNs (MacLeod and Laurent, 1996). In *Manduca* LNs generate full-size sodium spikes. But in the locust, LNs produce graded calcium potentials rather than all-or-none spikes. Because of its microglomerular structure and extensive multiglomerular connectivity, the locust olfactory system has sometimes been described as atypical (Hansson and Anton, 2000). Nevertheless, our results strongly suggest that, despite substantial differences in anatomical detail, the olfactory systems of these species function in a remarkably similar fashion.

Despite the striking similarities in odor coding mechanisms in locust and moth, we found small differences. The oscillatory phase relationship between spikes in PNs and LNs is slightly different in the two animals, possibly because of differences in the timing of spikes in LNs. In the locust the population of PNs spikes with the greatest synchrony upon odor onset (Mazor and Laurent, 2005) probably because the strong, non-adapted input can activate many LNs which coordinate the spike timings of PNs (Assisi *et al.*, 2007). In the moth, we found that odor inputs were strongest at the odor onset as well (Figure 2.10C,D). However, both across LNs and PNs, synchrony increased gradually over the course of a response (Figure 2.7). This is probably because, in the moth, oscillation frequency at the odor's onset shifted too quickly to permit full entrainment of the oscillatory network. Indeed, frequency shifts we observed in the moth over the course of a stimulus were typically greater than those in the locust (Figure 2.3; see also Perez-Orive, 2004). Our simplified rate model suggests this difference could be explained by greater net inhibition in the locust: we found that if we slightly increased the strength of inhibition in our simplified model of the moth AL, the model then produced frequency shifts similar to those observed in the locust (Figure 2.19). We speculate that, compared to the moth, the balance of net excitation and inhibition is slightly shifted toward stronger inhibition in locust.

2.3.2 Adaptation and saturation of ORN firing rate determine the oscillation frequency

Our recordings revealed that additional ORNs were recruited into the responsive population as odor concentration increased (Figure 2.10), a result consistent with a fundamental property of receptors: they become less selective as the concentrations

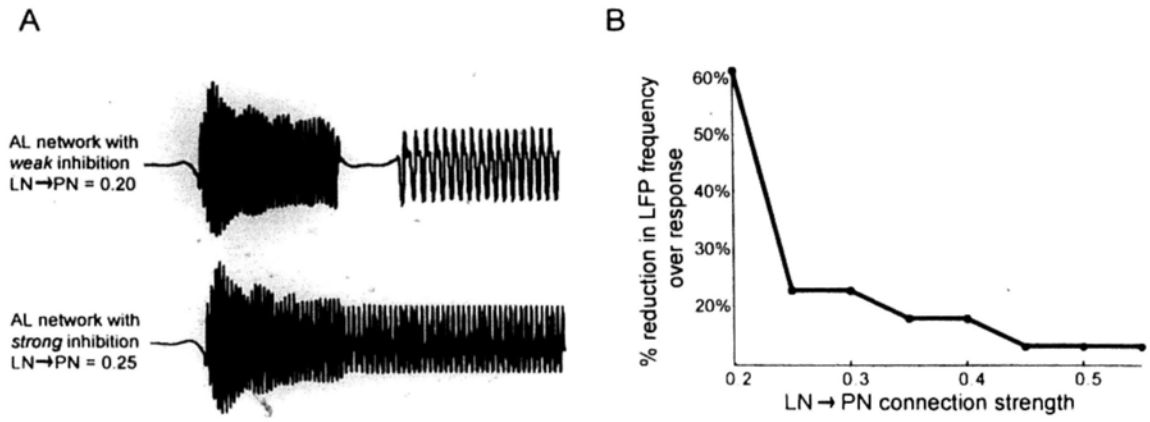

Figure 2.19. Overall strength of inhibition within the AL helps determine its response to adapting input.

(A) LFP oscillations driven by the same adapting odor input in models with relatively weak or strong overall inhibition. The network with weak inhibition resembles results obtained from the moth; the network with stronger inhibition resembles results obtained from the locust. (B) Relationship between the strength of inhibition and the shift in oscillatory frequency over the course of a response to a simulated odor pulse: When the strength of inhibition from LNs to PNs was set to be high, initially fast oscillations slowed down and then stabilized at a lower frequency.

of ligands increase. Yet, we found the range of response intensity of these ORNs was sharply constrained. Long odor pulses caused the most highly responsive ORNs to rapidly adapt their firing rates, with a time course similar to that of the shift in oscillation frequency (Figure 2.10L). Further, the firing rates of the most precisely tuned ORNs saturated when stimulated by low to moderate odor concentrations (Figure 2.10C-F).

Our electrophysiological and computational approaches allowed us to compare the relative contributions of the size of the responsive population and its response intensity. We found that in the periphery, coding of odor concentration was heavily dominated by the size of the set of responsive ORNs rather than by the intensity of

the response of the ORNs. At low odor concentrations, only those receptors most precisely tuned to the odor responded; as the concentration increased, the precisely-tuned ORNs continued to fire, but quickly adapted and saturated, and thus displayed strictly constrained increases in response intensity. However, additional, less well tuned ORNs began to participate in the response, thus encoding the concentration of the odor.

Several lines of evidence indicate that information about odors is encoded by a population of ORNs in a combinatorial fashion (Buck, 1996). A recent comprehensive study of all the receptor types on the *Drosophila* antenna (Hallem and Carlson, 2006) showed that the firing rates of ORNs often saturated at moderate concentration, that some ORNs decreased their firing rates at extremely high concentrations, and that, at high concentrations, individual ORNs tended to respond broadly to many odors. Studies using 2-deoxyglucose labeling, c-fos and calcium images have shown that the spatial pattern of glomerular activation can expand as odor concentration increases (for review, see Buck, 1996). Further, several studies suggest that ORNs can respond within a narrow dynamic range (Firestein *et al.*, 1993; Koulakov *et al.*, 2007; Stewart *et al.*, 1979). Indeed, a theoretical study of the locust olfactory system predicted that an intensity coding scheme like that shown here could explain the invariant frequency of odor-evoked oscillations over a wide range of stimulus intensity (Asissi *et al.*, 2007). These results are consistent with our quantitative finding that odor intensity is encoded mainly by the size of active ORN population rather than by firing rates.

We incorporated our findings in the moth into two types of computational models to determine how sensory input to an oscillatory circuit influences its frequency. Our

models robustly mimicked the frequency transition we observed between fast and slow oscillatory states as input intensity gradually decreased (Figures 2.12, 2.15, 2.17, and 2.19). Further, our models demonstrated that recruiting additional, but less well-tuned, ORNs could simulate responses to higher odor concentrations while causing only minimal changes in oscillation frequency (Figures 2.15, 2.17), similar to what we observed *in vivo* (Figures 2.8, 2.10). Our models also demonstrated how oscillation frequency can shift between fast and slow states (Figures 2.12, 2.17), depending mainly upon the varying output intensity of rapidly saturating and adapting receptors, rather than upon odor concentration.

In agreement with earlier work in locust (Stopfer *et al.*, 2003) our results show that increases in odor concentration led to large increases in the coherence of the odor-triggered oscillatory synchrony of PNs (Figure 2.8C). This large increase in coherence was accompanied by only small changes in the frequency of oscillation (Figure 2.8D), and was caused mainly by increasing the size of the activated ORN population. Our results show that, in the moth AL, the coherence and the firing rate of the PN ensemble are determined independently (for a discussion of theory see Salinas and Sejnowski, 2001). This independence enables an efficient strategy for dynamically matching the firing properties of PNs to the coincidence detection-based decoding properties of KCs (Perez-Orive *et al.*, 2002; Perez-Orive *et al.*, 2004).

What are the implications of this transition during an odor response? A comparison of the jitter in spike timing relative to the LFP before and after the frequency transition revealed an increase in spike time precision in LNs, PNs and KCs (Figure 2.7). Because little is known about how the output of KCs is decoded by cells that follow them, potential benefits of this increase in spike precision are not immediately

apparent. One possibility is that the increase in the synchrony of input to the KCs might help sustain highly specific firing in these cells even though the output of PNs decreases when ORNs adapt.

A similar frequency transition from gamma to beta oscillations has been noted in the rat olfactory bulb (Neville and Haberly, 2003), but the mechanism underlying the transition is quite different from that shown here. In the rat, oscillations of different frequency are generated by different neural circuits: odor-evoked gamma oscillations in the olfactory bulb arise locally, but beta oscillations require the participation of the olfactory cortex (Neville and Haberly, 2003).

It is well established that shifts in the balance of excitation and inhibition (Brunel and Wang, 2003) or changes in excitatory drive (Traub *et al.*, 1996; Whittington *et al.*, 1995) can influence the oscillation frequency of a neural network. However, sensory systems characterized *in vivo* often generate oscillations of invariant frequency when driven by a wide range of stimulus intensities (Bringuier *et al.*, 1997; Schadow *et al.*, 2007; Stopfer *et al.*, 2003). Our results suggest the extent to which oscillation frequency is sensitive to stimulus intensity depends at least in part on the properties (such as adaptation and saturation) of the neurons that provide inputs to the oscillatory network. In the retina, for example, some classes of ganglion cells have been shown to increase their firing rates as the velocity of a moving visual stimulus increases (Cleland and Harding, 1983); concomitantly, the frequency of gamma oscillations in the visual cortex monotonically increases (Gray and Prisco, 1997). On the other hand, in cortical areas responsive to the orientation or direction of a visual stimulus, oscillation frequency remains constant (Gray and Singer, 1989), likely because changing these stimuli only changes the population of active cells.

That many primary sensory neurons display tuning, saturation and adaptation characteristics may help explain why invariant oscillation frequency is often observed in sensory systems (Bringuier *et al.*, 1997; Schadow *et al.*, 2007; Stopfer *et al.*, 2003).

2.3.3 Oscillatory dynamics and fast-firing principal neurons

Fast 20-60 Hz synchronized oscillations are common in neuronal circuits. In one form of gamma oscillations (Interneuron Network Gamma, ING) a network of mutually inhibiting interneurons exclusively establishes the rhythm; pyramidal cells are simply entrained to it, and their low firing rates have little or no effect on network oscillations (Wang and Buzsaki 1996; Whittington *et al*, 2000). But in our models oscillations failed when synaptic input from PNs to LNs was blocked (data not shown). This suggests odor triggered oscillations in the moth AL are not entirely mediated by an ING-type inhibitory network but rather require the active participation of excitatory PNs to drive LNs (indeed, we observed that moth PNs fired slightly before LNs; Figure 2.4C) which in turn synchronized PNs through feedback inhibition. In this respect, odor triggered oscillations in the moth AL are similar to the persistent/transient forms of gamma oscillations (Pyramidal-Interneuron Network Gamma, PING) in the vertebrate cortex and hippocampus.

Our intracellular recordings from the AL network revealed, however, an unusual situation: most active PNs fired faster than the oscillation frequency (Figure 2.13). More typically, as in the case of transient gamma oscillations induced by tetanic stimulation of the hippocampus (Traub *et al.*, 1996; Whittington *et al.*, 1997), fast spiking interneurons and pyramidal cells both fire at the oscillation frequency. Also,

during persistent gamma activity in CA3 (Fisahn *et al.*, 1998) and neocortex (Buhl *et al.*, 1998), interneurons fire on every cycle or every other cycle; pyramidal cells fire at much lower rates. Notably, our model demonstrated that stable oscillations can nevertheless emerge from a network with fast-firing PNs (Figures 2.12B-D), a condition thought to be unstable since excessive excitatory feedback from PNs to LNs could potentially disrupt the rhythmic LN network.

The stability of the regime we observed in the moth could be explained by the combination of high-rate excitation and relatively low-efficiency $GABA_A$-mediated inhibition revealed by our recordings and our models. The overall weak inhibition we found in the moth AL (Figure 2.19) could also explain the relatively weak dependency of the network oscillation frequency upon the decay time constant of inhibition. Indeed, if fast, GABAergic inhibition were strong enough to prevent excitatory cells from firing, oscillatory frequency would depend strongly on the time constant of inhibition (Bazhenov *et al.*, 2008; Brunel and Wang, 2003; Buzsáki and Chrobak, 1995; Whittington *et al.*, 1995), something we did not observe here (Figure 2.14B,C). In moth, the net impact of inhibition seems restricted to influencing the timing of spikes in excitatory neurons, thus enabling periodic network rhythms. However, this inhibition appears too weak to prevent excitatory cells from firing, enabling them to maintain firing frequencies that exceed the network oscillation frequency. The oscillatory regime revealed here may be common, particularly in insects; unlike pyramidal cells, PNs in the AL of honeybee (Stopfer *et al.*, 1997), locust (Stopfer *et al.*, 2003), and *Drosophila* (Olsen *et al.*, 2007) can respond to stimuli with high firing rates.

2.4 Methods

Olfactory stimulation

Odor stimulation was modified from Brown *et al* (2005). Briefly, the odorized headspace in 60-ml glass bottles above mineral oil-diluted odorant solution (10 mL) was pushed by a controlled volume of humidified air (0.1 L/min) into an activated carbon-filtered, humidified air stream (0.75 L/min) flowing continuously across the antenna. The longest stimulus we used (4-s) would deplete only about 13% of the vapor in the headspace, making it likely that each odor pulse varied little in concentration throughout each stimulus. All chemicals were purchased from Sigma-Aldrich (St. Louis, MO) unless otherwise noted. Odorants were benzylalcohol, benzaldehyde, (+)-β-citronellene (Fluka Chemika, Buchs, Switzerland), cyclohexanone, geraniol, hexanol, cis-3-hexenyl acetate, (±)linalool (Aldrich Chemical Company Inc, Milwaukee, WI), methyl salicylate, methyl jasmonate, 1-octanol (Fluka Chemika, Buchs, Switzerland), trans-2-hexenal, trans-2-hexen-1-ol, oil extracts (strawberry, cinnamon, peach, lime, jasmine (Balducci's, Bethesda, MD), thyme (Thyme Red, Saidel Inc., Renton, WA), and wintergreen (Wagner's). Odorant solutions were diluted (vol/vol) to 1% in mineral oil (J.T. Baker, Phillipsburg, NJ) unless otherwise noted.

Electrophysiology

Physiological data were obtained from 145 adult moths (*Manduca sexta*) of both sexes reared from eggs (purchased from the NCSU Insectary, Raleigh, NC) in our laboratory on an artificial diet (Bell and Joachim, 1976), under a long-day photoperiod at 26 °C, and at more than 70% relative humidity. Adults 1 d

post-eclosion or older were dissected as described previously (Ito *et al.*, 2008 - this work, see Chapter 3). The head capsule was superfused with moth physiological saline (Christensen and Hildebrand, 1987) at room temperature.

EAGs were recorded using Ag/AgCl wire (127 μm o.d.) inserted into the distal tip of the antenna; the reference wire was inserted into the contralateral compound eye. Signals were amplified with a DC amplifier (Model 440; BrownLee Precision, San Jose, CA).

LFPs were recorded using saline-filled glass micropipettes with a long shank (o.d. ~3 μm, 4-10 MΩ), amplified and low-pass filtered (>100 Hz) by a DC amplifier (Brown-Lee Model 440). The long shank could be inserted deep into the calyx of the MB where axons of PNs and the dendrites of followers Kenyon cells make synaptic contacts. This technique allowed us to record LFP oscillations more robust than those we could detect by the method we use in locust (a blunt ended glass electrode with a short shank placed on the cell body layer of the MB; see Brown *et al.*, 2005).

Extracellular recordings of ORNs from were made from sensilla in either isolated antennae cut at their bases or intact antennae of restrained animals (both methods yielded identical results). The antenna was stabilized with epoxy carefully applied to leave the leading surface (where sensilla are located) accessible. An electrochemically-sharpened tungsten wire was inserted into the sensillar base under a stereomicroscope (Leica MZ7.5). For isolated antenna preparations, Ag/AgCl wires were placed in the cut ends. The proximal cut end was immersed in a drop of saline or sensillum lymph (Kaissling, 1995) which was covered with wax to prevent evaporation. For intact antenna preparations, Ag/AgCl wires were placed in the

distal end of the antenna and the contralateral compound eye. Signals were amplified by a differential amplifier (P55, GRASS Instruments; Telefactor, W. Warwick, RI) and sampled at 15 kHz (LabView software, PCI-MIO-16E-4 DAQ cards, National Instruments).

Intracellular recordings, subsequent fluorescent dye injection, histological steps and confocal imaging were made using sharp glass micropipettes as described previously (Ito *et al.*, 2008 - this work, see Chapter 3).

Full scale AL network model

The AL model included 820 PNs and 360 LNs (Homberg *et al.*, 1989) simulated using a reduced neuron model written in the form of difference equations (map; Rulkov 2002; Rulkov *et al.* 2004; Bazhenov *et al.* 2005; Rulkov and Bazhenov, 2008). The time evolution of membrane voltage V_n was described as nonlinear map $V_{n+1} = f_\alpha(V_n, I_n + \beta^e I_n^{ext})$, where I_n is a slow dynamical variable describing the effects of slow conductances, f_α is nonlinear function and n is a discrete time step (~0.5 ms). The model's properties and parameters are shown in Figure 2.20. This model, despite its low intrinsic dimensionality, produces a rich repertoire of dynamics and is able to mimic the dynamics of Hodgkin-Huxley type neurons both at the single cell level and in the context of network dynamics (Bazhenov *et al*, 2005; Rulkov *et al*, 2004; Rulkov and Bazhenov, 2008).

For synaptic connections, we used conventional first order kinetic models of fast synaptic conductances (Bazhenov *et al.* 2005; Rulkov *et al.* 2004) (see Figure 2.20). All intrinsic connections (LN-LN, LN->PN, PN->LN) were random with 0.5 probabilities. Maximal conductances (in dimensionless units; see Rulkov *et al.*,

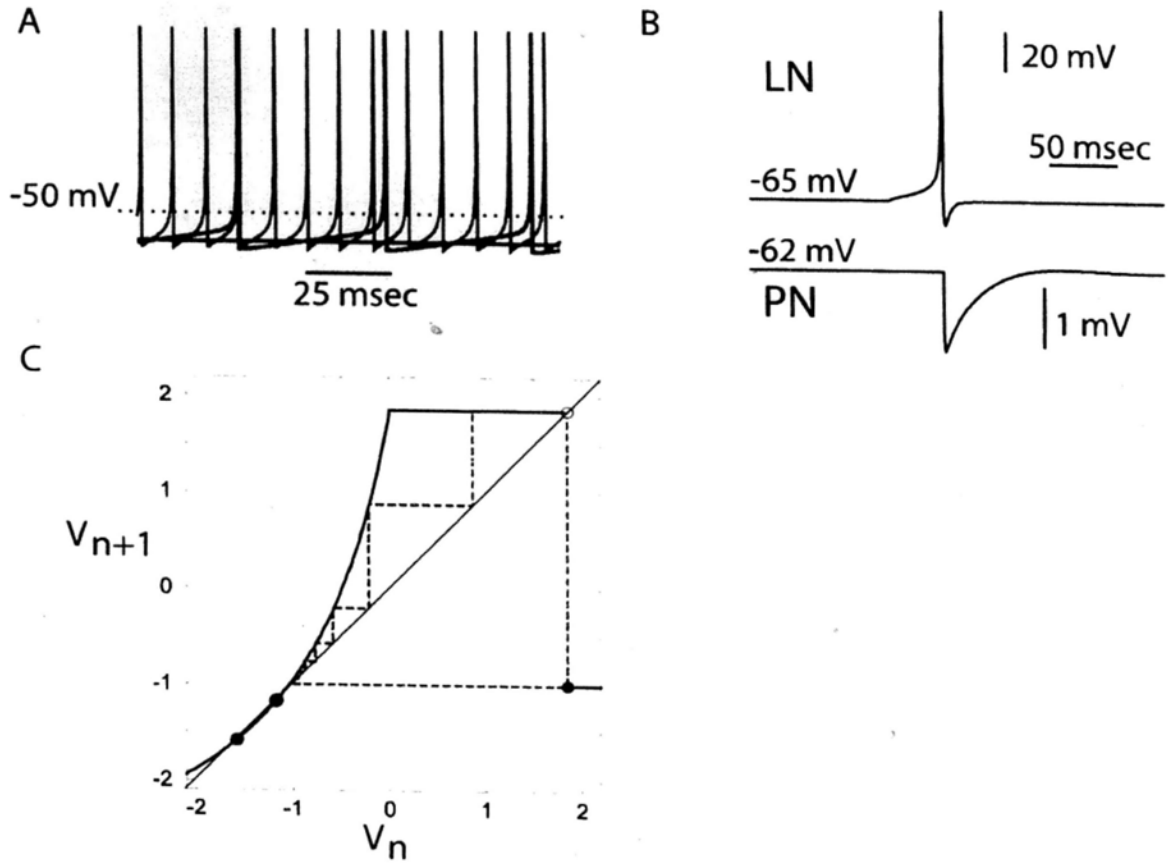

Figure 2.20. Reduced spiking models of the AL neurons.
Spiking neurons are described by the following reduced equations:

$$V_{n+1} = f_\alpha(V_n, I_n + \beta^e I_n^{ext}),\ I_{n+1} = I_n - \mu(V_n + 1) + \mu\sigma + \mu\sigma^e I_n^{ext},$$

$$f_\alpha(V_n, I_n) = \begin{cases} \alpha\ (1-V_n)^{-1} + I_n\ , & V_n \le 0 \\ \alpha + I_n\ , & 0 < V_n < \alpha + I_n \text{ and } V_{n-1} \le 0 \\ -1\ , & \alpha + I_n \le V_n \text{ or } V_{n-1} > 0 \end{cases}$$

where V_n is the membrane voltage, I_n is a slow dynamical variable describing the effects of slow conductances, and n is a discrete time step (=0.5 ms). Slow time evolution of I_n is achieved by using small values of the parameter $\mu << 1$. To convert the dimensionless "membrane potential" V to the physiological membrane potential V_{ph}, the following equation is applied: V_{ph}=*V*50-15* [mV]. The PN model parameters were set at $\alpha = 3.65$, $\sigma = 0.06$, $\mu = 0.0005$, $\beta^e = 0.133$, $\sigma^e = 1$. For LN model only first equation describing fast dynamics was used and parameters were set at $\alpha = 3.8$, $I = -2.9$, $\beta^e = 0.05$. The model parameter σ sets the resting

potential of PN neuron and, therefore, its state with respect to spiking threshold. To ensure variability of the resting potentials across population of neurons, this parameter was picked randomly from a uniform distribution with 2% variability.

To model synaptic interconnections, we used conventional first order kinetic models of synaptic conductances rewritten in the form of difference equations:

$$I_n^{syn} = -g_n^{syn}(V_n^{post} - V_{rp}), \qquad g_{n+1}^{syn} = \gamma g_n^{syn} - \begin{cases} g_{syn}, & \text{spike}_{pre}, \\ 0, & \text{otherwise}, \end{cases}$$

where g_{syn} is the strength of synaptic coupling, and indices *pre* and *post* stand for the presynaptic and postsynaptic variables, respectively. The first condition, "spike$_{pre}$", is satisfied when presynaptic spikes are generated. Parameter γ determines synaptic time constant $\tau = -1/\ln\gamma$ ($\gamma = 0.85$ for excitatory synapses and $\gamma = 0.8$ for inhibitory synapses); V_{rp} defines the reversal potential and, therefore, the type of synapse: excitatory or inhibitory ($V_{rp} = 0$ for excitatory synapses and $V_{rp} = -1.1$ for inhibitory synapses).

(A) Steady-state response pattern of an isolated PN neuron for 3 different levels of the resting potential. Black – σ=0.06, green – σ =0.09, blue – σ =0.17. (B) IPSP in the postsynaptic PN neuron (bottom trace) triggered by a spike in presynaptic LN neurons (top trace). (C) Function $f_\alpha(V_n, I_n)$ (red line) and the dynamics of the V_n (green line) computed with $\alpha = 5.6$ and fixed value of $I_n = -3.75$. The open circle at the function curve emphasizes that this point does not belong to the diagonal. Green and blue circles indicate equilibrium points of the voltage equation (Rulkov and Bazhenov, 2008).

2004) denoting the total excitation and inhibition received by a given cell were set in most of the simulations to G_{ACh}(PN-LN) = 0.00015, G_{GABA}(LN-PN) = 0.00035, G_{GABA}(LN-LN) = 0.00015.

The intensity (amplitude) of external (to mimic odor) stimuli to PNs and LNs followed a Gaussian distribution truncated at 0.1 to avoid stimulating all PNs (see Figure 2.15A). Which PNs and LNs received input with a particular intensity was determined randomly. The proportion of LNs receiving non-zero input was approximately one third that of PNs receiving non-zero input. For simplicity, we assumed that all ORNs (not only the best tuned ones) undergo sensory adaptation. To mimic data obtained *in vivo*, the temporal variation of the stimulus was approximated by the experimentally-measured function shown in Figure 2.10L.

Simplified firing rate model

This simplified model contained 80 PNs and 30 LNs; qualitatively similar results were obtained with a version of the model containing 800 PNs and 300 LNs. The dynamics of each neuron in the network was modeled as a difference equation:

$$\frac{dv_j}{dt} = -\frac{v_j(t)}{\tau} + \sum_{k=1}^{N} W_{kj}\varphi(v_k(t)) + I_j$$

where v_k is the firing rate of neuron k, τ is the membrane time constant of neuron (τ = 10 ms) and φ is a non-linear logistic function ($\varphi(x) = [1 + \exp(-a_1 \cdot (x - a_2))]^{-1}$; a_1 = 10, a_2 = 0.6). I_j is the input from *ORN* type j to PN_j. LNs did not receive direct input from ORNs. The connectivity matrix W included 50% connection probability: PN->LN (W_{PN_LN} = 0.125) and LN->PN (W_{LN_PN} = -0.2). No PN->PN or LN->LN connections were included. The integration step size (dt) was set to 1 ms. The

model LFP was computed by filtering summed PN activity (V). Since the number of PNs was reduced in this model, LFP traces shown appear noisy.

Each ORN response was modeled after our physiological recordings. The initial response from baseline to peak amplitude followed $t \cdot \exp(-t/\tau_{rise})$. Subsequently, ORN responses were reduced to reach an adapted state set at 60% of the peak amplitude following $\exp(-t/\tau_{adapt})$. Finally, after the odorant was removed, ORN responses returned back to baseline following $\exp(-t/\tau_{fall})$. τ_{rise}, τ_{adapt}, τ_{fall} for all 80 ORNs were set to 100 ms, 200 ms and 250 ms, respectively. For any odor 40% of PNs received non-zero ORN input. Peak ORN response amplitude was uniformly, randomly distributed between [0,1]. Model EAG responses (Figure 2.17G,I) were computed by summing individual ORN firing-rate responses.

Data analysis

All analyses except for spike sorting were performed using custom programs in MATLAB (MathWorks Inc., Natick, MA). For experiments examining the effect of odor pulse duration on oscillation frequency, 10 pre-trials (4 s) were first delivered to elicit short-term "fast learning" response plasticity (Stopfer and Laurent, 1999), and then 100, 250, 500, 750, 1000, 1500 ms duration pulses were examined in a pseudorandom sequence; this set was repeated 3 times in each animal. Spectrograms (500 ms sliding Hamming window with 90% overlap) were normalized by the maximum value in the last pre-trial. Results from 18 trials each from 3 animals of either sex (each animal tested with 2 odors) were averaged.

We used a magnitude squared coherence measure in Figure 2.1F to compare LFPs recorded in the AL and the MB; this approach allowed us to minimize the effect of

small variations in phase we found in AL recordings caused by differences in electrode placement. We calculated the magnitude squared coherence using an overlapping sliding Hamming window (0.25 s with 80% overlap) for fast (0.25-1 s) and slow (1-4 s) oscillations. For Figure 2.6B, which did not require phase comparisons across brain structures, we used the more standard cross-correlation measure.

We computed the phase of each spike relative to MB oscillations for fast (0.3-0.8 s) and slow (0.8-4 s) oscillations as described elsewhere (Mazor and Laurent, 2005) but modified as follows. LFP signals were acquired through an analog low-pass filter (>100 Hz) of a DC amplifier (BrownLee Model 440), which imposed a 7 ms delay, which we compensated for in MATLAB. For the phase analysis, LFP signals were then digitally filtered (5-55 Hz, Butterworth; zero phase distortion by filtfilt command in MATLAB).

We measured the frequencies of LFP oscillations evoked by different concentrations of three odors, each tested in blocks of 10 trials that were given in a randomized order. Power spectra were computed using the time series in the first 0.5 s of odor responses as well as in the 1 s before the odor responses (basal activity) and then averaged across 10 trials. The oscillation frequency was determined as the frequency with the maximum power in 14-54 Hz band in the average power spectrum.

Spike sorting of sensillum recordings was performed offline using Spike-o-Matic software (Pouzat *et al.*, 2002) implemented in Igor Pro (Wavemetrics, Lake Oswego, OR). In ORNs, spike amplitude can change somewhat as ORNs adapt to odors; to accommodate small changes in spike amplitude we allowed each cell cluster to

include events with varying amplitudes as long as different sorted clusters remained well-separated (by at least 5 times noise standard deviation), and, within a cluster, an appropriate inter-spike interval distribution was maintained throughout an experiment. For the population firing rate analysis shown in Figure 2.10D,E, in addition to well-sorted units, we included unsorted data as multiunit activity from a single sensillum. All other panels in Figure 2.10 include only well-sorted ORNs.

To fit the concentration responses of ORNs, we first counted the number of spikes in the first 1 s of odor response (same analysis bin as F1 in Figure 2.10D) and averaged over 10 trials for each concentration. Similarly, the baseline activity was measured from the 2 s just before the odor onset. ORN-odor combinations not showing odor-elicited changes in spiking (<5 spikes/response) were not included in this analysis.

2.5 Acknowledgements

The work presented in this chapter was previously published in *Neuron*, vol. 64, Iori Ito, Maxim Bazhenov, Rose Chik-ying Ong, Baranidharan Raman, and Mark Stopfer, "Frequency Transitions in Odor-Evoked Neural Oscillations," pp 692-706, 2009. This work is the product of a highly collaborative project among the authors. I contributed to moth electroatennogram, Kenyon cell intracellular, and sensilla recordings. Iori Ito contributed to electrophysiological recordings and computational modeling. Maxim Bazhenov and Baranidharan Raman performed computational modeling.

We are grateful to members of the Stopfer and Bazhenov laboratories for helpful discussions and to Dr. Marit Stranden for sensilla lessons. We also thank Dr. Kui Sun

for her excellent animal care. Microscopy imaging was performed at the Microscopy & Imaging Core (National Institute of Child Health and Human Development, NIH) with the kind assistance of Dr. Vincent Schram. This work was supported by the Japan Society for the Promotion of Science (00169, 70510) to I.I., Joint NIH-NIST postdoctoral fellowship award by National Research Council to B.R., grants from NIH-NIDCD and NIH-NINDS to M.B. and an intramural grant from NIH-NICHD to M.S.

3 Sparse odor representation and olfactory learning

Sensory systems create neural representations of environmental stimuli and these representations can be associated with other stimuli through learning. Are spike patterns the neural representations that get directly associated with reinforcement during conditioning? In the moth *Manduca sexta*, we found that odor presentations that support associative conditioning elicited only one or two spikes on the odor's onset (and sometimes offset) in each of a small fraction of Kenyon cells. Using associative conditioning procedures that effectively induced learning and varying the timing of reinforcement relative to spiking in Kenyon cells, we found that odor-elicited spiking in these cells ended well before the reinforcement was delivered. Furthermore, increasing the temporal overlap between spiking in Kenyon cells and reinforcement presentation actually reduced the efficacy of learning. Thus, spikes in Kenyon cells do not constitute the odor representation that coincides with reinforcement, and Hebbian spike timing–dependent plasticity in Kenyon cells alone cannot underlie this learning.

3.1 Introduction

The sense of smell is very flexible. For animals, odors can take on arbitrary meanings as warranted by the changing environment. Understanding how olfactory stimuli are represented in the brain is a prerequisite for studying how such representations become associated with other modalities.

The relatively simple structure of the insect brain makes it useful for studying the neural bases of sensory coding and associative learning. In insects, neural representations of odors begin in the antenna, where volatile molecules bind to olfactory receptor neurons, which respond with trains of action potentials and periods of inhibition (Hallem and Carlson, 2006). These receptor neurons send processes to the antennal lobe, where new odor representations arise from the circuit interactions of the receptor neurons, local interneurons and projection neurons. In the antennal lobe, representations of any given odor are transformed into elaborate and enduring spiking patterns that are distributed across a large fraction of the projection neuron population (Brown *et al.*, 2005; Daly *et al.*, 2004; Mazor and Laurent, 2005; Stopfer *et al.*, 2003). The projection neurons, which provide the only output from the antennal lobe, send processes to the mushroom body, where another set of odor representations arise. Here, the output of hundreds of projection neurons, each contributing dense bursts of spontaneous and odor-elicited spikes, is transformed into something markedly sparse: rare single spikes on a nearly silent background in a tiny fraction of the tens of thousands of Kenyon cells (Perez-Orive *et al.*, 2002). The Kenyon cells then send processes to the lobes of the mushroom body.

The mushroom bodies have long been linked to associative learning and memory. In

many insects, they are sites of multimodal convergence that include olfactory and gustatory inputs (Dacks *et al.*, 2005; Hammer, 1993; Schröter and Menzel, 2003). Furthermore, many types of studies indicate the mushroom bodies are important in olfactory learning. Insects that lack normally developed mushroom bodies suffer from learning and memory deficits (de Belle and Heisenberg, 1994; Heisenberg *et al.*, 1985). Experimentally inactivating the mushroom bodies by cooling them (Erber, 1976) or by conditionally blocking synaptic transmission from Kenyon cells (Davis, 2005; Heisenberg, 2003; Krashes *et al.*, 2007) prevents insects from forming or retaining associative memories. In *Drosophila*, work with mutants suffering from memory deficits found that proteins critical for memory are concentrated in the mushroom bodies (Keene and Waddell, 2007).

To understand how neural representations of odors become associated with reinforcement stimuli, we first sought to characterize the physiological responses of neurons along the olfactory pathway to odor pulses in the context of an associative learning procedure. The moth *Manduca sexta* has proved to be accessible for intracellular recording (Christensen and Hildebrand, 1987) and is also capable of performing an appetitive olfactory learning task, proboscis extension reflex (PER) conditioning (Daly and Smith, 2000). Thus, we examined neural representations of odor in the moth and performed PER training under identical conditions.

We used lengthy odor pulses (typically 4 s), as they correspond to odor exposures that moths encounter while feeding on flowers and because such pulses have often been used for studies of olfactory conditioning (Bitterman *et al.*, 1983; Daly and Smith, 2000; Fan *et al.*, 1997; Muller, 2000; Skiri *et al.*, 2005). With intracellular recordings, we found that projection neurons in the moth's antennal lobe responded

to long odor pulses with extended and complex firing patterns that varied with the odor. We found, with intracellular and multiunit recordings, that Kenyon cells were almost silent at rest; odor responses typically consisted of single spikes in a small population of Kenyon cells. Notably, spiking in Kenyon cells occurred almost entirely on an odor pulse's onset and sometimes offset, with few spikes occurring in between. For any given odor, the population of Kenyon cells responding to the stimulus onset was usually different from the population responding to the offset. This response feature allowed us to examine the ability of onset and offset spiking in Kenyon cells to support associative conditioning.

Having characterized the responses of Kenyon cells to these odor stimuli, we then used a set of behavioral studies to test whether pre- and postsynaptic neurons must both fire spikes nearly simultaneously, which is a key requirement of spike timing–dependent plasticity (STDP), a form of Hebbian learning. In the locust, STDP has been shown to occur between Kenyon cells and followers (Cassenaer and Laurent, 2007). To test the relationship between odor-evoked spikes in Kenyon cells and olfactory learning in the Kenyon cells, we used several behavioral procedures with different intervals between odor and reward. Our results indicate that reinforcement that was delivered seconds after the conclusion of spiking responses in Kenyon cells was able to support the formation and recall of associative memory. Thus, the acquisition of short-term memory does not require the concurrence of spikes in Kenyon cells with activation of a reward pathway in the moth. Furthermore, we found that reinforcement provided specifically following the off response (spiking occurring in 1.5 s of odor offset) could not support associative learning. These results indicate that appetitive associative conditioning cannot occur by a Hebbian STDP mechanism alone in the Kenyon cells.

3.2 Results

3.2.1 Odor representation in the antennal lobe and mushroom body

To characterize odor representations in the antennal lobe, we made intracellular recordings from projection neurons and analyzed their responses to odor pulses presented to the antenna. In all cases, we confirmed the cell type by dye injection and subsequent histological analysis (Figure 3.1). Consistent with earlier studies in locusts (Brown *et al.*, 2005; Mazor and Laurent, 2005; Stopfer *et al.*, 2003), moths (Carlsson *et al.*, 2005; Daly *et al.*, 2004) and *Drosophila* (Wilson *et al.*, 2004; Wilson and Laurent, 2005), we found that, over the course of an odor pulse, different projection neurons responded with slowly changing temporal patterns of spikes and periods of inhibition (Figure 3.2). These distributed, time-varying firing patterns were reliable over repeated trials and varied greatly with the odor. A standard test for information content (Brown *et al.*, 2005) showed that these odor-elicited patterns were sufficiently reliable and distinctive to allow for classification far exceeding chance (Figure 3.3); thus, these firing patterns could carry information about the odors. We were particularly interested in characterizing responses to relatively lengthy pulses of odor, which match the conditions in which moths naturally learn about food sources and which have often been used to test perception, learning and memory in insects, including moths (Daly and Smith, 2000; Fan *et al.*, 1997) and honeybees (Bitterman *et al.*, 1983; Müller, 2000). In projection neurons, responses to 4-s odor pulses generally consisted of lengthy trains of spikes, with 51% of odor-evoked spikes occurring in the first 0.6 s after odor arrived at the antenna

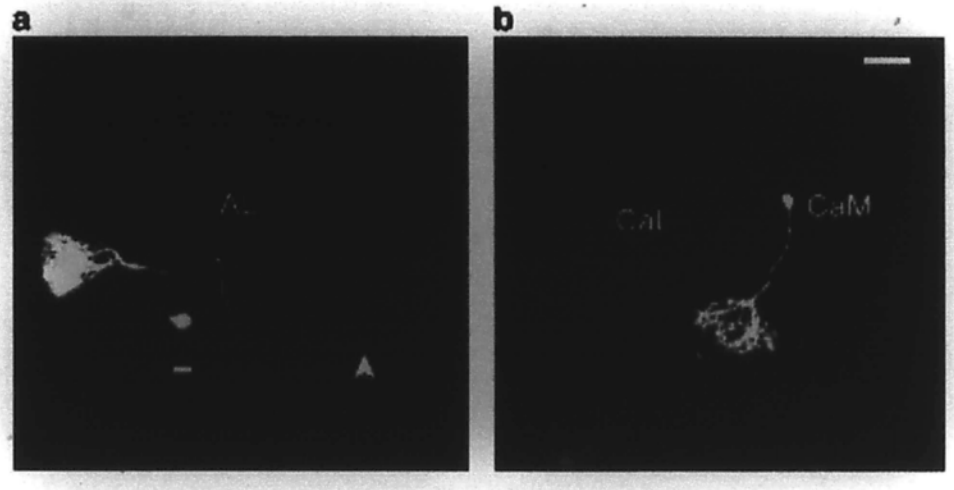

Figure 3.1. Morphological identification of cell type.
After physiological characterization, we injected fluorescent dye for morphological analysis of the recorded cell. Projection images of confocal stacks are shown. (a) Example of projection neuron morphology; anterior view of antennal lobe; projection neuron filled with Lucifer-yellow. The neuron's shape and the process exiting the antennal lobe (arrowhead) are characteristics of projection neurons. AL: antennal lobe. Scale bar: 20 µm. (b) Example of Kenyon cell morphology, posterior view of mushroom body; Kenyon cell filled with Lucifer-yellow. Scale bar: 50 µm. CaM: medial calyx; CaL: lateral calyx.

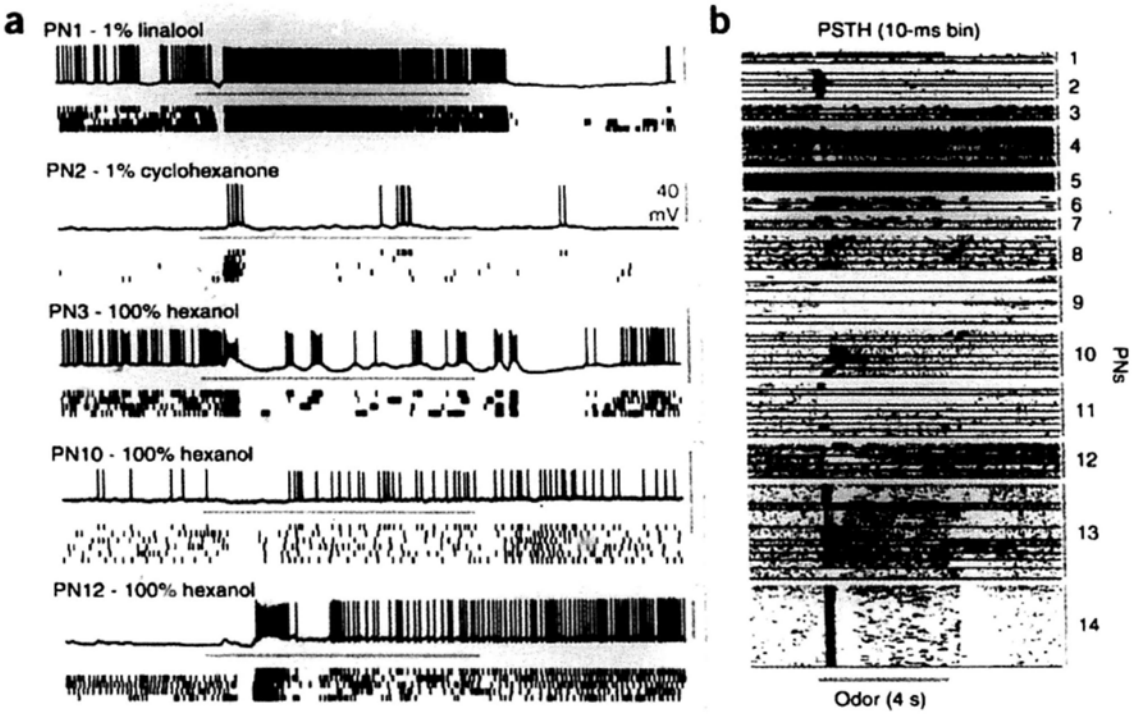

Figure 3.2. Projection neurons respond reliably to odors, and different odors evoke different temporally structured patterns of activity.
(a) Examples of intracellular recordings of projection neurons (PN) responding to 4-s odor pulses (stimulus duration indicated by horizontal bars). Top, intracellular record of 1 trial. Bottom, rasters showing spikes from multiple trials. In PN1, 1% linalool induced brief inhibition followed by sustained spiking that outlasted the stimulus and a prolonged period of inhibition at the offset. In PN2, 1% cyclohexanone evoked only brief excitation. PN3, PN10 and PN12 showed distinct patterns to the same odor (100% hexanol). PN3 and PN10 showed excitatory off responses as well. Vertical scale bars represent 40 mV. (b) Peri-stimulus time histograms (PSTHs) showed reliable odor responses in projection neurons to 4-s odor pulses. These firing patterns contained information about odors (see Figure 3.3). Spikes were binned (10 ms) and bins with at least one spike are indicated by a black dot. One row represents one trial, and 62 projection neuron–odor combinations, each separated by a horizontal black bar, are shown. All projection neurons (except PN14) were tested with more than one odor.

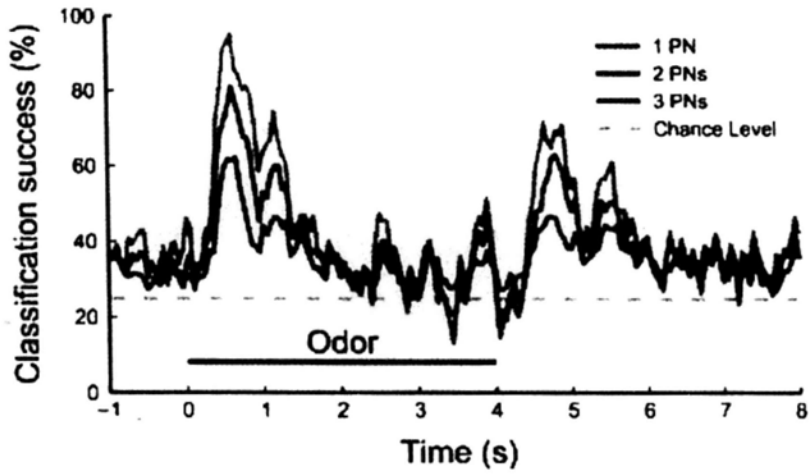

Figure 3.3. Projection neuron firing patterns reliably contain information about odors.
Classification success rates averaged over projection neuron-odor combinations (see Methods) plotted over time. Classification success was greatest at odor onset and offset. Classification success based upon the activity of a single projection neuron greatly exceeded chance level (25%), indicating that odors induced reliable and odor-specific firing activity. The classification success rate increased with the number of projection neurons, indicating that ensembles of projection neurons can encode the stimulus more reliably. Black horizontal bar: odor presentation.

(Figure 3.2; timing determined by reference to an electroantennogram, data not shown). We also found that odors evoked the oscillatory synchronization of projection neurons, which, in turn, regulated the fine timing of spiking in the Kenyon cells (I. Ito *et al.*, Soc. Neurosci. Abstr. 541.8, 2006).

To systematically examine the neural representation of odors by populations of Kenyon cells in the moth, we made intracellular recordings from Kenyon cells and extracellular recordings from the mushroom body with tetrodes (see Methods). Using 4-s pulses of each of a panel of 21 odors, we tested a set of 117 Kenyon cells (recorded extracellularly, 2,457 Kenyon cell–odor combinations, 10 trials per odor, each trial was 12 s long with an intertrial interval of 20 s, Figure 3.4a; a smaller set

of intracellular recordings from Kenyon cells revealed the same response properties, Figure 3.4b). We detected extremely little spontaneous activity in Kenyon cells in the pre-stimulation period (2 s) of each trial; in 24,570 trials (49,140 s), we observed only 203 spikes. This spontaneous firing rate (mean plusminus s.d., 0.0041 plusminus 0.0122 Hz; range, 0–0.1696 Hz; n = 117) was approx2,000-fold lower than the spontaneous firing rate that we observed in the projection neuron population (measured from intracellular recordings; mean plusminus s.d., 8.046 plusminus 5.899 Hz; range, 0–26 Hz; n = 15). Despite the strong and constant convergent and excitatory drive from spontaneously active projection neurons, Kenyon cells remained inactive.

We found that Kenyon cells responded mainly to the onset of a lengthy odor pulse: 72% of spikes evoked by an odor occurred in the first 0.6 s of a 4-s odor presentation (we refer to these early spikes as the 'on response') (Figure 3.4c). Additional spikes sometimes occurred just after an odor's offset (21% of spikes were off responses) and very few spikes occurred between these on and off responses (7% in the 3.4-s 'middle response' period). During the on responses, the mean firing rate, averaged over odors and trials, significantly increased ($P < 0.0001$, Wilcoxon signed rank test, n = 117 Kenyon cells, 0.6-s response bracket) about 21.5-fold from the basal firing level (activity during 2 s before odor stimulation). The mean firing rate during the off responses increased 3.5-fold ($P < 0.0001$, 3.4-s bracket) and increased by 1.3-fold during the middle responses ($P < 0.005$, 1.5-s bracket).

Most Kenyon cells responded to only a few of the 21 odors that we tested, although a subset of Kenyon cells responded to a broader range (Figure 3.4a). In some

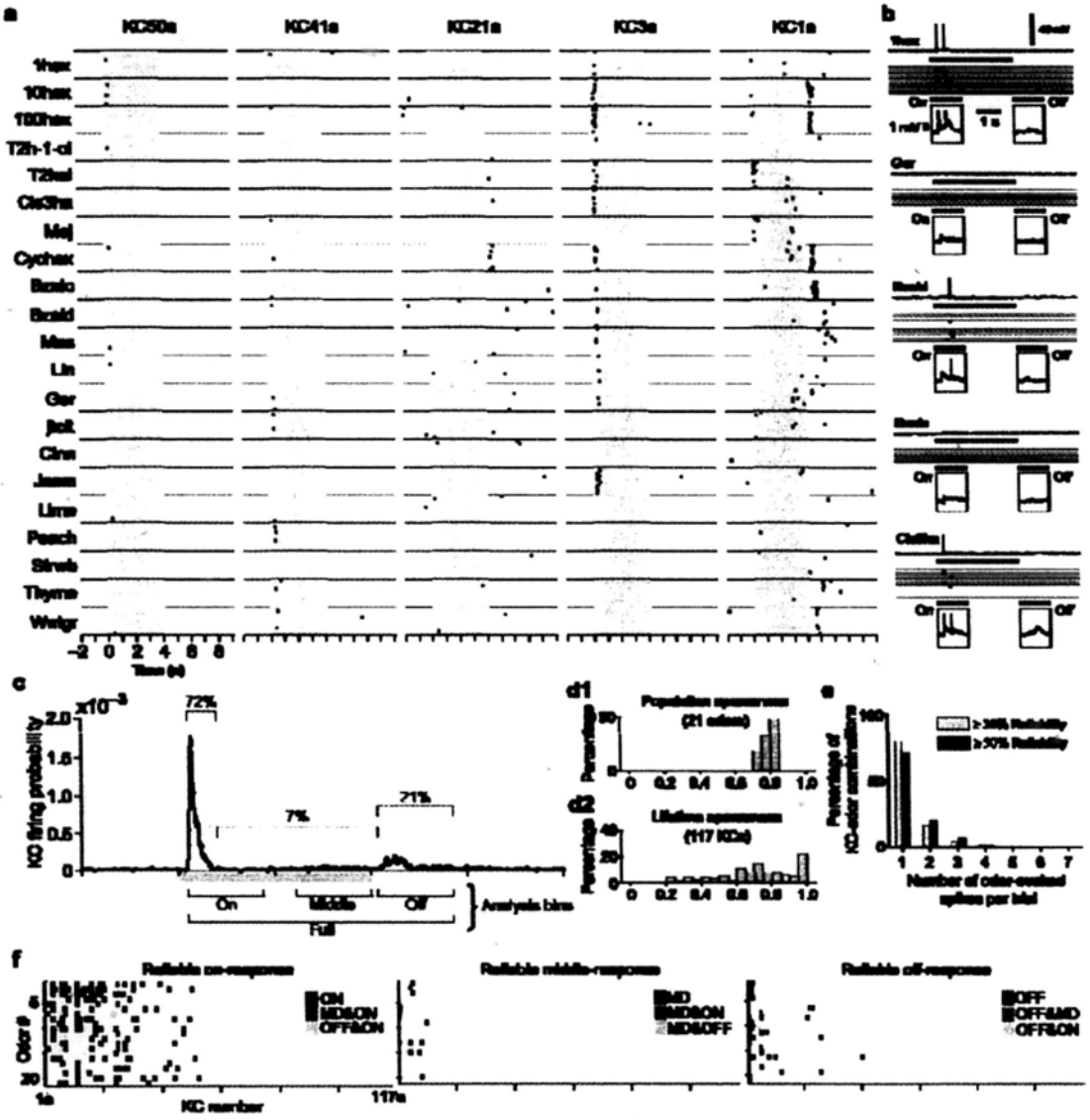

Figure 3.4. Odor-elicited spiking in Kenyon cells is brief and sparse.
(a) Examples of Kenyon cells (KC) responding to a panel of 21 odors. KC50a, KC41a and KC21a responded very sparsely, with either spikes at odor onset or offset. KC3a responded to a broader set of odors. KC1a was the most responsive cell in our set and fired reliably at different points in time for different odors. Ten trials were carried out for each odor. Rasters indicate spike times and the gray blocks indicate odor stimulation (4 s). See Methods for odors. (b) Spiking and subthreshold depolarization in Kenyon cells occurred mainly on odor onset and offset. The top trace indicates the intracellular voltage record and the dark horizontal line indicates odor delivery (4 s). The subsequent lines indicate the number of trials (one line per trial), and the rasters indicate spikes. Insets, enlarged membrane potential, averaged over first five trials, for on and off responses (times indicated as horizontal lines below rasters). (c) Histogram of Kenyon-cell firing probability (117 Kenyon cells, 10 trials each of 21 odors). The top brackets indicate the percentage of spikes during onset, middle and offset periods. The bottom brackets indicate the analysis bins used in subsequent panels. (d,e) Responses of Kenyon cells to odors were sparse. (e) Odor

responses usually consisted of a single spike. Frequency distributions of odor-evoked spikes per trial measured over the full analysis bin are shown. (f) Different Kenyon cell ensembles were usually active during on, middle and off responses (ON, MD and OFF, respectively). MD&ON, overlap in spiking between middle and on responses; OFF&ON, overlap between off and on responses; OFF&MD, overlap with off and middle responses.

experiments, we presented pulses of clean air as control stimuli. These presentations evoked no reliable responses (see Methods) in any of the 42 Kenyon cells that we tested this way. To characterize odor responses across the Kenyon cell population, we computed population sparseness (SP) and lifetime sparseness (SL) (Perez-Orive *et al.*, 2002, Vinje and Gallant2000) (see Methods). These measures, which take into account all of the odor-evoked spikes in all of the tested Kenyon cells, range from 0 to 1, where 1 is sparsest. Mean population sparseness SP (full) was 0.79 (Figure 3.4d), indicating that a given odor elicited responses in very few cells. Similarly, mean lifetime sparseness was 0.72 (Figure 3.4d), indicating that a given cell responded to a narrow range of odors, although a subset of Kenyon cells was more broadly tuned, as in the locust (Perez-Orive *et al.*, 2002). Most odor responses consisted of a single spike per trial and the maximum number of spikes in one responsive trial was 5 (Figure 3.4e). These results indicate that odor representations in the moth mushroom body are extremely sparse: they consist of very few spikes in very few neurons.

3.2.2 Spatiotemporal odor representations in Kenyon cells

When driven by a lengthy odor stimulus, the great majority of spikes that form the odor representation in the mushroom body occur at the onset and to a lesser extent the offset of an odor pulse (Figure 3.4c). Are the Kenyon cells that fire at the odor

onset the same ones that fire at odor offset? To analyze how spiking patterns in the mushroom body change over time, we divided the odor response time into three 1.5-s periods that together captured about 95% of all spikes (Figure 3.4c,f). We chose to focus on responses of Kenyon cell–odor combinations that were relatively strong and reliable, which consisted of at least three responsive trials out of ten (see Methods for rate and reliability criteria). Our set of Kenyon cell–odor combinations elicited 145 reliable on and 39 reliable off responses; of these, an odor elicited reliable spiking in the same Kenyon cell both during onset and offset in only six cases. We observed only 13 reliable Kenyon cell–odor combinations during the middle time period, with two overlaps with the on response and two overlaps with the off response (Figure 3.4f). Together, these findings indicate that odor responses in the mushroom body are spatially distributed and vary over the course of the stimulus. Thus, the moth olfactory system appears to use a time-varying, distributed spatiotemporal code to represent odors both in the antennal lobe and in the mushroom body.

To examine the effect of odor-pulse duration on Kenyon cells, we analyzed all of the spikes that we observed in another set of experiments (Figure 3.5) and found that the probability of off response spiking increased with the length of the odor pulse. We almost never observed off responses following odor pulses of less than 750 ms (examples of Kenyon cells selected for their prominent off responses are shown in Figure 3.5a). Odor pulses of at least 4 s produced the most off responses (Figure 3.5b–d). On and off responses elicited in Kenyon cells by long odor pulses (4 and 18 s) were distributed almost exclusively around two narrow time ranges, 0–600 ms after the odor arrived at the antenna (determined by reference to electroantennogram recordings, data not shown) and 0–800 ms after the odor was removed by vacuum (Figure 3.5c,d). On response spiking was maximal at around 65 ms after odor arrival.

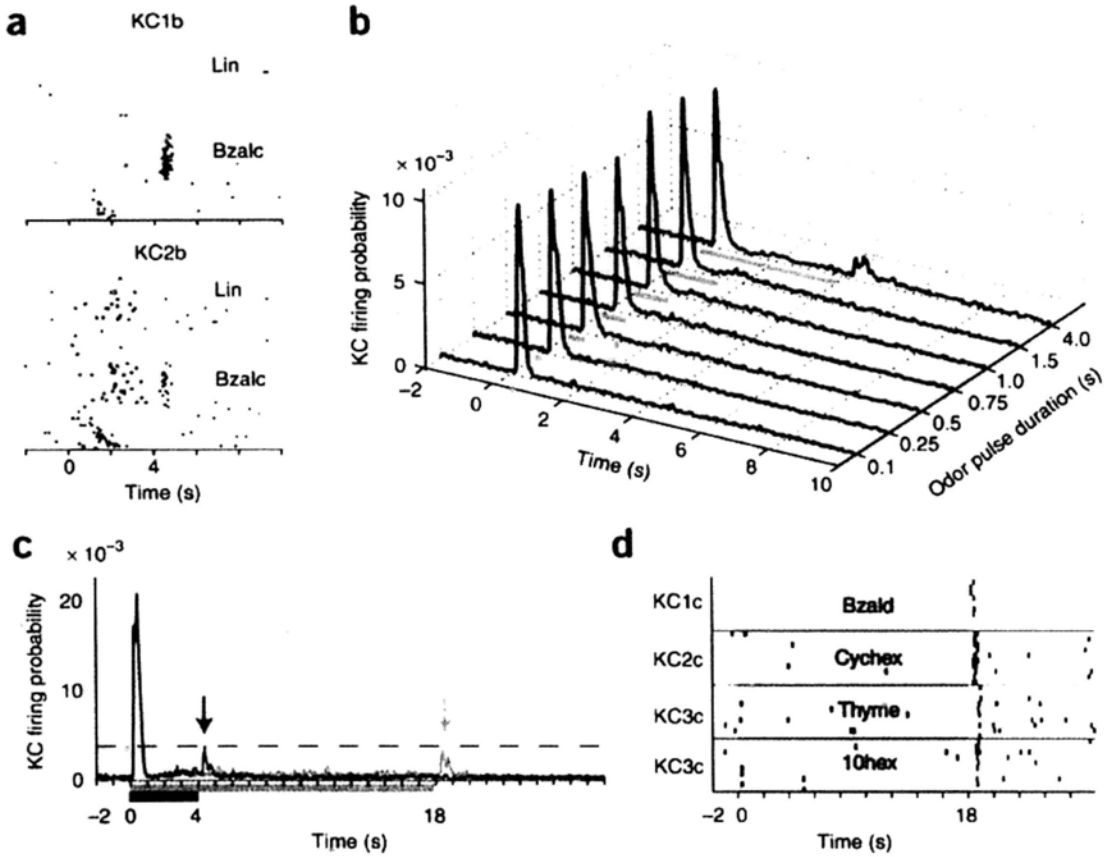

Figure 3.5. Kenyon cells responded only to the onset of brief odor pulses and to the onset and offset of long pulses.

(a) Kenyon cell responses varied with odor pulse duration. Pulses at least 4 s long were most likely to induce odor-specific off responses. Briefer odor pulses generally elicited weaker or no off responses (see also b). Examples shown were selected for prominent off responses. Trials are shown from top to bottom (20 trials of 4-s odor pulses, then 6 shorter pulses, 3 trials each). (b) Off response probability increased with stimulus duration. Multiunit recordings of Kenyon cells (including 117 sorted cells from 16 animals, see Methods) responding to odor pulses of different durations (gray bars, tested in a randomized order, ten trials each). The histogram (bin size, 1 ms) combines the responses to five odors. (c) Long 4-s (black) and 18-s (gray) odor pulses evoked comparable onset and offset responses (arrows indicate the corresponding off responses). Multiunit recordings of Kenyon cells averaged across the four odors shown in d and across multiple trials are shown. (d) Examples of Kenyon cells responding to the offset of 18-s odor pulses. See Methods for the odor labels in a and d.

3.2.3 STDP alone cannot mediate odor learning in Kenyon cells

Hebbian STDP mechanisms require the temporal convergence of activated neural pathways. Do the spikes that we observed in Kenyon cells constitute the odor representation that coincides with reinforcement that supports learning? To test this, we examined the relative timing of odor-elicited spiking in Kenyon cells and sucrose reinforcement in the context of a learning procedure. We trained several groups of moths and compared the amount of learning elicited by procedures in which we varied the temporal intervals between the odor and the reward (Figure 3.6).

Effective appetitive conditioning in honeybees (Bitterman *et al.*, 1983; Hammer and Menzel, 1998; Müller, 2000) and moths (Daly and Smith, 2000; Fan *et al.*, 1997; Skiri *et al.*, 2005) generally occurs when the unconditioned stimulus, a sucrose reward, is presented a few seconds after the onset of a lengthy conditioned stimulus, an odor pulse. Using a computer-controlled delivery system identical to (and frequently calibrated with) the olfactometer used for our electrophysiology experiments (see Methods), we precisely regulated the timing of both the conditioned and unconditioned stimuli in all procedures (Figure 3.6a).

The control 'unconditioned stimulus alone' procedure group received five trials of 3-s unconditioned stimulus presentations alone (n = 33; Figure 3.6a). This repeated delivery of sucrose alone may have caused some sensitization, as the spontaneous PER probability slightly increased from the baseline of 0 to 6.1% (not significant, P = 0.5, McNemar's exact test; Figure 3.6b).

For all associative conditioning procedures, the unconditioned stimulus duration was

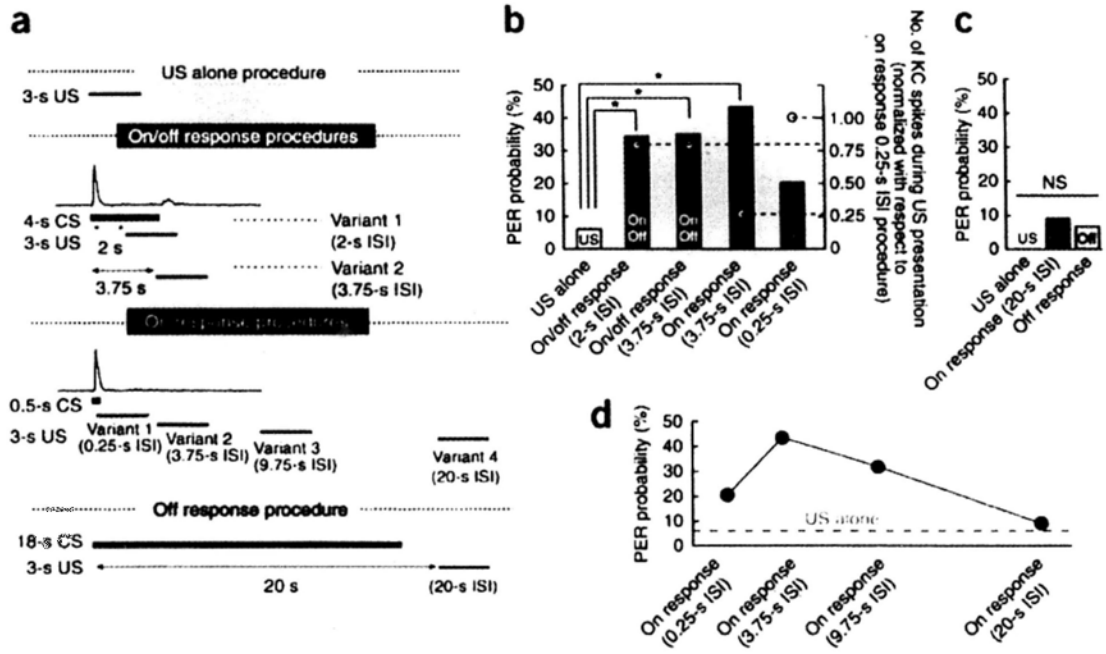

Figure 3.6. Greater temporal overlap between odor-elicited spiking in Kenyon cells and reinforcement delivery did not lead to more learning.

(a) Diagrams illustrate PER conditioning procedures used to vary temporal overlap between spiking in Kenyon cells and sucrose delivery. Black traces represent time course of Kenyon cell spike response probability and gray boxes indicate analysis time windows used to compute conditioned stimulus (CS, odor)-elicited Kenyon cell spike probability concurrent with the unconditioned stimulus (US, sucrose) presentation shown in b (right ordinate). Conditioned stimulus was always paired with the unconditioned stimulus five times with 5 min between trials. The unconditioned stimulus duration was always 3 s. Short-term memory was tested 5 min after training by presenting the conditioned stimulus without the unconditioned stimulus. (b,c) Bar graphs in b and c show the PER probability for short-term memory tests. Asterisks indicate significant difference ($P < 0.05$, Fisher's exact test with Bonferroni correction). More Kenyon cell spikes in the unconditioned stimulus period did not result in better learning. Open circles indicate normalized numbers of Kenyon cell spikes during the unconditioned stimulus presentation period (see Figure 3.5b); spike counts were normalized with respect to the maximum elicited during the on response procedure (0.25-s ISI). (c) Reinforcement provided following off response spiking in Kenyon cells does not support learning. (d) The most effective conditioning occurred when the unconditioned stimulus followed the burst of onset spiking in Kenyon cells by a delay of several seconds. A delay of 20 s elicited no learning. The graph shows PER probability during the short-term memory test for different on response procedure groups.

3 s and the conditioned stimulus was paired with the unconditioned stimulus five times with 5-min intertrial intervals. Short-term memory was assessed 5 min after training by delivering only the conditioned stimulus. Our 'on/off response' procedure (Figure 3.6a), one that is commonly used for training honeybees and moths, consisted of a 4-s conditioned stimulus (Daly and Smith, 2000; Müller, 2000) and a 2-s ISI from the onset of conditioned stimulus to the onset of unconditioned stimulus (Daly and Smith, 2000; Hammer and Menzel, 1998; Müller, 2000). Moths in the on/off response group (2-s ISI, n = 64) attained a 34.4% PER probability (Figure 3.6b). This amount of appetitive learning is typical for moths (Daly and Smith, 2000; Fan *et al.*, 1997; Skiri *et al.*, 2005), which, having fattened as caterpillars, do not need to eat as much as adults. Another group of moths trained with the on/off response procedure (2-s ISI, n = 23) and then tested with a different, non-trained odor did not respond to the different odor (Figure 3.7). This result indicates that learning was specific; moths learned to associate the odor, rather than unintended cues, with the reward. The amount of learning elicited by the on/off response procedure (2-s ISI) was significantly greater than that of the control, unconditioned stimulus alone procedure group (Fisher's exact test, P = 0.0024).

Notably, in this effective and commonly used learning procedure, sucrose reinforcement was delivered approx1.2 s after the end of the on response in the Kenyon cells, as we knew from our physiology experiments. Thus, successful conditioning occurred in the absence of any overlap between odor-elicited on response spikes in Kenyon cells and the sucrose reward.

To further explore the timing relationship of on-response spikes in Kenyon cells and sucrose reinforcement, we then used an on/off response procedure (3.75 s ISI) in

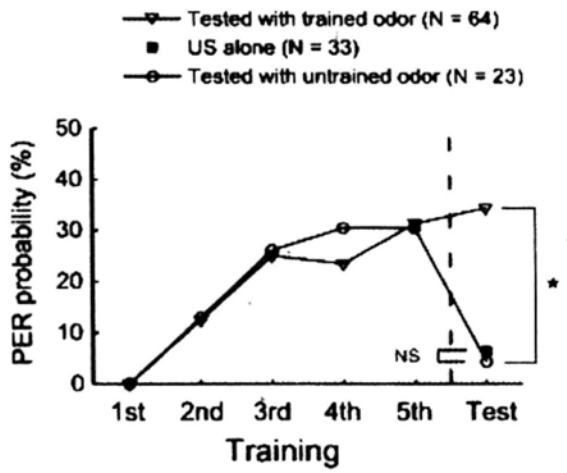

Figure 3.7. Trained moths learned about odors, not other non-specific cues. We trained two groups of moths with benzylaldehyde or cyclohexanone in the On/Off response procedure with 2 s ISI. In each group, half the animals were trained with each odor. After the training, we tested one group with the trained odor and the other group with the untrained odor. Moths responded only to the trained odor, not to the untrained odor. We determined statistical significance by Fisher's exact test with Bonferroni-corrected P values.

which conditioned stimulus and unconditioned stimulus were spaced further apart in time (4 s conditioned stimulus duration, 3.75 s ISI). We found that this group (n = 58) learned as well as that receiving the on/off response procedure with 2 s ISI (34.5%, Figure 3.6b), a level of learning significantly greater than that shown by the control, "unconditioned stimulus alone" procedure group (Fisher's exact test, P = 0.0021).

Our matching electrophysiology experiments found that brief odor pulses elicited only on response spikes in Kenyon cells (Figure 3.5b). To test the importance of overlapping on response spikes in Kenyon cells with sucrose reward, we conditioned a group of moths with brief (0.5 s) odor pulses, which were followed 0.25 s later by reinforcement (on response procedure, 0.25-s ISI, n = 61). Shifting the timing of the reward presentation closer to the on response spikes in Kenyon cells actually resulted

in decreased learning (18.0% PER probability, which was not significantly different from that elicited by the unconditioned stimulus alone procedure, P = 0.1299; Figure 3.6b).

Among these three groups, only the on response procedure (0.25-s ISI) elicited exclusively on response spikes in Kenyon cells, and was ineffective for learning. This raised the possibility that off response spiking in Kenyon cells (and possibly some middle response spiking) in the other two groups (on/off response procedures with 2-s and 3.75-s ISIs) may have contributed substantially to successful conditioning. To test this, we trained moths with a brief odor pulse in a trace procedure (on response procedure with 3.75-s ISI, 0.5-s conditioned stimulus duration, n = 23). Notably, conditioning with this procedure yielded learning (43.5%, significantly different from unconditioned stimulus alone procedure, Fisher's exact test, P = 0.0018) that was similar to that elicited by other conditioning procedures including off response spikes in Kenyon cells (on/off response procedures with 2-s and 3.75-s ISIs; Figure 3.6b). This suggests that the off response spikes contributed little or nothing to conditioning efficacy. We counted the number of spikes evoked in Kenyon cells during the time of unconditioned stimulus presentation in these procedures (Figure 3.5b). The on response procedure (3.75-s ISI) group, which elicited the highest learning rate, corresponded to the fewest spikes in Kenyon cells during the time of reinforcement (Figure 3.6b). To examine the limits of the interval between on response spikes in Kenyon cells and reinforcement to effectively support conditioning, we tried spacing the conditioned and unconditioned stimuli further and further apart. When we set the conditioned stimulus duration to 0.5 s to induce almost exclusively on response spikes (Figure 3.5) and gradually increased the interval between the conditioned and unconditioned stimuli, we found that the PER

probability peaked at the 3.75-s ISI (43.5%) and gradually decreased (at the 9.75-s ISI, 31.8%, n = 22, not significantly different from the unconditioned stimulus alone procedure, Fisher's exact test, P = 0.022, not significant after Bonferroni correction) and reached the control level at around the 20-s ISI (9.1%, n = 22, not significantly different from the unconditioned stimulus alone procedure, Fisher's exact test, P = 1; Figure 3.6d).

Notably, effective conditioning was possible even when sucrose reinforcement was delivered many seconds after the spiking responses in Kenyon cells had returned to baseline levels. These results indicate that appetitive olfactory conditioning in the moth Kenyon cells cannot be mediated by a Hebbian STDP process that requires the near-overlap of spikes elicited by the odor stimulus and spikes elicited by the reinforcement; spiking in Kenyon cells cannot be the representation that coincides with appetitive reinforcement during associative conditioning.

Finally, we asked whether off response spikes alone in Kenyon cells could support associative learning. Drawing on the results of our on response procedures, we used an ISI that was long enough to separate the onset and offset spiking in Kenyon cells by an interval that exceeded that which can support trace conditioning (Figure 3.6c,d); we used an extra-long conditioned stimulus (18 s, which induced small off responses similar to those elicited by 4-s odor pulses; Figure 3.5c,d) and delivered the unconditioned stimulus at a 20-s ISI (2 s after the beginning of the off response). This allowed us to selectively reinforce the off response spikes, but not the on response spikes (off response procedure group, 6.7%, n = 30; Figure 3.6c). This procedure did not lead to PER conditioning that was significantly different from the control level (Fisher's exact test, P = 1). Therefore, we concluded that off response

spiking alone cannot support learning. This absence of learning may result because off responses were generally small, consisting of far fewer spikes than the on responses (Figure 3.6b,c). As middle response spikes were much less frequent than off response spikes, we conclude that only the on response spikes contributed substantially to learning. Responses occurring after the on response could be important for other tasks that require temporal integration. The apparent importance of odor onset for associative conditioning suggests that, at least for our simple learning task, moths were prepared to make rapid behavioral choices. Consistent with this analysis, we found that moths tended to respond rapidly with proboscis extension on the onset of an odor pulse regardless of its duration or time of reinforcement during training (Figure 3.8).

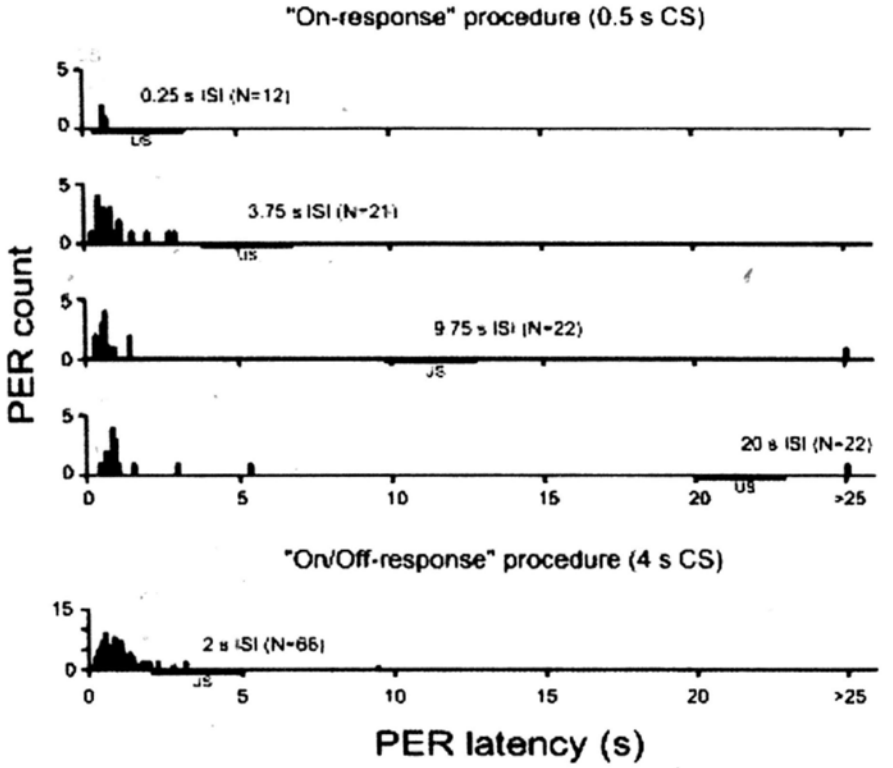

Figure 3.8. Moths responded to odor onset regardless of reward timing. In these experiments, we measured the latencies of all PER responses during training and testing from video recordings. We trained different groups of moths with different CS-US intervals. Most moths quickly responded to the odor pulse (the CS) within 1 s regardless of the training interval. Frequency histograms show time after odor onset when the start of proboscis extension was noted. The bins labeled > 25 s include responses occurring between 25 s and 60 s after CS onset. N: number of moths in the group. Yellow boxes: the CS presentation time. Black horizontal bars under histograms: the US (sucrose) presentation time.

3.3 Discussion

3.3.1 Odor representations in the moth olfactory system

Olfaction, with only a few layers of neurons separating input from output, provides a useful model for understanding a succession of neural representations of sensory events. Consistent with earlier findings in moths (Daly *et al.*, 2004) and locusts (Mazor and Laurent, 2005), our intracellular recordings from projection neurons revealed high spontaneous firing rates and odor-specific, temporally complex patterns of robust spiking and inhibition (Figure 3.2). We provide, to the best of our knowledge, the first characterization of odor responses in the Kenyon cells of moths; they showed markedly low background firing rates and typically responded to odors with one spike at the odor onset or, less often, at the offset (Figure 3.4). Thus, in the moth, as has been observed in locusts (Perez-Orive *et al.*, 2002), honeybees (Szyszka *et al.*, 2005) and *Drosophila* (Turner *et al.*, 2007; Wang *et al.*, 2004), dense spatiotemporal patterns in the projection neurons were transformed into sparse representations in the Kenyon cells. We found that largely distinct ensembles of Kenyon cells spiked at the onset and offset of odor pulses in the moth, with a very low level of spiking in between onset and offset (Figures 3.2 and 3.5).

In moths, as in other animals, the meanings of odors are readily adjusted by learning experiences. Needless to say, the odorants themselves are not matched with conditioning reinforcements in the brain, but rather neural representations of odors, presumably spiking activity in olfactory neurons, must undergo this matching process. Having characterized the responses of olfactory neurons to odor stimuli such as those used in conditioning procedures, we asked what was the neural

representation of the odor that coincides with the reward. Memory traces are, in general, distributed across multiple neural populations. Specifically, short-term memory induced by appetitive olfactory conditioning, such as the PER procedures that we used here, appears to involve both the antennal lobe and the mushroom body (Hammer and Menzel, 1998; Thum *et al.*, 2007) and possibly other areas. We focused on the timing of odor-elicited firing patterns of the intrinsic neurons of the mushroom bodies, the Kenyon cells, and the timing of reinforcement stimuli that leads to effective associative conditioning. In a number of conditioning procedures, we found that reinforcement stimuli that were delivered at times that did not coincide with odor-elicited spiking in Kenyon cells could still effectively support associative conditioning (Figure 3.6).

Recent work in vertebrates and insects has focused on the role of STDP, a form of Hebbian learning, which requires precise, millisecond-scale correlation between spiking in pre- and postsynaptic neurons that undergo plasticity. Notably, we found that the most behaviorally effective reinforcement occurred long after, sometimes seconds past, the cessation of all odor-elicited spiking in the Kenyon cells. Thus, it is not possible for spikes in Kenyon cells to interact, in a STDP temporal window, with spikes arriving via any pathway bearing the reinforcement. Plasticity cannot occur in these cells through any type of Hebbian mechanism that requires spiking in both pre- and postsynaptic neurons to occur in a temporal window of less than several hundred milliseconds. Plasticity here must occur through a different mechanism.

Neurotransmission from Kenyon cells is required for memory retrieval, as shown by behavioral studies in transgenic flies in which neurotransmission from a subset of Kenyon cells ($\alpha\beta$ neurons) was conditionally regulated by temperature shifts (Davis,

2005; Heisenberg, 2003). A recent study investigating the role of another subset of Kenyon cells, the α'β' neurons (Keene and Waddell, 2007; Krashes *et al.*, 2007), indicated that neurotransmission from α'β' neurons is required during the acquisition of memory and contributes to stabilizing the memory. These results are consistent with an earlier finding in honeybees, where the neuromodulator octopamine, injected specifically into the mushroom body, can induce olfactory learning by substituting for the sucrose reward (Hammer and Menzel, 1998). Studies such as these show that Kenyon cells are involved in memory acquisition (plasticity in the antennal lobe may be involved as well) (Hammer and Menzel, 1998; Thum, 2007). However, the precise mechanism by which Kenyon cell activity contributes to the acquisition of associative memory remains unknown. Any such mechanism would require the temporal convergence of the neural representations of the odorant and sucrose.

3.3.2 Sparse coding and associative learning

Accumulating evidence shows that organisms spanning locusts (Perez-Orive *et al.*, 2002) to humans (Quiroga *et al.*, 2005) make use of sparse neural coding strategies to represent stimuli. Sparse codes, in which stimuli elicit very low spike rates in a small fraction of a large population of mostly silent neurons, maximize coding space between representations of different sensory stimuli (Olshausen and Field, 2004). This increases associative memory capacity and also readily allows for efficient formation of learned associations via a local rule. Hebbian mechanisms, through which synapses are strengthened if spikes in the presynaptic neurons contribute to produce an action potential in the postsynaptic neurons, seem ideally suited for efficiently modifying sparsely coded neural representations of stimuli (Marr, 1971; Willshaw *et al.*, 1969). Thus, Hebbian plasticity has become a common component

of associative neural network models, particularly in the context of sparse codes (Olshausen and Field, 2004).

Indeed, a recent study found millisecond-scale STDP in the olfactory pathway of the locust, demonstrating that insects have synapses that exemplify Hebb's rule (Cassenaer and Laurent, 2007). Behavioral studies in *Drosophila* have revealed the sort of bidirectional plasticity that is typical of STDP, but with conditioned stimulus–unconditioned stimulus pairing time scales on the order of seconds rather than milliseconds (Tanimoto *et al.*, 2004). Computational studies suggest that the time scale mismatch between behavioral and physiological STDP characteristics can be resolved if the pre- and postsynaptic neurons responding to conditioned and unconditioned stimuli show sustained firing that slowly decays (Drew and Abbott, 2006). However, our finding that Kenyon cells respond only sparsely and very briefly to odor pulses that support conditioning is not consistent with this model. It is possible that STDP mechanisms may contribute to olfactory conditioning when combined with slower biochemical processes (Izhikevich, 2007). Might the responses of Kenyon cells to odor become altered by conditioning such that spikes then temporally overlap with the reward? This seems to be an unlikely explanation for our results. First, we found that the most learning occurred during the first training trial; that is, before any potential learning-induced changes could have occurred (on/off response procedure with 2-s ISI; Figure 3.7). Second, odor responses of Kenyon cells in moths that had been successfully trained to associate that odor with reward were no less sparse than responses from Kenyon cells in untrained moths (data not shown). Therefore, we conclude that STDP mechanisms alone cannot account for the learning in Kenyon cells that we observed in moths.

Our physiological and behavioral studies indicate that spikes in Kenyon cells cannot, in and of themselves, constitute the odor representation that coincides with appetitive reinforcement. We suggest instead that the odor representation in Kenyon cells that is paired with reward may be a sustained biochemical process, perhaps second messenger responses (Davis, 2005; Heisenberg, 2003; Schwaerzel *et al.*, 2003) that are triggered by very transient spiking. The situation may be different in other neurons or species. Recent recordings from *Drosophila* Kenyon cells found that odor-elicited somatic subthreshold excitatory postsynaptic potentials are close in amplitude to those attained by spikes (Turner *et al.*, 2007). If excitatory postsynaptic potentials alone suffice to activate voltage-dependent calcium channels, for example, reinforceable odor representations might include neurons that are not firing spikes.

3.4 Methods

Experimental animals

Moths (*Manduca sexta*) were reared from eggs (purchased from the NCSU Insectary) in our laboratory on an artificial diet (Bell and Joachim, 1976) under a long-day photoperiod at 26 °C, and at more than 70% relative humidity.

Olfactory stimulation

The odor-stimulation method that we used was modified from our previous study (Brown *et al.*, 2005). Briefly, the odorized headspace in 60-ml glass bottles above mineral oil–diluted odorant solution was pushed by a controlled volume of humidified air (0.1 l min-1) into an activated carbon–filtered, humidified air stream (0.75 l min-1) that flowed continuously across the antenna. The inner diameter of the odor delivery tube was 6.5 mm and the air speed at the end of tube was about 9.4 cm s-1. Excess odorants were continuously drawn by vacuum from the back of the preparation. All chemicals were purchased from Sigma-Aldrich unless otherwise noted. The odorants that we used were benzylalcohol (Bzalc), benzaldehyde (Bzald), (+)-β-citronellene (βcit, Fluka Chemika), cyclohexanone (Cychex), geraniol (Ger), hexanol (1hex, 10hex and 100hex), cis-3-hexenyl acetate (Cis3ha), (plusminus)linalool (Lin, Aldrich), methyl salicylate (Mes), methyl jasmonate (Mej), 1-octanol (Oct, Fluka Chemika), trans-2-hexenal (T2hal), trans-2-hexen-1-ol (T2h-1-ol), oil extracts, strawberry (Strwb), cinnamon (Cinn), peach, lime, jasmine (Jasm, Balducci's), thyme (Thyme Red, Saidel) and wintergreen (Wntgr, Wagner's). Monomolecular odorant solutions were diluted to 1% (vol/vol) in mineral oil unless otherwise noted. Oil extracts were used undiluted. The odor vapor drawn from the

headspace was further diluted when mixed into the constant air stream.

Electrophysiology

Physiological data were obtained from 38 adult moths of both sexes. Adults that were 1 d post-eclosion or older were dissected following a procedure described for locusts (Laurent and Naraghi, 1994). The brain was treated for 1–3 min with 3% collagenase-dispase (Roche Diagnostics) that had been dissolved in saline. The antennal lobe and mushroom body were then carefully desheathed with fine forceps. The head capsule was superfused with moth physiological saline (Christensen and Hildebrand, 1987) at room temperature (about 25 °C).

Intracellular recordings were made using sharp glass micropipettes pulled horizontally (P87, Sutter Instrument Company) to yield 50–150 MOmega electrodes for antennal lobe neurons and 50–200 MOmega electrodes for Kenyon cells when filled with one of the internal solutions (details are given in Figure 3.1). Multiunit recordings from Kenyon cells were made using 8-channel, custom-made, twisted wire tetrodes (Perez-Orive *et al.*, 2002), amplified with a custom 16-channel amplifier (Biology Electronics Shop, Caltech) and digitized at 15 kHz (details on spike sorting43 are given in Figure 3.9).

Behavioral experiments

A total of 336 moths were used for behavioral experiments. Moths that were 1–4 d post eclosion were restrained in plastic tubes (inner diameter, 1.5 cm.) with the head protruding. The proboscis was made to extend partially by threading it through flexible polyethylene tubing (inner diameter, 0.86 mm.) with the proboscis tip exposed to allow sucrose application. To eliminate visual cues during training and

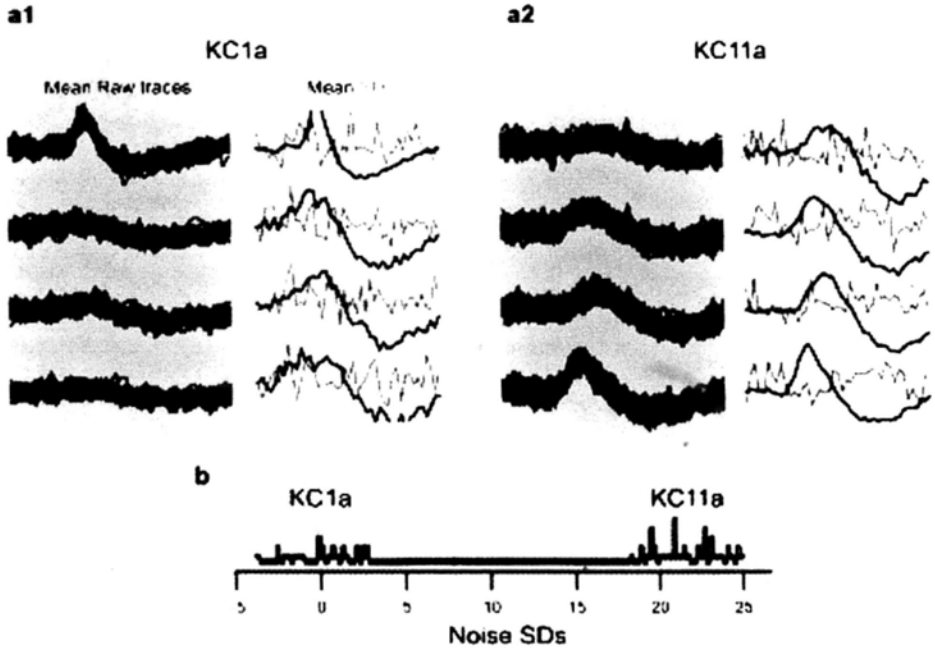

Figure 3.9. Examples of spike sorting.
We performed spike sorting conservatively, taking into account the full waveform of each spike event from four channels43. We made extracellular recordings of Kenyon cell activity using custom-made twisted wire tetrodes. To collect a representative sample of Kenyon cells, electrodes were placed at random locations within the mushroom body. Spike sorting was achieved offline, using the best 4 of the 8 channels recorded, and consistent with conservative statistical principles43 (Spike-o-Matic) implemented in IGOR Pro (Wavemetrics, Lake Oswego, OR). A total of 266 Kenyon cells (117 for Figure 3.4f, another 117 for Figure 3.5a,b and 32 more for Figure 3.5c,d) were recorded from 36 moths of either sex. In most cases, both right and left sides of the mushroom bodies were tested in each animal. (a) Example of individual events (black), their mean (red), and the SD (gray) in each of the four channels for all events classified as KC1a (a1) and KC11a (a2), respectively. (b) Histogram obtained by projecting KC1a and KC11a events onto the line connecting their means. We considered only well separated clusters, with centers separated by at least five times the noise SD.

testing, the compound eyes were covered with black ink at least 15 min before training began.

Moths were classically conditioned during the dark photoperiod with the four types of training procedures described above (shown in Figure 3.6a). Time- and pressure-regulated odor stimuli (1% cyclohexanone or 1% benzaldehyde) were pulsed onto one antenna as described above. These two odors, as with the others in our set, evoked mainly on response spiking and weaker off response spiking in Kenyon cells (Figure 3.10). The equipment that we used for odor presentation in these behavioral experiments was identical to, and with settings daily cross-calibrated with, the equipment that we used for the physiology experiments. For taste reward presentation, air driven by a picopump pushed approx10 mul of sucrose solution (40% wt/vol in water) from a glass capillary (inner diameter: 0.058 mm) to the tip region of the proboscis. The two pneumatic picopumps used for odor and sucrose stimuli were controlled by a programmable pulse generator (Master-8, A.M.P. Instruments). Proboscis extension was monitored visually by an investigator. Responses were recorded if PER occurred within 1 min of the odor onset. For some experiments, response latency was measured from video images (see Methods).

Data analysis

All analyses, except for spike sorting, were carried out using custom programs in MATLAB (MathWorks). Given the sparseness of Kenyon cell spiking, it was not always clear when a Kenyon cell was responding to an odor. Therefore, for some analyses of our extracellular Kenyon cell records (Figure 3.4e,f) we used rate and reliability criteria modified from an earlier study (Perez-Orive *et al.*, 2002). To meet our rate criterion, Kenyon cell firing was averaged over all ten trials in each Kenyon

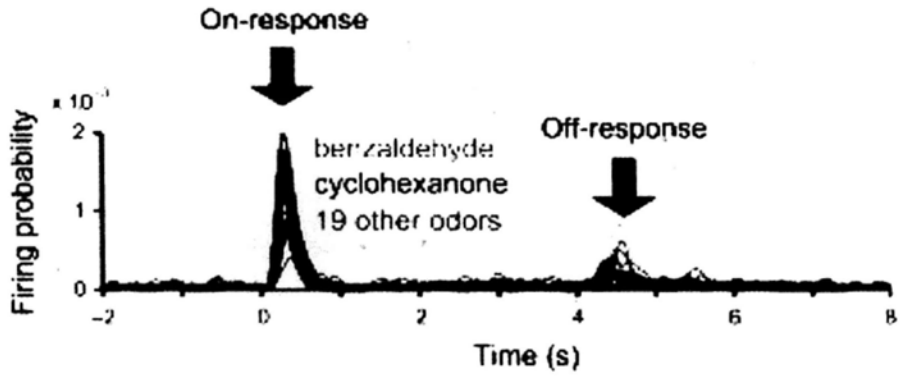

Figure 3.10. All odors, including those used to test behavior, evoked similar temporal spiking characteristics in Kenyon cells.
Each line represents a histogram (bin size: 1 ms) that combines 1,170 trials from 117 cells. Odors used for behavioral training (benzaldehyde and cyclohexanone) evoked overall temporal activity patterns in Kenyon cells (strong on-responses and much weaker off-responses) similar to those of all other odors tested. Yellow bar: odor presentation.

cell–odor combination set and segmented into successive, nonoverlapping 250-ms bins that spanned the 5.5-s full analysis window. Firing had to exceed 3.5 s.d. of the mean baseline rate (2 s before stimulation) in at least one of the bins; background activity was so low that in almost all cases a single spike in any bin in any trial sufficed. Therefore, we defined a responsive trial as one with at least one spike. To meet the reliability criterion, the response probability (number of trials showing at least one spike divided by the number of trials tested) had to exceed 30%. We evaluated the usefulness of this threshold by estimating the probability that at least one spike in our dataset would occur during the pre-stimulus period (in the absence of odorant, 2 s). We made this estimate for each Kenyon cell (normalizing for test windows of different duration) using all 210 trials. These probabilities for individual Kenyon cells had a median of 0 and a mean of 0.0058. Except for two extremes (0.125 and 0.0929) all Kenyon cells showed a probability lower than 0.0607. At P = 0.0607, the binomial probability theorem shows that the probability that at least one

spike would occur in the absence of odorant in more than three trials in 10 (30% reliability) was less than 0.02. For the two extreme cases, the probabilities estimated in the same way were just above the 0.05 level of significance ($P < 0.12$ or 0.06). Thus, we judged our 30% threshold to be appropriate for detecting odor responses in Kenyon cells. We also provide results using a 50% criterion to allow for comparison with results obtained in locusts (Perez-Orive *et al.*, 2002).

The distribution of spike number per trial was analyzed by counting the number of spikes occurring within 5.5 s of odor onset using only the cell-odor pairs that included odor responses (that is, met the response reliability criteria given above). To compute the sparseness of Kenyon cell responses, we used measures of population (SP) and lifetime (SL) sparseness (Perez-Orive *et al.*, 2002; Vinje and Gallant, 2000). SP estimates the proportion of cells not responding to each stimulus:

$$S_P = \frac{1}{\left(1 - \frac{1}{N}\right)} \left(1 - \frac{\left[\sum_{j=1}^{N} r_j / N \right]^2}{\sum_{j=1}^{N} r_j^2 / N} \right)$$

where N is the total number of Kenyon cells and rj is the number of spikes detected in cell j over ten trials. SP takes values from 0 to 1, with SP = 1 being sparsest. To estimate the response intensity (rj), we segmented the 5.5-s full response window into 250-ms bins and calculated the mean spike count in each bin averaged over ten trials for each cell-odor pair. The mean baseline activity in the 2-s pre-stimulus period was then subtracted from all of the bins. Finally, only the bins showing more than the mean basal activity (values greater than 0) were added to obtain rj. SL estimates the range of responses of each cell and was calculated in the same way as SP, except that index j corresponds to each odor and N to the total number of odors

tested with each cell.

Statistical tests were made using SAS version 9.0 (SAS Institute) and R version 2.4.1 (http://www.r-project.org/) for behavioral data and using Statistical toolbox version 5.2 for MATLAB for physiological data. All of the statistical tests for physiology were two-tailed and significance was judged at $P = 0.05$. To make conservative multiple comparisons of results from behavioral experiments, we judged significance by more stringent, Bonferroni-corrected P values. For evaluation of sensitization, spontaneous PER probability was estimated using the 1-min window before the beginning of the unconditioned stimulus alone procedure and compared with the PER probability of the test period with McNamar's exact test. PER probabilities between different procedures were compared with Fisher's exact test.

Histology

After electrophysiological characterization, we stained cells by passing current pulses (for fluorescent dyes – 1 to – 10 nA, 0.5 s duration, 1 Hz; for neurobiotin + 3 nA, 0.5 s duration, 1 Hz) for 5–40 min. We then fixed brains with 4% paraformaldehyde in phosphate buffer (pH 7.4) overnight. We visualized neurobiotin by incubating brains overnight in a 0.1% solution of streptavidin-Alexa conjugate in phosphate buffer containing 1% Triton (Alexa-Fluor-568 or 633 conjugated streptavidin, Invitrogen). We dehydrated fixed brains through a graded ethanol series and cleared with methyl salicylate. We imaged the brains with a laser-scanning confocal microscope (LSM 510 Upright 2-Photon Meta, Carl Zeiss Inc., Thornwood, NY) equipped with a 458 Argon ion laser, a 543 nm Helium-Neon laser, and a 633 nm Helium-Neon laser. We obtained projection images of confocal stacks using the projection function of Zeiss LSM Image Browser version 4.2.0.121

(Carl Zeiss Inc) in transparent mode.

Classification analysis

To test the reliability and information content of projection neuron firing patterns, we performed a standard classification analysis (Brown *et al.*, 2005) using single and multiple projection neuron ensemble responses (up to 3 projection neurons) based upon dataset shown in Figure 3.2. Among the 62 projection neuron-odor combinations, we included only those projection neuron singlets, pairs, and triplets that were tested for the same three odors at least three trials for each odor for this analysis. This resulted in a total of 227 combinations for classification based on single projection neuron activity, 88 and 19 combinations for projection neuron pair and triplet cases, respectively (each combination represents a separate classification problem).

We constructed a response vector by concatenating projection neuron firing rates in five consecutive 50 ms bins (250 ms activity) from single or multiple projection neurons. To predict the odor label of a response vector in the test trial, we computed the Euclidean distance between the test trial response vectors with each of the remaining trials (corresponding response vectors); we then assigned the test vector the odor label of the closest trial (smallest Euclidean distance). We used the first three trials for each of the three odors (a total of 9 trials), thus each classification task had one test trial and 8 remaining trials. Therefore, the classification success by chance was 25% (2 out of 8). We used a standard leave-one out validation method to ensure every trial served as a test trial in the classification analysis. We averaged the classification rates across different combinations. We repeated this analysis for 50 ms step sliding windows over the course of each trial. We obtained

similar results with a range of bin sizes.

Projection neuron activities at odor onset and offset supported successful odor classification that significantly exceeded chance level (25%). We judged statistical significance ($P < 0.05$) by estimating the probability of getting the observed classification success probability or higher, assuming a random binomial process. We performed the analysis separately for singlet, pair and triplet projection neuron ensembles.

Video analysis

In some experiments, we recorded training and testing with a digital video camcorder (PV-GS400, Panasonic, Japan) at 29 frames/s. Odor onset was indicated by a flashing LED controlled by the odor pulse generator; we defined PER latency as the time difference from the first frame showing the LED illuminated to the first frame showing the beginning of a proboscis extension response. We measured timing with video processing software (VirtualDub 1.6.17, http://www.virtualdub.org). We measured the latencies of all PER responses during training and test phases except for the first training trials to exclude spontaneous PERs.

3.5 Acknowledgements

The work presented in this chapter was previously published in *Nature Neuroscience*, vol. 11, Iori Ito, Rose Chik-ying Ong, Baranidharan Raman, and Mark Stopfer, "Sparse odor representation and olfactory learning", pp 1177-1184, 2008. Iori Ito and Rose Chik-ying Ong contributed equally to this work. This work is the product of a highly collaborative project among the authors. I contributed to moth Kenyon

cell intracellular and extracellular recordings, and behavioral data. Iori Ito contributed to electrophysiological recordings and behavioral data. Baranidharan Raman performed data analysis on Kenyon cell extracellular data.

We are grateful to members of the Stopfer laboratory for helpful discussions. We especially thank K. Sun for her excellent animal care. Micrographs were made at the Microscopy and Imaging Core (US National Institute of Child Health and Development, NICHD) with the assistance of V. Schram. We thank C. Wu in the Biometry and Mathematical Statistics Branch, US National Institutes of Health (NIH)/NICHD for his advice on the statistical analysis of the behavioral experiments. This work was supported by grants from the Japan Society for the Promotion of Science (00169, 70510) to I.I., a joint NIH–National Institutes of Standards and Technology postdoctoral fellowship award by the National Research Council to B.R. and an intramural grant from NIH-NICHD to M.S.

4 Concluding remarks

In the previous two chapters I presented two projects about olfactory coding. Here, I will summarize the major findings, and the significance of these findings.

4.1 Frequency transitions in odor-evoke neural oscillations

The work presented in Chapter 2 clarified several concepts in olfactory coding. We demonstrated that, in moths, oscillations can be triggered by a wide range of general, non-pheromonal odors including host-plant volatiles and common food blends at a wide range of concentrations. The mechanism through which oscillations generated in moths appears to be similar to that found in other insects (locusts: Laurent and Davidowitz, 1994; bees: Stopfer *et al.*, 1997; flies: Tanaka *et al.*, 2009). Spikes generated by olfactory neurons (PNs, LNs, and KCs) are phase-locked to the LFP oscillations (Figures 2.4 and 2.6). LFP oscillations detected in the AL and MB are coherent (Figure 2.1). Injection of picrotoxin into the AL abolishes odor-evoked oscillations. Together, all these results confirm that oscillations arise within the AL circuitry.

Our results contradict several earlier reports. Previously, odors (pheromones) were found to induce highly localized LFP oscillations only within the AL (Heinbockel *et al.*, 1998). Coherent LFP oscillations between the MB and AL have never been observed (Christensen *et al.*, 2003). Further, intra- and extracellular recordings in PNs showed no consistent synchrony; only brief, non-oscillatory synchrony is

observed (Christensen *et al.*, 2003; Lei *et al.*, 2002). These observations led to the proposal that *Manduca* uses a non-oscillatory mechanism to encode odor (Lei *et al.*, 2002).

The differences between our results and those reported earlier probably arise from both our focus on the general olfactory system and differences in recording techniques. Thus, our results provide an important new perspective by demonstrating that the moth's pheromone system may not present a good model for the study of olfactory coding of general odors. And, we confirmed that odor is encoded through a mechanism common to several diverse insect species.

Further, we found that the frequency of odor-evoked oscillations changed over the course of a lengthy odor presentation. Odor-evoked oscillation frequency was initially ~40 Hz after odor onset, then suddenly decreased to ~15-20 Hz after ~1 s. Our investigation of this phenomenon led to an analysis of how odor concentration is encoded in the periphery. With electrophysiological recordings, we found that longer odor pulses caused the most active ORNs to adapt their firing rates, with a time course similar to that of the oscillation frequency transition (Figure 2.10L, 2.11). On the other hand, firing rates of the most precisely tuned ORNs saturated when stimulated by low to moderate odor concentrations (Figure 2.10F). Thus, ORN activities are tightly constrained by adaptation and saturation.

Combining these results with computational models, we showed that oscillation frequency in moth is determined by the input intensities of ORNs to the AL, set by the adaptation and saturation of ORN responses. Changing stimuli intensity by increasing odor concentration, on the other hand, recruits additional, but less well-tuned ORNs to respond. Thus, we revealed an important principle: to a very

large extent, odor concentration is encoded by the number of responsive ORNs rather than by the firing rates of these ORNs.

4.2 Sparse odor representation and olfactory learning

The work presented in Chapter 3 produced several novel findings about olfactory coding and associative learning mechanisms. Our work provided the first characterization of odor responses in the KCs of moths (Figures 3.4, 3.5). Similar to the KCs in locusts, moth KCs showed extremely low spontaneous firing rates, with extremely high population and lifetime sparseness. Moth KCs typically responded to odors with one spike at odor onset and sometimes at odor offset. Thus, despite differences in anatomical detail in the AL, KCs in locusts and moths appear to respond to odors in similar way.

Hebbian STDP is widely observed in a wide range of species from insects to humans (Cassenaer and Laurent, 2007; for review, see Dan and Poo, 2004). This physiological phenomenon is believed to be the cellular mechanism for associative learning. However, STDP requires a millisecond-scale temporal correlation of spiking activity between the pre- and postsynaptic neurons, but animals can learn to associate a sensory cue and a reward presented seconds later. Thus, for STDP to mediate associative learning, neurons must retain information about the sensory cue as spiking activity until reinforcement arrives.

We tested this requirement in *Manduca*. We conditioned moths to associate an odor with a sucrose water reward. By varying the amount of temporal overlap between

KC spikes and the sucrose reward, we showed that the most learning happened when KC spiking activity had no overlap with the reward presentation. Increasing this temporal overlap actually reduced the learning efficacy (Figure 3.6). Taken together, our physiological and behavioral results indicate that spikes in KCs alone cannot constitute the odor representation that coincides with sucrose reward. Instead, our findings lead to an alternative hypothesis that sustained biochemical processes triggered by the transient KC spikes may be paired with the sucrose reward. This pairing can bring about changes in presynaptic terminals in KCs as a form to store the learned associations in the neural network.

References

Abdel-Latief M. A family of chemoreceptors in Tribolium castaneum (Tenebrionidae: Coleoptera)., *PLoS One* 2: e1319, 2007.

Ache BW, Young JM. Olfaction: diverse species, conserved principles., *Neuron* 48: 417-430, 2005.

Adams *et al.* The genome sequence of *Drosophila melanogaster*., *Science* 287: 2185-2195, 2000.

Adrian ED. Olfactory reactions in the brain of the hedgehog., *J. Physiol.* 100: 459-473, 1942.

Altner H, Routil C, Loftus R. The structure of bimodal chemo-, thermo-, and hygroreceptive sensilla on the antenna of Locusta migratoria., *Cell Tissue Res* 215: 289-308, 1981.

Anton S, Homberg U. Antennal lobe structure. *In: Insect Olfaction.* Hansson BS (Ed.), Springer-Verlag, Berlin, 1999.

Araneda RC, Kini AD, Firestein S. The molecular receptive range of an odorant receptor., *Nat Neurosci* 3: 1248-1255, 2000.

Assisi C, Stopfer M, Laurent G, Bazhenov M. Adaptive regulation of sparseness by feedforward inhibition., *Nat Neurosci* 10: 1176-1184, 2007.

Baker TC, Willis MA, Haynes KF, Phelan PL. A Pulsed Cloud Of Sex-Pheromone Elicits Upwind Flight In Male Moths, *Physiological Entomology* 10: 257-265, 1985.

Barlow HB. Single units and sensation: a neuron doctrine for perceptual psychology?, *Perception* 1: 371-394, 1972.

Bathellier B, Buhl DL, Accolla R, Carleton A. Dynamic Ensemble Odor Coding in the Mammalian Olfactory Bulb: Sensory Information at Different Timescales., *Neuron* 57: 586-598, 2008.

Bazhenov M, Rulkov NF, Fellous J.-M, Timofeev I. Role of network dynamics in shaping spike timing reliability., *Phys Rev E Stat Nonlin Soft Matter Phys* 72: 041903, 2005.

Bazhenov M, Rulkov NF, Timofeev I. Effect of synaptic connectivity on long-range synchronization of fast cortical oscillations., *J Neurophysiol* 100: 1562-1575, 2008.

Bazhenov M, Stopfer M, Rabinovich M, Abarbanel HD, Sejnowski TJ, Laurent G. Model of cellular and network mechanisms for odor-evoked temporal patterning in the locust antennal lobe., *Neuron* 30: 569-581, 2001.

Bell RA, Joachim FA. Techniques for rearing laboratory colonies of tobacco hornworms and pink bollworms lepidoptera-sphingidae-gelechiidae., *Ann. Entomol. Soc. Am.* 69: 365-373, 1976.

Belle JS, Heisenberg M. Associative odor learning in *Drosophila* abolished by chemical ablation of mushroom bodies., *Science* 263: 692-695, 1994.

Belluscio L, Katz LC. Symmetry, stereotypy, and topography of odorant representations in mouse olfactory bulbs., *J Neurosci* 21: 2113-2122, 2001.

Benton R. On the ORigin of smell: odorant receptors in insects., *Cell Mol Life Sci* 63: 1579-1585, 2006.

Benton R, Sachse S, Michnick SW, Vosshall LB. Atypical membrane topology and heteromeric function of *Drosophila* odorant receptors *in vivo*., *PLoS Biol* 4: e20, 2006.

Berg MVD, Ziegelberger G. On the function of the pheromone binding protein in

the olfactory hairs of *Antheraea polyphemus*, *Journal of Insect Physiology* 37: 79-85, 1991.

Bhalerao S, Sen A, Stocker R, Rodrigues V. Olfactory neurons expressing identified receptor genes project to subsets of glomeruli within the antennal lobe of *Drosophila melanogaster*., *J Neurobiol* 54: 577-592, 2003.

Bigiani A, Mucignat-Caretta C, Montani G, Tirindelli R. Pheromone reception in mammals., *Rev Physiol Biochem Pharmacol* 154: 1-35, 2005.

Bitterman ME, Menzel R, Fietz A, Schäfer S. Classical conditioning of proboscis extension in honeybees (*Apis mellifera*)., *J Comp Psychol* 97: 107-119, 1983.

Boeckh J, Ernst KD, Selsam P. Neurophysiology and neuroanatomy of the olfactory pathway in the cockroach., *Ann N Y Acad Sci* 510: 39-43, 1987.

Boeckh J, Tolbert LP. Synaptic organization and development of the antennal lobe in insects., *Microsc Res Tech* 24: 260-280, 1993.

Breed MD, Guzmán-Novoa E, Hunt GJ. Defensive behavior of honey bees: organization, genetics, and comparisons with other bees., *Annu Rev Entomol* 49: 271-298, 2004.

Bressler SL, Freeman WJ. Frequency analysis of olfactory system EEG in cat, rabbit, and rat., *Electroencephalogr Clin Neurophysiol* 50: 19-24, 1980.

Bringuier V, Frégnac Y, Baranyi A, Debanne D, Shulz DE. Synaptic origin and stimulus dependency of neuronal oscillatory activity in the primary visual cortex of the cat., *J Physiol* 500 (Pt 3): 751-774, 1997.

Brown SL, Joseph J, Stopfer M. Encoding a temporally structured stimulus with a temporally structured neural representation., *Nat. Neurosci.* 8: 1568-1576, 2005a.

Bruce HM. Pheromones., *Br Med Bull* 26: 10-13, 1970.

Brunel N, Wang XJ. What determines the frequency of fast network oscillations with irregular neural discharges? I. Synaptic dynamics and excitation-inhibition balance., *J. Neurophysiol.* 90: 415-430, 2003.

de Bruyne M, Clyne PJ, Carlson JR. Odor coding in a model olfactory organ: the *Drosophila* maxillary palp., *J Neurosci* 19: 4520-4532, 1999.

de Bruyne M, Foster K, Carlson JR. Odor coding in the *Drosophila* antenna., *Neuron* 30: 537-552, 2001.

Buck L, Axel R. A novel multigene family may encode odorant receptors: a molecular basis for odor recognition., *Cell* 65: 175-187, 1991.

Buck LB. Information coding in the vertebrate olfactory system., *Annu. Rev. Neurosci.* 19: 517-544, 1996.

Buhl EH, Tamás G, Fisahn A. Cholinergic activation and tonic excitation induce persistent gamma oscillations in mouse somatosensory cortex *in vitro*., *J. Physiol.* 513: 117-126, 1998.

Buzsáki G, Chrobak JJ. Temporal structure in spatially organized neuronal ensembles: a role for interneuronal networks., *Curr Opin Neurobiol* 5: 504-510, 1995.

Carlsson MA, Knüsel P, Verschure PF. MJ, Hansson BS. Spatio-temporal Ca2+ dynamics of moth olfactory projection neurones., *Eur J Neurosci* 22: 647-657, 2005.

Cassenaer S, Laurent G. Hebbian STDP in mushroom bodies facilitates the synchronous flow of olfactory information in locusts., *Nature* 448: 709-713, 2007.

Christensen TA, Harrow ID, Cuzzocrea C, Randolph PW, Hildebrand JG. Distinct projections of two populations of olfactory receptor axons in the antennal lobe of the sphinx moth *Manduca sexta*., *Chem Senses* 20: 313-323, 1995.

Christensen TA, Hildebrand JG. Male-specific, sex pheromone-selective projection neurons in the antennal lobes of the moth *Manduca sexta*., *J Comp Physiol*

A 160: 553-569, 1987.
Christensen TA, Lei H, Hildebrand JG. Coordination of central odor representations through transient, non-oscillatory synchronization of glomerular output neurons., *Proc Natl Acad Sci USA* 100: 11076-11081, 2003.
Christensen TA, Pawlowski VM, Lei H, Hildebrand JG. Multi-unit recordings reveal context-dependent modulation of synchrony in odor-specific neural ensembles., *Nat. Neurosci.* 3: 927-931, 2000.
Cleland BG, Harding TH. Response to the velocity of moving visual stimuli of the brisk classes of ganglion cells in the cat retina., *J Physiol* 345: 47-63, 1983.
Clyne PJ, Warr CG, Freeman MR, Lessing D, Kim J, Carlson JR. A novel family of divergent seven-transmembrane proteins: candidate odorant receptors in *Drosophila*., *Neuron* 22: 327-338, 1999.
Couto A, Alenius M, Dickson BJ. Molecular, anatomical, and functional organization of the *Drosophila* olfactory system., *Curr Biol* 15: 1535-1547, 2005.
Dacks AM, Christensen TA, Agricola HJ, Wollweber L, Hildebrand JG. Octopamine-immunoreactive neurons in the brain and subesophageal ganglion of the hawkmoth *Manduca sexta*., *J Comp Neurol* 488: 255-268, 2005.
Daly KC, Durtschi ML, Smith BH. Olfactory-based discrimination learning in the moth, *Manduca sexta*., *J Insect Physiol* 47: 375-384, 2001.
Daly KC, Smith BH. Associative olfactory learning in the moth *Manduca sexta*., *J Exp Biol* 203: 2025-2038, 2000.
Daly KC, Wright GA, Smith BH. Molecular features of odorants systematically influence slow temporal responses across clusters of coordinated antennal lobe units in the moth *Manduca sexta*., *J Neurophysiol* 92: 236-254, 2004.
Dan Y, Poo MM. Spike timing-dependent plasticity of neural circuits., *Neuron* 44: 23-30, 2004.
Datta SR, Vasconcelos ML, Ruta V, Luo S, Wong A, Demir E, Flores J, Balonze K, Dickson BJ, Axel R. The *Drosophila* pheromone cVA activates a sexually dimorphic neural circuit., *Nature* 452: 473-477, 2008.
Davis RL. Olfactory memory formation in *Drosophila*: from molecular to systems neuroscience., *Annu Rev Neurosci* 28: 275-302, 2005.
Demmer H, Kloppenburg P. Intrinsic membrane properties and inhibitory synaptic input of kenyon cells as mechanisms for sparse coding?, *J Neurophysiol* 102: 1538-1550, 2009.
Dethier VG. Five hundred million years of olfaction., *In: Keywords in Evolutionary Biology.*, Keller EF, Lloyd EA (Eds.), Harvard University Press, Cambridge, Massachusetts, 170-179, 1994.
DeWeese MR, Wehr M, Zador AM. Binary spiking in auditory cortex., *J Neurosci* 23: 7940-7949, 2003.
Distler PG, Boeckh J. Synaptic connections between identified neuron types in the antennal lobe glomeruli of the cockroach, Periplaneta americana: I. Uniglomerular projection neurons., *J Comp Neurol* 378: 307-319, 1997.
Distler PG, Boeckh J. Synaptic connections between identified neuron types in the antennal lobe glomeruli of the cockroach, Periplaneta americana: II. Local multiglomerular interneurons., *J Comp Neurol* 383: 529-540, 1997a.
Dobritsa AA, van der Goes van Naters W, Warr CG, Steinbrecht RA, Carlson JR. Integrating the molecular and cellular basis of odor coding in the *Drosophila* antenna., *Neuron* 37: 827-841, 2003.
Drew PJ, Abbott LF. Extending the effects of spike-timing-dependent plasticity to behavioral timescales., *Proc Natl Acad Sci U S A* 103: 8876-8881, 2006.

Du G, Prestwich GD. Protein structure encodes the ligand binding specificity in pheromone binding proteins., *Biochemistry* 34: 8726-8732, 1995.
Duchamp-Viret P, Duchamp A, Chaput MA. Peripheral odor coding in the rat and frog: quality and intensity specification., *J Neurosci* 20: 2383-2390, 2000.
Dudareva N, Pichersky E. Biochemical and molecular genetic aspects of floral scents., *Plant Physiol* 122: 627-633, 2000.
Eeckman FH, Freeman WJ. Correlations between unit firing and EEG in the rat olfactory system., *Brain Res* 528: 238-244, 1990.
Eisthen HL. Why are olfactory systems of different animals so similar?, *Brain Behav Evol* 59: 273-293, 2002.
Elmore T, Ignell R, Carlson JR, Smith DP. Targeted mutation of a *Drosophila* odor receptor defines receptor requirement in a novel class of sensillum., *J Neurosci* 23: 9906-9912, 2003.
Engsontia P, Sanderson AP, Cobb M, Walden KKO, Robertson HM, Brown S. The red flour beetle's large nose: an expanded odorant receptor gene family in Tribolium castaneum., *Insect Biochem Mol Biol* 38: 387-397, 2008.
Erber J. Retrograde amnesia in honeybees (*Apis mellifera carnica*)., *J Comp Physiol Psychol* 90: 41-46, 1976.
Erber J. Localization of short-term-memory in the bran of the bee, *Apis mellifera.*, *Physiological entomology* 5 : 343-358, 1980.
Ernst KD, Boeckh J, Boeckh V. A neuroanatomical study on the organization of the central antennal pathways in insects., *Cell Tissue Res.* 176: 285-306, 1977.
Fan RJ, Anderson P, Hansson BS. Behavioural analysis of olfactory conditioning in the moth *Spodoptera littoralis* (Boisd.) (Lepidoptera: noctuidae)., *J Exp Biol* 200 (Pt 23): 2969-2976, 1997.
Farivar SS. Cytoarchitecture of the locust olfactory system., Ph.D. thesis, California Institute of Technology, Pasadena, 2005.
Farris SM. Evolution of insect mushroom bodies: old clues, new insights., *Arthropod Structure & Development* 34: 211-234, 2005.
Farris SM, Sinakevitch I. Development and evolution of the insect mushroom bodies: towards the understanding of conserved developmental mechanisms in a higher brain center., *Arthropod Struct Dev* 32: 79-101, 2003.
Felicioli A, Ganni M, Garibotti M, Pelosi P. Multiple types and forms of odorant-binding proteins in the Old-World porcupine *Hystrix cristata.*, *Comp Biochem Physiol B* 105: 775-784, 1993.
Firestein S, Picco C, Menini A. The relation between stimulus and response in olfactory receptor cells of the tiger salamander., *J Physiol* 468: 1-10, 1993.
Fisahn A, Pike FG, Buhl EH, Paulsen O. Cholinergic induction of network oscillations at 40 Hz in the hippocampus *in vitro.*, *Nature* 394: 186-189, 1998.
Fishilevich E, Vosshall LB. Genetic and functional subdivision of the *Drosophila* antennal lobe., *Curr Biol* 15: 1548-1553, 2005.
Fonta C, Sun XJ, Masson C. Morphology and spatial-distribution of bee antennal lobe interneurons responsive to odors., *Chemical Senses* 18: 101-119, 1993.
Friedrich RW, Laurent G. Dynamic optimization of odor representations by slow temporal patterning of mitral cell activity., *Science* 291: 889-894, 2001.
Fuentes RA, Aguilar MI, Aylwin ML, Maldonado PE. Neuronal activity of mitral-tufted cells in awake rats during passive and active odorant stimulation., *J Neurophysiol* 100: 422-430, 2008.
Galambos R, Makeig S, Talmachoff PJ. A 40-Hz auditory potential recorded from the human scalp., *Proc Natl Acad Sci U S A* 78: 2643-2647, 1981.

Galizia CG, Nägler K, Hölldobler B, Menzel R. Odour coding is bilaterally symmetrical in the antennal lobes of honeybees (*Apis mellifera*)., *Eur J Neurosci* 10: 2964-2974, 1998.
Galizia CG, Sachse S, Rappert A, Menzel R. The glomerular code for odor representation is species specific in the honeybee *Apis mellifera*., *Nat Neurosci* 2: 473-478, 1999.
Gamboa GJ, Grudzien TA, Espelie KE, Bura EA. Kin recognition pheromones in social wasps: combining chemical and behavioural evidence., *Animal Behaviour* 51: 625-629, 1996.
Gao Q, Chess A. Identification of candidate *Drosophila* olfactory receptors from genomic DNA sequence., *Genomics* 60: 31-39, 1999.
Gao Q, Yuan B, Chess A. Convergent projections of *Drosophila* olfactory neurons to specific glomeruli in the antennal lobe., *Nat Neurosci* 3: 780-785, 2000.
Garibotti M, Navarrini A, Pisanelli AM, Pelosi P. Three odorant-binding proteins from rabbit nasal mucosa., *Chem Senses* 22: 383-390, 1997.
Gelperin A, Tank DW. Odour-modulated collective network oscillations of olfactory interneurons in a terrestrial mollusc., *Nature* 345: 437-440, 1990.
Gilad Y, Wiebe V, Przeworski M, Lancet D, Pääbo S. Loss of olfactory receptor genes coincides with the acquisition of full trichromatic vision in primates., *PLoS Biol* 2: E5, 2004.
Gillies MT. The role of carbon dioxide in host-finding by mosquitoes (Diptera: Culicidae): a review., *Bulletin of Entomological Research* 70: 525-532, 1980.
Gorman ML. A mechanism for individual recognition by odour in Herpestes auropunctatus (Carnivora: Viverridae), *Animal Behaviour* 24: 141-145, 1976.
Gray CM, König P, Engel AK, Singer W. Oscillatory responses in cat visual cortex exhibit inter-columnar synchronization which reflects global stimulus properties., *Nature* 338: 334-337, 1989.
Gray CM, Prisco GVD. Stimulus-dependent neuronal oscillations and local synchronization in striate cortex of the alert cat., *J Neurosci* 17: 3239-3253, 1997.
Gray CM, Singer W. Stimulus-specific neuronal oscillations in orientation columns of cat visual cortex., *Proc Natl Acad Sci U S A* 86: 1698-1702, 1989.
Gronenberg W. Subdivisions of hymenopteran mushroom body calyces by their afferent supply., *J Comp Neurol* 435: 474-489, 2001.
Haddad R, Khan R, Takahashi YK, Mori K, Harel D, Sobel N. A metric for odorant comparison., *Nat Methods* 5: 425-429, 2008.
Hallem EA, Carlson JR. Coding of odors by a receptor repertoire., *Cell* 125: 143-160, 2006.
Hallem EA, Ho MG, Carlson JR. The molecular basis of odor coding in the *Drosophila* antenna., *Cell* 117: 965-979, 2004.
Hammer M. An identified neuron mediates the unconditioned stimulus in associative olfactory learning in honeybees, *Nature* 366: 59-63, 1993.
Hammer M, Menzel R. Multiple sites of associative odor learning as revealed by local brain microinjections of octopamine in honeybees., *Learn Mem* 5: 146-156, 1998.
Hansson BS, Anton S. Function and morphology of the antennal lobe: new developments., *Annu. Rev. Entomol.* 45: 203-231, 2000.
Hansson BS, Carlsson MA, Kalinova B. Olfactory activation patterns in the antennal lobe of the sphinx moth, *Manduca sexta*., *J Comp Physiol A Neuroethol Sens Neural Behav Physiol* 189: 301-308, 2003.
Heimbeck G, Bugnon V, Gendre N, Keller A, Stocker RF. A central neural circuit

for experience-independent olfactory and courtship behavior in *Drosophila melanogaster.*, *Proc Natl Acad Sci U S A* 98: 15336-15341, 2001.
Heinbockel T, Kaissling KE. Variability of olfactory receptor neuron responses of female silkmoths (*Bombyx mori* L) to benzoic acid and (+/-)-linalool, *Journal Of Insect Physiology* 42: 565-578, 1996.
Heinbockel T, Kloppenburg P, Hildebrand JG. Pheromone-evoked potentials and oscillations in the antennal lobes of the sphinx moth *Manduca sexta.*, *J. Comp. Physiol. [A]* 182: 703-714, 1998.
Heisenberg M. Mushroom body memoir: from maps to models., *Nat Rev Neurosci* 4: 266-275, 2003.
Heisenberg M, Borst A, Wagner S, Byers D. *Drosophila* mushroom body mutants are deficient in olfactory learning., *J Neurogenet* 2: 1-30, 1985.
Hildebrand JG. Analysis of chemical signals by nervous systems., *Proc Natl Acad Sci U S A* 92: 67-74, 1995.
Hildebrand JG, Shepherd GM. Mechanisms of olfactory discrimination: converging evidence for common principles across phyla., *Annu Rev Neurosci* 20: 595-631, 1997.
Hill CA, Fox AN, Pitts RJ, Kent LB, Tan PL, Chrystal MA, Cravchik A, Collins FH, Robertson HM, Zwiebel LJ. G protein-coupled receptors in Anopheles gambiae., *Science* 298: 176-178, 2002.
Homberg U, Christensen TA, Hildebrand JG. Structure and function of the deutocerebrum in insects., *Annu Rev Entomol* 34: 477-501, 1989.
Homberg U, Hoskins SG, Hildebrand JG. Distribution of acetylcholinesterase activity in the deutocerebrum of the sphinx moth *Manduca sexta.*, *Cell Tissue Res* 279: 249-259, 1995.
Homberg U, Montague RA, Hildebrand JG. Anatomy of antenno-cerebral pathways in the brain of the sphinx moth *Manduca sexta.*, *Cell Tissue Res* 254: 255-281, 1988.
Hudson R. Do newborn rabbits learn the odor stimuli releasing nipple-search behavior?, *Dev Psychobiol* 18: 575-585, 1985.
Hughes JR, Mazurowski JA. Studies on the supracallosal mesial cortex of unanesthetized, conscious mammals. II. Monkey. B. Responses from the olfactory bulb., *Electroencephalogr Clin Neurophysiol* 14: 635-645, 1962.
Ignell R, Anton S, Hansson BS. The antennal lobe of orthoptera - anatomy and evolution., *Brain Behav Evol* 57: 1-17, 2001.
Ito I, Bazhenov M, Ong RC, Raman B, Stopfer M. Frequency Transitions in Odor-Evoked Neural Oscillations., *Neuron* 64: 692-706, 2009.
Ito I, Ong RC, Raman B, Stopfer M. Sparse odor representation and olfactory learning., *Nat Neurosci* 11: 1177-1184, 2008.
Izhikevich EM. Solving the distal reward problem through linkage of STDP and dopamine signaling., *Cereb Cortex* 17: 2443-2452, 2007.
Jayaraman V, Laurent G. Evaluating a genetically encoded optical sensor of neural activity using electrophysiology in intact adult fruit flies., *Front Neural Circuits* 1: 3, 2007.
Jefferis GS. XE, Potter CJ, Chan AM, Marin EC, Rohlfing T, Maurer CR, Luo L. Comprehensive maps of *Drosophila* higher olfactory centers: spatially segregated fruit and pheromone representation., *Cell* 128: 1187-1203, 2007.
Jemiolo B, Andreolini F, Xie TM, Wiesler D, Novotny M. Puberty-affecting synthetic analogs of urinary chemosignals in the house mouse, *Mus domesticus.*, *Physiol Behav* 46: 293-298, 1989.

Joerges J, Kuttner A, Galizia CG, Menzel R. Representations of odours and odour mixtures visualized in the honeybee brain, *Nature* 387: 285-288, 1997.
Johnson BA, Xu Z, Ali SS, Leon M. Spatial representations of odorants in olfactory bulbs of rats and mice: similarities and differences in chemotopic organization., *J Comp Neurol* 514: 658-673, 2009.
Johnston RE. Communication by mosaic signals: Individual recognition and underlying neural mechanisms., *In: Chemical Signals in Vertebrates.*, Robert T, Mason MPL, Müller-Schwarze D (Eds.), Springer US, 269-282, 2005.
Johnston RE. Chemical communication in rodents: From pheromones to individual recognition, *Journal Of Mammalogy* 84: 1141-1162, 2003.
Jones WD, Nguyen TAT, Kloss B, Lee KJ, Vosshall LB. Functional conservation of an insect odorant receptor gene across 250 million years of evolution., *Curr Biol* 15: R119-R121, 2005.
Jortner RA, Farivar SS, Laurent G. A simple connectivity scheme for sparse coding in an olfactory system., *J Neurosci* 27: 1659-1669, 2007.
Kaissling K. Single unit and electroantennogram recordings in insect olfactory organs., *In: Experimental cell biology of taste and olfaction: current techniques and protocols.*, Spielman A, Brand J. (Eds.), CRC press, Boca Raton, FL., 367-377, 1995.
Kaissling KE. Peripheral mechanisms of pheromone reception in moths., *Chem Senses* 21: 257-268, 1996.
Kaissling KE. A quantitative model of odor deactivation based on the redox shift of the pheromone-binding protein im moth antennae., *Ann N Y Acad Sci* 855: 320-322, 1998.
Kaissling KE, Strausfeld CZ, Rumbo ER. Adaptation processes in insect olfactory receptors. Mechanisms and behavioral significance., *Ann N Y Acad Sci* 510: 104-112, 1987.
Kanzaki R, Arbas EA, Strausfeld NJ, Hildebrand JG. Physiology and morphology of projection neurons in the antennal lobe of the male moth *Manduca sexta.*, *J Comp Physiol A* 165: 427-453, 1989.
Kanzaki R, Mishima T. Pheromone-triggered 'flipflopping' neural signals correlate with activities of neck motor neurons of a male moth, *Bombyx mori*, *Zoological Science* 13: 79-87, 1996.
Kanzaki R, Sugi N, Shibuya T. Self-Generated Zigzag Turning Of *Bombyx mori* Males During Pheromone-Mediated Upwind Walking, *Zoological Science* 9: 515-527, 1992.
Karlson P, Luscher M. 'Pheromones': a new term for a class of biologically active substances., *Nature* 183: 55-56, 1959.
Kashiwadani H, Sasaki YF, Uchida N, Mori K. Synchronized oscillatory discharges of mitral/tufted cells with different molecular receptive ranges in the rabbit olfactory bulb., *J Neurophysiol* 82: 1786-1792, 1999.
Kay LM, Stopfer M. Information processing in the olfactory systems of insects and vertebrates., *Semin Cell Dev Biol* 17: 433-442, 2006.
Keene AC, Waddell S. *Drosophila* olfactory memory: single genes to complex neural circuits., *Nat Rev Neurosci* 8: 341-354, 2007.
Kennedy JS, Ludlow AR, Sanders CJ. Guidance-system used in moth sex attraction, *Nature* 288: 475-477, 1980.
Kennedy JS, Ludlow AR, Sanders CJ. Guidance of flying male moths by wind-borne sex-pheromone, *Physiological Entomology* 6: 395-412, 1981.
Kitamoto T. Targeted expression of temperature-sensitive dynamin to study neural

mechanisms of complex behavior in *Drosophila*., *J Neurogenet* 16: 205-228, 2002.
Koulakov A, Gelperin A, Rinberg D. Olfactory coding with all-or-nothing glomeruli., *J Neurophysiol* 98: 3134-3142, 2007.
Krashes MJ, Keene AC, Leung B, Armstrong JD, Waddell S. Sequential use of mushroom body neuron subsets during *Drosophila* odor memory processing., *Neuron* 53: 103-115, 2007.
Krieger J, Klink O, Mohl C, Raming K, Breer H. A candidate olfactory receptor subtype highly conserved across different insect orders., *J Comp Physiol A Neuroethol Sens Neural Behav Physiol* 189: 519-526, 2003.
Krieger J, Raming K, Dewer YME, Bette S, Conzelmann S, Breer H. A divergent gene family encoding candidate olfactory receptors of the moth Heliothis virescens., *Eur J Neurosci* 16: 619-628, 2002.
Larsson MC, Domingos AI, Jones WD, Chiappe ME, Amrein H, Vosshall LB. Or83b encodes a broadly expressed odorant receptor essential for *Drosophila* olfaction., *Neuron* 43: 703-714, 2004.
Laurent G. Olfactory network dynamics and the coding of multidimensional signals., *Nat. Rev. Neurosci.* 3: 884-895, 2002.
Laurent G, Davidowitz H. Encoding of Olfactory Information with Oscillating Neural Assemblies., *Science* 265: 1872-1875, 1994.
Laurent G, Wehr M, Davidowitz H. Temporal representations of odors in an olfactory network., *J Neurosci* 16: 3837-3847, 1996.
Leal WS, Nikonova L, Peng G. Disulfide structure of the pheromone binding protein from the silkworm moth, *Bombyx mori*., *FEBS Lett* 464: 85-90, 1999.
Lee JK, Strausfeld NJ. Structure, distribution and number of surface sensilla and their receptor cells on the olfactory appendage of the male moth *Manduca sexta*., *J Neurocytol* 19: 519-538, 1990.
Lei H, Christensen TA, Hildebrand JG. Local inhibition modulates odor-evoked synchronization of glomerulus-specific output neurons., *Nat. Neurosci.* 5: 557-565, 2002.
Leitch B, Laurent G. GABAergic synapses in the antennal lobe and mushroom body of the locust olfactory system., *J Comp Neurol* 372: 487-514, 1996.
Li Y, Strausfeld NJ. Morphology and sensory modality of mushroom body extrinsic neurons in the brain of the cockroach, *Periplaneta americana*., *J Comp Neurol* 387: 631-650, 1997.
Li Y, Strausfeld NJ. Multimodal efferent and recurrent neurons in the medial lobes of cockroach mushroom bodies., *J Comp Neurol* 409: 647-663, 1999.
Linn CE, Campbell MG, Roelofs WL. Pheromone Components and Active Spaces: What Do Moths Smell and Where Do They Smell It?, *Science* 237: 650-652, 1987.
Linn CE, Roelofs WL. Response specificity of male moths to multicomponent pheromones, *Chemical Senses* 14: 421-437, 1989.
Lundin C, Käll L, Kreher SA, Kapp K, Sonnhammer EL, Carlson JR, Heijne G, Nilsson I. Membrane topology of the *Drosophila* OR83b odorant receptor., *FEBS Lett* 581: 5601-5604, 2007.
Luo L, Callaway EM, Svoboda K. Genetic Dissection of Neural Circuits, *Neuron* 57: 634-660, 2008.
MacLeod K, Bäcker A, Laurent G. Who reads temporal information contained across synchronized and oscillatory spike trains?, *Nature* 395: 693-698, 1998.
MacLeod K, Laurent G. Distinct mechanisms for synchronization and temporal patterning of odor-encoding neural assemblies., *Science* 274: 976-979, 1996.
Mafraneto A, Carde RT. Fine-scale structure of pheromone plumes modulates

upwind orientation of flying moths, *Nature* 369: 142-144, 1994.
Maida R, Mameli M, Müller B, Krieger J, Steinbrecht RA. The expression pattern of four odorant-binding proteins in male and female silk moths, *Bombyx mori.*, *J Neurocytol* 34: 149-163, 2005.
Maida R, Proebstl T, Laue M. Heterogeneity of odorant-binding proteins in the antennae of *Bombyx mori.*, *Chem Senses* 22: 503-515, 1997.
Malnic B, Hirono J, Sato T, Buck LB. Combinatorial receptor codes for odors., *Cell* 96: 713-723, 1999.
Marchlewska-Koj A, Cavaggioni A, Mucignat-Caretta C, Olejniczak P. Stimulation of estrus in female mice by male urinary proteins, *Journal Of Chemical Ecology* 26: 2355-2366, 2000.
Marr D. Simple memory: a theory for archicortex., *Philos Trans R Soc Lond B Biol Sci* 262: 23-81, 1971.
Martín F, Charro MJ, Alcorta E. Mutations affecting the cAMP transduction pathway modify olfaction in *Drosophila.*, *J Comp Physiol A* 187: 359-370, 2001.
Mazor O, Laurent G. Transient dynamics versus fixed points in odor representations by locust antennal lobe projection neurons., *Neuron.* 48: 661-73, 2005.
McKenna MP, Hekmat-Scafe DS, Gaines P, Carlson JR. Putative *Drosophila* pheromone-binding proteins expressed in a subregion of the olfactory system., *J Biol Chem* 269: 16340-16347, 1994.
Melo ACA, Rützler M, Pitts RJ, Zwiebel LJ. Identification of a chemosensory receptor from the yellow fever mosquito, Aedes aegypti, that is highly conserved and expressed in olfactory and gustatory organs., *Chem Senses* 29: 403-410, 2004.
Mizunami M, Okada R, Li Y, Strausfeld NJ. Mushroom bodies of the cockroach: activity and identities of neurons recorded in freely moving animals., *J Comp Neurol* 402: 501-519, 1998.
Mizunami M, Weibrecht JM, Strausfeld NJ. Mushroom bodies of the cockroach: their participation in place memory., *J Comp Neurol* 402: 520-537, 1998a.
Moncho-Bogani J, Lanuza E, Hernández A, Novejarque A, Martínez-García F. Attractive properties of sexual pheromones in mice: innate or learned?, *Physiol Behav* 77: 167-176, 2002.
Mori K, Yoshihara Y. Molecular recognition and olfactory processing in the mammalian olfactory system., *Prog Neurobiol* 45: 585-619, 1995.
Morè L. Mouse major urinary proteins trigger ovulation via the vomeronasal organ., *Chem Senses* 31: 393-401, 2006.
Murlis J, Elkinton JS, Carde RT. Odor plumes and how insects use them, *Annual Review Of Entomology* 37: 505-532, 1992.
Murlis J, Jones CD. Fine-scale structure of odor plumes in relation to insect orientation to distant pheromone and other attractant sources, *Physiological Entomology* 6: 71-86, 1981.
Müller U. Prolonged activation of cAMP-dependent protein kinase during conditioning induces long-term memory in honeybees., *Neuron* 27: 159-168, 2000.
Nakagawa T, Sakurai T, Nishioka T, Touhara K. Insect sex-pheromone signals mediated by specific combinations of olfactory receptors., *Science* 307: 1638-1642, 2005.
Nathans J, Thomas D, Hogness DS. Molecular genetics of human color vision: the genes encoding blue, green, and red pigments., *Science* 232: 193-202, 1986.
Nei M, Niimura Y, Nozawa M. The evolution of animal chemosensory receptor gene repertoires: roles of chance and necessity., *Nat Rev Genet* 9: 951-963, 2008.

Neuhaus EM, Gisselmann G, Zhang W, Dooley R, Störtkuhl K, Hatt H. Odorant receptor heterodimerization in the olfactory system of *Drosophila melanogaster*., *Nat Neurosci* 8: 15-17, 2005.

Neville KR, Haberly LB. Beta and gamma oscillations in the olfactory system of the urethane-anesthetized rat., *J Neurophysiol* 90: 3921-3930, 2003.

Nishikawa M, Yokohari F, Ishibashi T. Central projections of the antennal cold receptor neurons and hygroreceptor neurons of the cockroach *Periplaneta americana*., *J Comp Neurol* 361: 165-176, 1995.

Novotny MV, Jemiolo B, Wiesler D, Ma W, Harvey S, Xu F, Xie TM, Carmack M. A unique urinary constituent, 6-hydroxy-6-methyl-3-heptanone, is a pheromone that accelerates puberty in female mice., *Chem Biol* 6: 377-383, 1999.

Olberg RM. Pheromone-triggered flip-flopping interneurons in the ventral nerve cord of the silkworm moth, *Bombyx mori*, *Journal of Comparative Physiology A: Neuroethology, Sensory, Neural, and Behavioral Physiology* 152: 297-307, 1983.

Olender T, Lancet D, Nebert DW. Update on the olfactory receptor (OR) gene superfamily., *Hum Genomics* 3: 87-97, 2008.

Olsen SR, Bhandawat V, Wilson RI. Excitatory Interactions between Olfactory Processing Channels in the *Drosophila* Antennal Lobe., *Neuron* 54: 89-103, 2007.

Olsen SR, Wilson RI. Cracking neural circuits in a tiny brain: new approaches for understanding the neural circuitry of *Drosophila*., *Trends Neurosci* 31: 512-520, 2008.

Olsen SR, Wilson RI. Lateral presynaptic inhibition mediates gain control in an olfactory circuit., *Nature* 452: 956-960, 2008a.

Olshausen BA, Field DJ. Sparse coding of sensory inputs., *Curr Opin Neurobiol* 14: 481-487, 2004.

Ong RC, Stopfer M. Olfactory coding: Unusual conductances contribute to sparse neural representations., *J Neurophysiol* , 2009. *In press.*

Parkes AS, Bruce HM. Pregnancy-Block In Female Mice Placed In Boxes Soiled By Males, *Journal Of Reproduction And Fertility* 4: 303-308, 1962.

Pelosi P. Odorant-Binding Proteins, *Critical Reviews in Biochemistry and Molecular Biology* 29: 199-228, 1994.

Pelosi P, Baldaccini NE, Pisanelli AM. Identification of a specific olfactory receptor for 2-isobutyl-3-methoxypyrazine., *Biochem J* 201: 245-248, 1982.

Perez-Orive J. Neural oscillations and the decoding of sensory information., Ph.D. thesis, California Institute of Technology, Pasadena, 2004.

Perez-Orive J, Bazhenov M, Laurent G. Intrinsic and circuit properties favor coincidence detection for decoding oscillatory input., *J. Neurosci.* 24: 6037-6047, 2004.

Perez-Orive J, Mazor O, Turner GC, Cassenaer S, Wilson RI, Laurent G. Oscillations and sparsening of odor representations in the mushroom body., *Science* 297: 359-365, 2002.

Pes D, Pelosi P. Odorant-binding proteins of the mouse., *Comp Biochem Physiol B Biochem Mol Biol* 112: 471-479, 1995.

Pikielny CW, Hasan G, Rouyer F, Rosbash M. Members of a family of *Drosophila* putative odorant-binding proteins are expressed in different subsets of olfactory hairs., *Neuron* 12: 35-49, 1994.

Pitts RJ, Fox AN, Zwiebel LJ. A highly conserved candidate chemoreceptor expressed in both olfactory and gustatory tissues in the malaria vector Anopheles gambiae., *Proc Natl Acad Sci U S A* 101: 5058-5063, 2004.

Porter RH, Winberg J. Unique salience of maternal breast odors for newborn

infants., *Neurosci Biobehav Rev* 23: 439-449, 1999.
Pouzat C, Mazor O, Laurent G. Using noise signature to optimize spike-sorting and to assess neuronal classification quality., *J Neurosci Methods* 122: 43-57, 2002.
Prestwich GD, Du G, LaForest S. How is pheromone specificity encoded in proteins?, *Chem Senses* 20: 461-469, 1995.
Quiroga RQ, Reddy L, Kreiman G, Koch C, Fried I. Invariant visual representation by single neurons in the human brain., *Nature* 435: 1102-1107, 2005.
Reiff DF, Ihring A, Guerrero G, Isacoff EY, Joesch M, Nakai J, Borst A. *In vivo* performance of genetically encoded indicators of neural activity in flies., *J Neurosci* 25: 4766-4778, 2005.
Rekwot PI, Ogwu D, Oyedipe EO, Sekoni VO. The role of pheromones and biostimulation in animal reproduction., *Anim Reprod Sci* 65: 157-170, 2001.
Ressler KJ, Sullivan SL, Buck LB. Information coding in the olfactory system: evidence for a stereotyped and highly organized epitope map in the olfactory bulb., *Cell* 79: 1245-1255, 1994.
Raguso RA, Willis MA. Synergy between visual and olfactory cues in nectar feeding by naïve hawkmoths, *Manduca sexta*, *Animal Behaviour* 64: 685, 2002.
Robertson HM, Wanner KW. The chemoreceptor superfamily in the honey bee, *Apis mellifera*: expansion of the odorant, but not gustatory, receptor family., *Genome Res* 16: 1395-1403, 2006.
Robertson HM, Warr CG, Carlson JR. Molecular evolution of the insect chemoreceptor gene superfamily in *Drosophila melanogaster.*, *Proc Natl Acad Sci U S A* 100 Suppl 2: 14537-14542, 2003.
Rodrigues V. Spatial coding of olfactory information in the antennal lobe of *Drosophila melanogaster.*, *Brain Res* 453: 299-307, 1988.
Rospars JP, Hildebrand JG. Anatomical identification of glomeruli in the antennal lobes of the male sphinx moth *Manduca sexta.*, *Cell Tissue Res.* 270: 205-227, 1992.
Rubin BD, Katz LC. Optical imaging of odorant representations in the mammalian olfactory bulb., *Neuron* 23: 499-511, 1999.
Ruebenbauer A, Schlyter F, Hansson BS, Löfstedt C, Larsson MC. Genetic variability and robustness of host odor preference in *Drosophila melanogaster.*, *Curr Biol* 18: 1438-1443, 2008.
Rulkov N, Bazhenov M. Oscillations and Synchrony in Large-scale Cortical Network Models, *J. Biol. Phys.* 34: 279-299, 2008.
Rulkov NF. Modeling of spiking-bursting neural behavior using two-dimensional map., *Phys Rev E Stat Nonlin Soft Matter Phys* 65: 041922, 2002.
Rulkov NF, Timofeev I, Bazhenov M. Oscillations in large-scale cortical networks: map-based model., *J Comput Neurosci* 17: 203-223, 2004.
Sachse S, Galizia CG. The coding of odour-intensity in the honeybee antennal lobe: local computation optimizes odour representation., *Eur J Neurosci* 18: 2119-2132, 2003.
Sachse S, Rappert A, Galizia CG. The spatial representation of chemical structures in the antennal lobe of honeybees: steps towards the olfactory code., *Eur J Neurosci* 11: 3970-3982, 1999.
Salinas E, Sejnowski TJ. Correlated neuronal activity and the flow of neural information., *Nat Rev Neurosci* 2: 539-550, 2001.
Sandeman DC, Sandeman RE. Orthodromically and antidromically evoked local field potentials in the crayfish olfactory lobe., *J Exp Biol* 201 (Pt 9): 1331-1344, 1998.
Sato K, Pellegrino M, Nakagawa T, Nakagawa T, Vosshall LB, Touhara K.

Insect olfactory receptors are heteromeric ligand-gated ion channels., *Nature* 452: 1002-1006, 2008.

Satou M. Synaptic organization, local neuronal circuitry, and functional segregation of the teleost olfactory bulb., *Prog Neurobiol* 34: 115-142, 1990.

Scaloni A, Monti M, Angeli S, Pelosi P. Structural analysis and disulfide-bridge pairing of two odorant-binding proteins from *Bombyx mori*., *Biochem Biophys Res Commun* 266: 386-391, 1999.

Schadow J, Lenz D, Thaerig S, Busch NA, Fründ I, Herrmann CS. Stimulus intensity affects early sensory processing: sound intensity modulates auditory evoked gamma-band activity in human EEG., *Int J Psychophysiol* 65: 152-161, 2007.

Schmuker M, Bruyne M, Hähnel M, Schneider G. Predicting olfactory receptor neuron responses from odorant structure., *Chem Cent J* 1: 11, 2007.

Schröter U, Menzel R. A new ascending sensory tract to the calyces of the honeybee mushroom body, the subesophageal-calycal tract., *J Comp Neurol* 465: 168-178, 2003.

Schwaerzel M, Monastirioti M, Scholz H, Friggi-Grelin F, Birman S, Heisenberg M. Dopamine and octopamine differentiate between aversive and appetitive olfactory memories in *Drosophila*., *J Neurosci* 23: 10495-10502, 2003.

Shanbhag SR, Hekmat-Scafe D, Kim MS, Park SK, Carlson JR, Pikielny C, Smith DP, Steinbrecht RA. Expression mosaic of odorant-binding proteins in *Drosophila* olfactory organs., *Microsc Res Tech* 55: 297-306, 2001.

Shang Y, Claridge-Chang A, Sjulson L, Pypaert M, Miesenböck G. Excitatory local circuits and their implications for olfactory processing in the fly antennal lobe., *Cell* 128: 601-612, 2007.

Shariff S, Suh M, Zhao M, Ma H, Schwartz TH. Recent developments in oximetry and perfusion-based mapping techniques and their role in the surgical treatment of neocortical epilepsy., *Epilepsy Behav* 8: 363-375, 2006.

Sharp FR, Kauer JS, Shepherd GM. Local sites of activity-related glucose metabolism in rat olfactory bulb during olfactory stimulation., *Brain Res* 98: 596-600, 1975.

Shields VD, Hildebrand JG. Recent advances in insect olfaction, specifically regarding the morphology and sensory physiology of antennal sensilla of the female sphinx moth *Manduca sexta*., *Microsc Res Tech* 55: 307-329, 2001.

Shields VDC, Hildebrand JG. Responses of a population of antennal olfactory receptor cells in the female moth *Manduca sexta* to plant-associated volatile organic compounds, *J Comp Physiol A* 186: 1135-1151, 2000.

Skiri HT, Galizia CG, Mustaparta H. Representation of primary plant odorants in the antennal lobe of the moth Heliothis virescens using calcium imaging., *Chem Senses* 29: 253-267, 2004.

Skiri HT, Stranden M, Sandoz JC, Menzel R, Mustaparta H. Associative learning of plant odorants activating the same or different receptor neurones in the moth Heliothis virescens., *J Exp Biol* 208: 787-796, 2005.

Smith TE, Tomlinson AJ, Mlotkiewicz JA, Abbott DH. Female marmoset monkeys (*Callithrix jacchus*) can be identified from the chemical composition of their scent marks., *Chem Senses* 26: 449-458, 2001.

Sorensen PW. Biological responsiveness to pheromones provides fundamental and unique insight into olfactory function., *Chem Senses* 21: 245-256, 1996.

Soucy ER, Albeanu DF, Fantana AL, Murthy VN, Meister M. Precision and diversity in an odor map on the olfactory bulb., *Nat Neurosci* 12: 210-220, 2009.

Spors H, Wachowiak M, Cohen LB, Friedrich RW. Temporal dynamics and

latency patterns of receptor neuron input to the olfactory bulb., *J Neurosci* 26: 1247-1259, 2006.
Steinbrecht RA. Are odorant-binding proteins involved in odorant discrimination?, *Chem Senses* 21: 719-727, 1996.
Steinbrecht RA. Odorant-binding proteins: expression and function., *Ann N Y Acad Sci* 855: 323-332, 1998.
Stewart WB, Kauer JS, Shepherd GM. Functional organization of rat olfactory bulb analysed by the 2-deoxyglucose method., *J Comp Neurol* 185: 715-734, 1979.
Stocker RF. The organization of the chemosensory system in *Drosophila melanogaster*: a review., *Cell Tissue Res* 275: 3-26, 1994.
Stocker RF, Lienhard MC, Borst A, Fischbach KF. Neuronal architecture of the antennal lobe in *Drosophila melanogaster*., *Cell Tissue Res* 262: 9-34, 1990.
Stopfer M, Bhagavan S, Smith BH, Laurent G. Impaired odour discrimination on desynchronization of odour-encoding neural assemblies., *Nature* 390: 70-74, 1997.
Stopfer M, Jayaraman V, Laurent G. Intensity versus identity coding in an olfactory system., *Neuron* 39: 991-1004, 2003.
Stopfer M, Laurent G. Short-term memory in olfactory network dynamics., *Nature* 402: 664-668, 1999.
Strausfeld NJ. Organization of the honey bee mushroom body: representation of the calyx within the vertical and gamma lobes., *J Comp Neurol* 450: 4-33, 2002.
Strausfeld NJ, Hildebrand JG. Olfactory systems: common design, uncommon origins?, *Curr Opin Neurobiol* 9: 634-639, 1999.
Strausfeld NJ, Li Y. Organization of olfactory and multimodal afferent neurons supplying the calyx and pedunculus of the cockroach mushroom bodies., *J Comp Neurol* 409: 603-625, 1999.
Suh GSB, Wong AM, Hergarden AC, Wang JW, Simon AF, Benzer S, Axel R, Anderson DJ. A single population of olfactory sensory neurons mediates an innate avoidance behaviour in *Drosophila*., *Nature* 431: 854-859, 2004.
Szyszka P, Ditzen M, Galkin A, Galizia CG, Menzel R. Sparsening and temporal sharpening of olfactory representations in the honeybee mushroom bodies., *J Neurophysiol* 94: 3303-3313, 2005.
Sánchez-Gracia A, Vieira FG, Rozas J. Molecular evolution of the major chemosensory gene families in insects., *Heredity* 103: 208-216, 2009.
Tanaka NK, Awasaki T, Shimada T, Ito K. Integration of chemosensory pathways in the *Drosophila* second-order olfactory centers., *Curr Biol* 14: 449-457, 2004.
Tanaka NK, Ito K, Stopfer M. Odor-evoked neural oscillations in *Drosophila* are mediated by widely branching interneurons., *J Neurosci* 29: 8595-8603, 2009.
Tanimoto H, Heisenberg M, Gerber B. Experimental psychology: event timing turns punishment to reward., *Nature* 430: 983, 2004.
Thum AS, Jenett A, Ito K, Heisenberg M, Tanimoto H. Multiple memory traces for olfactory reward learning in *Drosophila*., *J Neurosci* 27: 11132-11138, 2007.
Tichy H, Loftus R. Response of moist-air receptor on antenna of the stick insect, *Carausius morosus*, to step changes in temperature, *J Comp Physiol A* 166: 507-516, 1990.
Tirindelli R, Dibattista M, Pifferi S, Menini A. From pheromones to behavior., *Physiol Rev* 89: 921-956, 2009.
Tolbert LP, Hildebrand JG. Organization and synaptic ultrastructure of glomeruli in the antennal lobes of the moth *Manduca sexta*: a study using thin sections and freeze-fracture, *Proc R Soc Lond [Biol]* 213: 279-301, 1981.
Touhara K, Vosshall LB. Sensing odorants and pheromones with chemosensory

receptors., *Annu Rev Physiol* 71: 307-332, 2009.
Traub RD, Whittington MA, Colling SB, Buzsáki G, Jefferys JG. Analysis of gamma rhythms in the rat hippocampus *in vitro* and *in vivo.*, *J Physiol* 493 (Pt 2): 471-484, 1996.
Turin L, Yoshii F. Structure-Odor Relationship., *In: Handbook of olfaction and gustation.*, Doty RL (Ed.), Informa HealthCare, 457-492, 2003.
Turner GC, Bazhenov M, Laurent G. Olfactory representations by *Drosophila* mushroom body neurons., *J Neurophysiol* 99: 734-746, 2008.
Uchida N, Takahashi YK, Tanifuji M, Mori K. Odor maps in the mammalian olfactory bulb: domain organization and odorant structural features., *Nat Neurosci* 3: 1035-1043, 2000.
Vassar R, Chao SK, Sitcheran R, Nuñez JM, Vosshall LB, Axel R. Topographic organization of sensory projections to the olfactory bulb., *Cell* 79: 981-991, 1994.
Vickers NJ, Baker TC. Reiterative responses to single strands of odor promote sustained upwind flight and odor source location by moths., *Proc Natl Acad Sci U S A* 91: 5756-5760, 1994.
Vinje WE, Gallant JL. Sparse coding and decorrelation in primary visual cortex during natural vision., *Science* 287: 1273-1276, 2000.
Vogt RG, Prestwich GD, Lerner MR. Odorant-binding-protein subfamilies associate with distinct classes of olfactory receptor neurons in insects.ste, *J Neurobiol* 22: 74-84, 1991.
Vogt RG, Riddiford LM. Pheromone binding and inactivation by moth antennae., *Nature* 293: 161-163, 1981.
Vosshall LB. Scent of a fly., *Neuron* 59: 685-689, 2008.
Vosshall LB, Amrein H, Morozov PS, Rzhetsky A, Axel R. A spatial map of olfactory receptor expression in the *Drosophila* antenna., *Cell* 96: 725-736, 1999.
Vosshall LB, Wong AM, Axel R. An olfactory sensory map in the fly brain., *Cell* 102: 147-159, 2000.
Wachowiak M, Cohen LB. Representation of odorants by receptor neuron input to the mouse olfactory bulb., *Neuron* 32: 723-735, 2001.
Waldrop B, Christensen TA, Hildebrand JG. GABA-mediated synaptic inhibition of projection neurons in the antennal lobes of the sphinx moth, *Manduca sexta.*, *J. Comp. Physiol. [A]* 161: 23-32, 1987.
Wang JW, Wong AM, Flores J, Vosshall LB, Axel R. Two-photon calcium imaging reveals an odor-evoked map of activity in the fly brain., *Cell* 112: 271-282, 2003.
Wang XJ, Buzsáki G. Gamma oscillation by synaptic inhibition in a hippocampal interneuronal network model., *J Neurosci* 16: 6402-6413, 1996.
Wang Y, Guo H.-F, Pologruto TA, Hannan F, Hakker I, Svoboda K, Zhong Y. Stereotyped odor-evoked activity in the mushroom body of *Drosophila* revealed by green fluorescent protein-based Ca2+ imaging., *J Neurosci* 24: 6507-6514, 2004.
Wehr M, Laurent G. Odour encoding by temporal sequences of firing in oscillating neural assemblies., *Nature* 384: 162-166, 1996.
Weinstock *et al.* Insights into social insects from the genome of the honeybee *Apis mellifera.*, *Nature* 443: 931-949, 2006.
Weliky M, Fiser J, Hunt RH, Wagner DN. Coding of natural scenes in primary visual cortex., *Neuron* 37: 703-718, 2003.
Whittington MA, Stanford IM, Colling SB, Jefferys JG, Traub RD. Spatiotemporal patterns of gamma frequency oscillations tetanically induced in the rat hippocampal slice., *J Physiol* 502 (Pt 3): 591-607, 1997.

Whittington MA, Traub RD, Jefferys JG. Synchronized oscillations in interneuron networks driven by metabotropic glutamate receptor activation., *Nature* 373: 612-615, 1995.
Whittington MA, Traub RD, Kopell N, Ermentrout B, Buhl EH. Inhibition-based rhythms: experimental and mathematical observations on network dynamics., *Int J Psychophysiol* 38: 315-336, 2000.
Wicher D, Schäfer R, Bauernfeind R, Stensmyr MC, Heller R, Heinemann SH, Hansson BS. *Drosophila* odorant receptors are both ligand-gated and cyclic-nucleotide-activated cation channels., *Nature* 452: 1007-1011, 2008.
Willis MA, Arbas EA. Odor-modulated upwind flight of the sphinx moth, *Manduca sexta* L., *J. Comp. Physiol. [A]* 169: 427-40, 1991.
Willmore B, Tolhurst DJ. Characterizing the sparseness of neural codes., *Network* 12: 255-270, 2001.
Willshaw DJ, Buneman OP, Longuet-Higgins HC. Non-holographic associative memory., *Nature* 222: 960-962, 1969.
Wilson RI, Laurent G. Role of GABAergic inhibition in shaping odor-evoked spatiotemporal patterns in the *Drosophila* antennal lobe., *J Neurosci* 25: 9069-9079, 2005.
Wilson RI, Turner GC, Laurent G. Transformation of olfactory representations in the *Drosophila* antennal lobe., *Science* 303: 366-370, 2004.
Wright GA. Bee pheromones: signal or agent of manipulation?, *Curr Biol* 19: R547-R548, 2009.
Wright GA, Carlton M, Smith BH. A honeybee's ability to learn, recognize, and discriminate odors depends upon odor sampling time and concentration., *Behav Neurosci* 123: 36-43, 2009.
Xia *et al*. The genome of a lepidopteran model insect, the silkworm *Bombyx mori*., *Insect Biochem Mol Biol* 38: 1036-1045, 2008.
Yasuyama K, Meinertzhagen IA, Schürmann FW. Synaptic connections of cholinergic antennal lobe relay neurons innervating the lateral horn neuropile in the brain of *Drosophila melanogaster*., *J Comp Neurol* 466: 299-315, 2003.
Young MP, Yamane S. Sparse population coding of faces in the inferotemporal cortex., *Science* 256: 1327-1331, 1992.
Zhang K, Guo JZ, Peng Y, Xi W, Guo A. Dopamine-mushroom body circuit regulates saliency-based decision-making in *Drosophila*., *Science* 316: 1901-1904, 2007.
Zhang W, Ge W, Wang Z. A toolbox for light control of *Drosophila* behaviors through Channelrhodopsin 2-mediated photoactivation of targeted neurons., *Eur J Neurosci* 26: 2405-2416, 2007a.
Ziegelberger G. Redox-shift of the pheromone-binding protein in the silkmoth Antheraea polyphemus., *Eur J Biochem* 232: 706-711, 1995.
Zimmermann B. Differentiation of the thermosensitive hygrosensitive (no-pore) sensilla on the antenna of *Antheraea pernyi* (Lepidoptera, Saturniidae) - a study of cryofixed material, *Cell And Tissue Research* 266: 427-440, 1991.
Zufall F, Hatt H. Dual activation of a sex pheromone-dependent ion channel from insect olfactory dendrites by protein kinase C activators and cyclic GMP., *Proc Natl Acad Sci U S A* 88: 8520-8524, 1991.
Zufall F, Stengl M, Franke C, Hildebrand JG, Hatt H. Ionic currents of cultured olfactory receptor neurons from antennae of male *Manduca sexta*., *J Neurosci* 11: 956-965, 1991.

Bibliography

Ong RC, Stopfer M. Olfactory coding: Unusual conductances contribute to sparse neural representation. Focus on "Intrinsic membrane properties and inhibitory synaptic input of Kenyon cells as mechanisms for sparse coding?", *J Neurophysiol* 103:2-3, 2010.

Ito I, Bazhenov M, Ong RC, Raman B, Stopfer M. Frequency transitions in odor-evoked neural oscillations., *Neuron* 64: 692-706, 2009.

Ito I, Ong RC, Raman B, Stopfer M. Olfactory learning and spike timing dependent plasticity., *Commun Integr Biol* 1:170-171, 2008.

Ito I*, Ong RC*, Raman B, Stopfer M. Sparse odor representation and olfactory learning., *Nat Neurosci* 11: 1177-1184, 2008.
*equal contributions

Ong RC, Lei J, Lee RK, Cheung JY, Fung KP, Lin C, Ho HP, Yu B, Li M, Kong SK. Polyphyllin D induces mitochondrial fragmentation and acts directly on the mitochondria to induce apoptosis in drug-resistant HepG2 cells., *Cancer letter*, 261(2): 158-164, 2008.

Cheung JY, **Ong RC**, Suen YK, Ooi VEC, Wong H, Mak TTW, Fung KP, Yu B, Kong SK. Polyphyllin D is a potent apoptosis inducer in drug-resistant HepG2 cells., *Cancer letter*, 217(2): 203-211, 2005.